

# STUDY OF THE BREAKING OF RELATIVISTICALLY INTENSE LONGITUDINAL WAVES IN A HOMOGENEOUS PLASMA

*By*

ARGHYA MUKHERJEE

PHYS06201204004

INSTITUTE FOR PLASMA RESEARCH, GANDHINAGAR

*A thesis submitted to the  
Board of Studies in Physical Sciences*

*In partial fulfillment of the requirements*

*For the Degree of*

DOCTOR OF PHILOSOPHY

*of*

HOMI BHABHA NATIONAL INSTITUTE




February, 2018


# Homi Bhabha National Institute

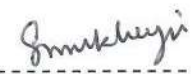
## Recommendations of the Viva Voce Board


As members of the Viva Voce Board, we recommend that the dissertation prepared by **Arghya Mukherjee** entitled "Study of the Breaking of Relativistically Intense Longitudinal Waves in a Homogeneous Plasma" may be accepted as fulfilling the dissertation requirement for the Degree of Doctor of Philosophy.

-----  ----- Date : 26-7-18  
Chairman : Prof. Amita Das

-----  ----- Date : 26/07/2018  
Convener : Prof. Sudip Sengupta

-----  ----- Date : 26/07/2018.  
Examiner : Dr. Amar Kakad


-----  ----- Date : 26/07/2018  
Member : Prof. Subroto Mukherjee

-----  ----- Date : 26.07.18  
Member : Prof. Prabal K Chattopadhyay

-----  ----- Date : 26/07/2018  
Member : Dr. Mrityunjay Kundu

Final approval and acceptance of this dissertation is contingent upon the candidate's submission of the final copies of the dissertation to HBNI.

I hereby certify that I have read this dissertation prepared under my direction and recommend that it may be accepted as fulfilling the dissertation requirement.

-----  ----- Date : 26/07/2018  
Guide : Prof. Sudip Sengupta



## STATEMENT BY AUTHOR

This dissertation has been submitted in partial fulfilment of requirements for an advanced degree at Homi Bhabha National Institute (HBNI) and is deposited in the Library to be made available to borrowers under rules of the HBNI.

Brief quotations from this dissertation are allowable without special permission, provided that accurate acknowledgement of source is made. Requests for permission for extended quotation from or reproduction of this manuscript in whole or in part may be granted by the Competent Authority of HBNI when in his or her judgement the proposed use of the material is in the interests of scholarship. In all other instances, however, permission must be obtained from the author.

*Arghya Mukherjee*

Arghya Mukherjee

## DECLARATION

I, hereby declare that the investigation presented in the thesis has been carried out by me. The work is original and the work has not been submitted earlier as a whole or in part for a degree/diploma at this or any other Institution or University.

*Arghya Mukherjee*

Arghya Mukherjee

*In dedication to  
my family, my teachers  
and  
my “Hero”*

## ACKNOWLEDGEMENTS

*“What memories and thoughts crowd into my mind, as, at the threshold of the afternoon of my wandering life, I sit down to write the story of its morning hours!”*

*- Sarat Chandra Chattopadhyay (in “Srikanto” novel)*

First and foremost, I would like to express my sincere gratitude to my advisor Prof. Sudip Sengupta for his continuous support in my PhD work and related research, for his patience, motivation, and immense knowledge. His guidance helped me in all the time of research and writing of this thesis. I could not have imagined having a better advisor and mentor for my PhD study, his encouragement made it possible to achieve the goal. He is the person who introduced me to basic tools and concepts of plasma physics. Each round of discussions with him inspired me to think in more and more depth. He is a great teacher and his special lectures on “Lagrange coordinates and Wave breaking” during the course work influenced me a lot and helped me to choose him as a advisor of my thesis without thinking a twice. Apart from this, another thing that I have learnt from my advisor is how to remain calm in adverse situations which is very necessary in research career. The discussions with him on various topics (from Richard Feynman to the songs of Kishore Kumar) during tea time is never forgettable.

I would also like to thank the rest of my Doctoral committee members: Prof. Amita Das, Prof. Prabal K Chattopadhyay, Prof. Subroto Mukherjee and Dr. Mrityunjay Kundu, for their encouragement, insightful comments, and hard questions during the review meetings. I want to acknowledge my Doctoral committee chairman, Prof. Amita Das, whose help and sympathetic attitude at every point during

my research helped me to work in time. I would like to express my warm thank to Dr. Mrityunjay Kundu and Prof. Prabal K Chattopadhyay who supported me at every bit, specially during the making of presentations. Their critical review and valuable comments on my presentations always helped me to convey the main message easily to the audiences during the oral talks. I acknowledge them for their valuable times. I wish to thank Prof. Subroto Mukherjee, Academic Dean of Institute for Plasma Research (IPR), whose reminders and constant motivation always encouraged me to complete the jobs in due time and before the deadlines.

I wish to extend my thank to all the faculty members (including the academic committee) of IPR, who taught us during the course work. Dr. Daniel Raju and Dr. R. Srinivasan deserve special thanks for critically reading my manuscripts and providing valuable inputs on them. I am also very grateful to Dr. Vikrant Saxena, Dr. Rameswar Singh and Dr. Abhishek Atreya for reading my synopsis report and for pointing out the necessary corrections. I am extremely grateful to Sagar (one of my close friends at IPR) and Roopendra who always helped me whenever I had some difficulties in numerical programming. The numerical help I got from Sagar (at a very critical stage of PhD) to begin my work in Udbhav and Uday cluster is indeed unforgettable. Big thanks to Avadhesh Maurya and some people from administration (Silel Sir), computer center (Hemant Sir), library, accounts, stores for their unconditional co-operation throughout my PhD.

I gratefully acknowledge the National Initiative in Strong Field Science and Homi Bhabha National Institute for providing travel funds to present my work in ICPP - 2016 and EPS - 2017. I have received a great appreciation there.

Time spent at IPR was made enjoyable due to the presence of many friends, juniors and seniors that became a part of my life specially Patel (Amit), Narayan,

Surabhi, Sagar, Sandeep, Rupak, Subroto, Soumen, Satadal, Devshree, Dr. Harish, Dr. Soumen , Dr. Sayak and Dr. Vikram. A big hug goes to Patel (he was a true friend since we started to share our office) and Surabhi (she was a good listener since we started the physics discussion after 1st review). Physics discussions with Ratan, Shivam and Nidhi has always been very enjoyable. In addition to the above I am also grateful to some of my very close friends specially Pranay, Satyajit, Debaditya, Arijit, Mousumi, Sudeshna and Rai for tolerating my madness. I am also lucky to have family friends like Mr. and Mrs. Shah in Ahmedabad. A big thank to Jiva bhai and his wife for preparing delicious foods (specially sev-tomato ki sabji and kofta) at IPR hostel.

My life was also enriched by the thoughts and philosophy of some of my teachers since my school days which have brought me at this stage. I am highly influenced by the thoughts of Mr. Rudradaman Dutta, ex-headmaster of our school Chakdaha Purbachal Vidyapith. During the holiday times, whenever I went to him, he always gave me inspirations to find out new things. Till date, he is the best person of my life and a source of endless positive energy. Apart from this, he was the person, who introduced me to my science teacher Mr. Tarun Debnath (Tarun Da). Tarun da was the first person who implanted the seed of interest in science in my mind and he has always been a critic of mine (fortunately!). During my higher secondary study, Tarun da took me to my first physics teacher Late Mr. Rabindranath Mandal (Robin Sir) who watered that seed and inspired me to love physics & to choose physics for higher studies. I really miss you Sir !

Nobody has been more important to me in the pursuit of this thesis than my family members. I would like to thank my parents (though they are beyond my thank), whose love, guidance and blessings were always with me. Whatever I have



achieved till date is due to their sacrifice in their life to fulfil my demands. A big thank to my sisters Tikli, Riku & Miku and my uncle (jethu) to take care of my parents in my absence. A warm thank to my eleven years old nephew Debalay who always asks many questions (from atomic structure to string theory) and helps me to think physics from different angles.

I have no words left with me to thank my beloved wife Poulami. Since my college days, she was always with me as a close friend and always inspired me to believe on myself. She was always there to listen about my problems and frustrations. From the date we got married, she took the responsibilities of my home and parents so that I can focus on my research. I deeply acknowledge her for her patience that she has shown in last few months during my PhD. Without her support it would not have been possible. I am really grateful to the God for sending her in my messy life. Therefore this acknowledgement would be incomplete if I do not thank the almighty by uttering the following lines of Rabindranath Tagore (Translated by Deepankar Choudhury):

*“You make me endless, such is a coffee you brew.*

*Emptying me, you fill me again till I am born a new.*

*So many hilltops and many a waterside.*

*You carried me, a flute, far and wide.*

*Endless tunes you evoke, in each stride;*

*To whom I may say so !”*

# List of Publications arising from the thesis

## Publications in Peer Reviewed Journals:

- Analytical estimate of phase mixing time of longitudinal Akhiezer-Polovin waves,  
[Arghya Mukherjee](#) and Sudip Sengupta  
Physics of Plasmas 21, 112104 (2014)
- Phase mixing of relativistically intense longitudinal wave packets in a cold plasma,  
[Arghya Mukherjee](#) and Sudip Sengupta  
Phys of Plasmas 23, 092112 (2016)
- Relativistic electron beam driven longitudinal wake-wave breaking in a cold plasma,  
Ratan Kumar Bera, [Arghya Mukherjee](#), Sudip Sengupta and Amita Das  
Physics of Plasmas 23, 083113 (2016)
- Breaking of large amplitude relativistically intense electron plasma waves in a warm plasma,  
[Arghya Mukherjee](#) and Sudip Sengupta  
arXiv:1802.05670v1 (To be submitted)
- Wave breaking amplitude of a self-consistent electron plasma wave in a Maxwellian plasma,  
[Arghya Mukherjee](#) and Sudip Sengupta  
To be submitted

- **Nonlinear dynamics of relativistically intense waves in cylindrical and spherical geometry,**

[Arghya Mukherjee](#) and Sudip Sengupta

To be submitted

## Conferences

### International Participation:

- **Relativistic Cylindrical and Spherical Plasma Waves (Poster presentation).**

[Arghya Mukherjee](#) and Sudip Sengupta.

Asia Plasma And Fusion Association (APFA), 14th - 18th December 2015, Gandhinagar, India.

- **Wave Breaking in a Maxwellian Plasma (Oral presentation).**

[Arghya Mukherjee](#) and Sudip Sengupta.

International Conference on Plasma Science, Technology and Application (ICPSTA 2016), 20th - 21st January 2016, Amity University, Lucknow, India.

- **Breaking of Large Amplitude Electron Plasma Waves in a Maxwellian Plasma (Poster presentation).**

[Arghya Mukherjee](#) and Sudip Sengupta.

International Congress on Plasma Physics (ICPP 2016), 27th June - 1st July 2016, Kaohsiung, Taiwan.

- **Breaking of Large Amplitude Relativistically Intense Waves in a Warm Plasma (Poster presentation).**

[Arghya Mukherjee](#) and Sudip Sengupta.

44th International Conferences on Plasma Physics (EPS 2017), 26th - 30th June 2017, Belfast, Northern Ireland, United Kingdom.

**National Participation:**

- **Nonlinear Dynamics of Relativistically Intense Waves in Cylindrical and Spherical Geometry (Poster presentation).**

[Arghya Mukherjee](#) and Sudip Sengupta.

28th National Symposium on Plasma Science and Technology (PSSI 2013), 3rd - 6th December 2013, KIIT University, Bhubaneswar, India.

- **Phase Mixing of Longitudinal Akhiezer - Polovin Wave : An Analytical Treatment (Oral presentation).**

[Arghya Mukherjee](#) and Sudip Sengupta.

3rd PSSI-Plasma Scholars Colloquium (PSC 2014), 3rd - 5th July 2014, VIT University, Chennai, India.

- **Analytical Estimate of Phase Mixing Time of Longitudinal Akhiezer-Polovin Waves (Poster Presentation).**

[Arghya Mukherjee](#) and Sudip Sengupta.

29th National Symposium on Plasma Science and Technology (PSSI 2014), 8th - 11th December 2014, M. G. University, Kottayam, Kerala, India.

- **Nonlinear Dynamics of Relativistically Intense Waves in Cylindrical and Spherical Geometry (Oral presentation).**

[Arghya Mukherjee](#) and Sudip Sengupta.

4th PSSI-Plasma Scholars Colloquium (PSC - 2015) , 16th - 17th August 2015, Jadavpur University, Kolkata, India.

- **Phase Mixing of Relativistically Intense Wave Packets in a Cold Plasma (Oral presentation).**

Arghya Mukherjee and Sudip Sengupta.

30th National Symposium on Plasma Science and Technology (PSSI 2015),  
1st - 4th December 2015, SINP, Kolkata, India.

- **Phase Mixing of Relativistically Intense Wave Packets in a Cold Plasma (Buti Young Scientist Award Talk).**

Arghya Mukherjee and Sudip Sengupta.

32nd National Symposium on Plasma Science and Technology (PSSI 2017),  
7th - 10th November 2017, IPR, Gandhinagar, India.

#### Schools/Workshops:

- **DST-SERB School on Tokamaks and Magnetized Plasma Fusion.**

25 February - 15 March 2013,

Institute for Plasma Research, Gandhinagar, India.

- **DST-SERB School on High Intensity Laser Plasma Application. Theory and Simulations.**

05 - 23 May, 2014,

Indian Institute of Technology Delhi, New Delhi.

- **CERN Accelerator School.**

23-29 November 2014,

CERN, Geneva, Switzerland.

*Arghya Mukherjee*

Arghya Mukherjee

Synopsis . . . . .	ix
List of Figures . . . . .	xxiii
<b>1 Introduction</b>	<b>1</b>
1.1 Nonlinear Plasma Waves and Wave Breaking (Overview) . . . . .	1
1.2 Review of earlier works and Motivation . . . . .	5
1.2.1 Wave breaking in a nonrelativistic cold plasma . . . . .	5
1.2.2 Wave breaking in a relativistic cold plasma . . . . .	6
1.2.3 Wave breaking in a nonrelativistic warm plasma . . . . .	8
1.2.4 Wave breaking in a relativistic warm plasma . . . . .	10
1.3 Scope and outline of this thesis . . . . .	11
<b>2 Overview of Sheet Simulations and Particle-in-Cell Simulations</b>	<b>15</b>
2.1 Why Simulations ? . . . . .	15
2.2 Brief overview of Sheet Simulations . . . . .	16
2.2.1 Sheet Model in planar geometry . . . . .	16
2.2.2 Sheet Model in cylindrical and spherical geometry . . . . .	19
2.3 Brief overview of 1-D Particle-in-Cell Simulations . . . . .	21
<b>3 Breaking of Large Amplitude Relativistically Intense Wave Pack-</b> <b>ets in a Cold Plasma</b>	<b>23</b>
3.1 Introduction . . . . .	23
3.2 Equation of Motion and its Solution . . . . .	25
3.3 Results from Sheet Simulations . . . . .	28
3.4 Summary . . . . .	31



<b>4</b>	<b>Analytical Estimate of Phase Mixing Time of Longitudinal Akhiezer - Polovin Wave</b>	<b>33</b>
4.1	Introduction . . . . .	34
4.2	Relativistic Travelling Wave Solution . . . . .	35
4.3	Estimation of Phase Mixing Time . . . . .	37
4.4	Results from Sheet Simulations . . . . .	39
4.5	Discussion and Summary . . . . .	44
<b>5</b>	<b>Nonlinear Dynamics of Relativistically Intense Plasma Waves in Cylindrical and Spherical Geometry</b>	<b>47</b>
5.1	Introduction . . . . .	47
5.2	Governing Equations . . . . .	49
5.2.1	Fluid Variables in Cylindrical Geometry . . . . .	50
5.2.2	Fluid Variables in Spherical Geometry . . . . .	52
5.3	Dynamics of Nonlinear Cylindrical & Spherical Plasma Oscillations and Calculation of Phase Mixing Time . . . . .	54
5.3.1	Breaking of Cylindrical Plasma Oscillations . . . . .	55
5.3.2	Breaking of Spherical Plasma Oscillations . . . . .	59
5.4	Summary . . . . .	62
<b>6</b>	<b>Wave Breaking Amplitude of a Self-consistent Electron Plasma Wave in a Maxwellian Plasma</b>	<b>65</b>
6.1	Introduction . . . . .	65
6.2	Theoretical Model (Using “Water-Bag”) . . . . .	67
6.3	Particle-In-Cell Simulation . . . . .	71
6.3.1	Simulation Model . . . . .	71

6.3.2	Results from Simulation and Its Interpretation . . . . .	73
6.4	Summary . . . . .	85
<b>7</b>	<b>Breaking of Large Amplitude Relativistically Intense Electron Plasma Waves in a Warm Plasma</b>	<b>87</b>
7.1	Introduction . . . . .	88
7.2	Relativistic Particle-in-Cell Simulations Results . . . . .	92
7.2.1	Regime 1 - Relativistic Landau Damping . . . . .	93
7.2.2	Regime 2 - Wave breaking (via phase mixing) . . . . .	95
7.3	Estimation of Phase Mixing Time . . . . .	103
7.4	Summary and Discussions . . . . .	108
<b>8</b>	<b>Conclusion and Future Scope</b>	<b>111</b>
8.1	Conclusions and Summary . . . . .	111
8.2	Future Scope . . . . .	116
	<b>Appendices</b>	<b>123</b>
<b>A</b>	<b>Lindstedt - Poincaré Perturbation Technique (In Planar Geome- try)</b>	<b>125</b>
A.1	Perturbative Solution of $\ddot{\xi} + \omega_p^2 \xi + \epsilon_1 \xi \dot{\xi}^2 \approx 0$ : . . . . .	126
A.2	Perturbative Solution of $\ddot{\xi} + \omega_p^2 \xi + \epsilon_2 \xi \dot{\xi}^4 \approx 0$ : . . . . .	128
<b>B</b>	<b>Lindstedt - Poincaré Perturbation Technique (In Cylindrical and Spherical Geometry)</b>	<b>131</b>
B.1	Perturbative solution of $\ddot{\rho} + \omega_p^2 \rho + \epsilon_2 \rho^2 = 0$ . . . . .	132
B.2	Perturbative solution of $\ddot{\rho} + \omega_p^2 \rho + \epsilon_3 \rho^3 = 0$ . . . . .	134
B.3	Frequency of Oscillation in Cylindrical Geometry: . . . . .	136

B.4	Frequency of Oscillation in Spherical Geometry: . . . . .	136
<b>C</b>	<b>Derivation of Relativistic Warm Plasma Dispersion Relation</b>	<b>139</b>
C.1	Derivation of Linear Dispersion Relation . . . . .	139
C.2	Case 1: $\alpha \gg 1$ , Weakly Relativistic limit . . . . .	142
C.3	Case 2: $\alpha \ll 1$ , Strongly Relativistic limit . . . . .	142

## SYNOPSIS

A plasma is a collection of charged and neutral particles which exhibits collective behaviour. Under equilibrium condition a plasma is macroscopically neutral or quasi-neutral *i.e.* it has an equal mix of electrons and ions which are interacting via electromagnetic forces. Being a highly complex medium, plasma exhibits an assortment of normal modes which are usually termed as plasma waves [1–3]. These waves are often distinguished by their characteristic frequencies, the presence or absence of magnetic fields and the plasma temperature. Waves in plasmas can be classified as electromagnetic or electrostatic respectively, according to whether or not there is an associated oscillating magnetic field. Under certain conditions, mixed modes also can exist. For plane waves Faraday’s law of induction indicates that an electrostatic wave in plasma must be longitudinal. In an unmagnetized plasma (no external magnetic field) two types of electrostatic normal modes can exist: (i) Electron Plasma Oscillations/Waves and (ii) Ion Acoustic Waves. Dynamics of electron plasma oscillation/wave depends on mass and temperature of the electrons in the plasma, where the ions are assumed to be infinitely massive and hence stationary. On the other side, the characteristics of the ion acoustic mode depends on the ion mass and electron temperature; electrons are assumed to be massless and hence follow the Boltzmann distribution. In response to a given perturbation, the acceleration of the electron will be much greater than that of an ion. For this reason, the characteristic frequency of electron motion is much higher than the ion. The reciprocals of the characteristic electron frequency and of the characteristic ion frequency determine the fast and slow time-scale respectively [4]. Depending on the strength of the applied perturbation (or driver that excites the oscillation/wave) and pattern of motion (geometry of motion) of the

oscillating species a variety of high frequency longitudinal modes can be excited in an unmagnetized homogeneous plasma. These modes are the subject of our present exposition.

The most simplest mode that describes the characteristics of a plasma is the electron plasma oscillation [5,6] which is excited when the quasi-neutrality condition of the plasma is disturbed. In fact, when the electrons are instantaneously disturbed from their equilibrium positions, the resulting self-consistent electric field builds up to pull back the electrons in order to restore the quasi-neutrality condition. Because of the inertia, the electrons overshoot from their equilibrium positions and oscillate around their equilibrium positions with a characteristic frequency known as the plasma frequency which mathematically can be expressed as  $\omega_p = \sqrt{4\pi n_0 e^2 / m}$ , where  $n_0$  is the equilibrium density of the electrons and  $e$  &  $m$  respectively are the charge and mass of an electron. Here, the necessary restoring force for oscillation is provided only by the self-consistent electric field.

The theory of cold plasma oscillation does not take into account the random thermal motion of the electrons. If we let the electrons to have a finite temperature, then the electron pressure also acts as a restoring force in addition to the electric field and the oscillation propagates with a characteristic frequency greater than the above cold plasma frequency. This was first reported by Bohm & Gross [7] and known as Electron Plasma Wave (EPW) or Langmuir Wave.

Such space charge oscillations/waves are capable of generating very high electric fields within a short distance and under certain conditions the work done by this self-consistent electric field  $E$  of the wave, over a distance of the order of wavelength ( $\lambda_p$ ) of the wave may approach the electron rest mass energy *i.e*  $eE\lambda_p \sim mc^2$ . Under such conditions, the electrons quiver with a velocity which is

close to the velocity of light in free space ( $c$ ) and the oscillations/waves become relativistically intense. Such kind of relativistically intense oscillations/waves are usually generated by passing a high intensity laser pulse [8] ( $\sim 10^{18} \text{ Watt/cm}^2$  for a  $1\mu\text{m}$  wavelength laser ) or an ultrarelativistic electron beam pulse through an underdense plasma [9]. Apart from its great academic relevance in nonlinear plasma theory [10–13], the study of such kind of relativistically intense oscillations/waves has received a great deal of attention in a number of systems ranging from laboratory plasmas to astrophysical plasmas [14–16]. For instance, oscillations/waves with relativistic amplitudes are regularly encountered in laser assisted nuclear fusion [17–19] and particle acceleration experiments [8, 20–26]. In laser fusion experiments, an intense laser pulse falls on an overdense plasma and excites plasma waves through mode conversion [19] whereas in particle acceleration experiments, an intense laser/beam pulse, propagating through an underdense plasma, excites a large amplitude wakefield through ponderomotive forces/electrostatic forces, which then traps the background plasma electrons or externally injected electrons and accelerates them to higher energy [14–16]. Recent experiments [14, 16, 20–24, 26] indicate that plasma waves excited in the wake of a laser/beam pulse could generate accelerating gradients of the order of  $100 \text{ GV/m}$  in plasma-based accelerator experiments - this is as high as 1000 times stronger accelerating field as compared to the conventional RF accelerators. These energetic particles are useful in a wide variety of fields, ranging from medicine and biology to high-energy physics experiments. These energetic particles are also desirable for producing a hot spot to initiate ignition in an already compressed pellet for fast ignition applications of laser fusion [19].

It is natural to expect that, the larger the amplitude of plasma wave, the greater



the acceleration would be. In fact, the amplitudes of these space charge waves are limited by a phenomena called wave breaking which occurs via several nonlinear processes. In 1959, J. M. Dawson [5] presented a pioneering work where he modelled electrons as independently oscillating sheets of charges (hereinafter referred as Dawson Sheet Model) and demonstrated that for nonrelativistic cold plasma oscillations (where thermal velocity is negligible with respect to the quiver velocity of the electrons) in slab/planar geometry, the amplitude of applied perturbation can not be increased beyond a critical limit, known as wave breaking limit, as the trajectories of the neighbouring sheets constituting the oscillation/wave start crossing each other beyond this limit. This results in fine scale mixing of various parts of the oscillation which destroys the oscillation/wave within a period.

Inclusion of relativistic effects change the dynamics of these oscillations/waves dramatically. The maximum electric field amplitude that can be sustained by a relativistically intense non-linear wave in a cold plasma was first reported by Akhiezer and Polovin [27], before Dawson introduced the phenomenon of “wave breaking” [5]. Using non-linear, relativistic, cold fluid equations in one dimension, Akhiezer and Polovin showed that, the maximum electric field amplitude ( $E_{max}$ ) that can be sustained by a relativistically intense travelling wave in a cold plasma is given by  $eE_{max}/m\omega_p c = \sqrt{2(\gamma_\phi - 1)}$ , where  $\gamma_\phi = 1/\sqrt{1 - \frac{v_\phi^2}{c^2}}$  is the Lorentz factor associated with the phase velocity  $v_\phi$  of the wave. However later it has been discovered that this Akhiezer - Polovin limit does not hold for arbitrary initial conditions. In 1989, Infeld and Rowlands [28] presented an exact space-time dependent solution of the relativistic cold plasma fluid-Maxwell equations using Lagrange coordinates [6]. The solution presented by them exhibits explosive behaviour for all initial conditions, except for the one which is needed to excite Akhiezer - Polovin

waves. Physically this explosive behaviour arises due to the relativistic electron mass variation which causes the characteristic electron plasma frequency to acquire spatial dependency, due to which neighbouring electrons gradually go out of phase and eventually cross causing the wave to break at arbitrarily small initial perturbation. This phenomena is known as phase mixing [29–32]. This mechanism of wave breaking through gradual phase mixing is not exhibited by a pure longitudinal Akhiezer - Polovin wave. In fact, longitudinal Akhiezer - Polovin mode is a very special combination of frequency ( $\omega$ ), wavenumber ( $k$ ) and their harmonics such that the resultant profile propagates as a coherent nonlinear structure with a constant phase velocity [32]. In 2012 Verma *et. al.* [33], by performing extensive numerical simulation, showed that even a longitudinal Akhiezer - Polovin wave breaks through the gradual process of phase mixing at an amplitude well below its wave breaking limit, when it is subjected to an arbitrarily small amplitude longitudinal perturbation. However an analytical expression for the phase mixing time scale of this mode as a function of its parameters is yet to be discovered. Further, in relation to laser/beam driven wakefield experiments, it has been recently pointed out that [33] if the phase mixing time (wave breaking time) is shorter than the dephasing time of an electron in the wake wave, then the maximum energy gain cannot be achieved as the wake wave gets damped because of phase mixing before the dephasing time is reached. Therefore, the estimation of phase mixing time (wave breaking time) of these relativistically intense plasma waves are relevant for these experiments.

Now we would like to note that, in addition to the relativistic mass variation effects, phase mixing also arises because of the geometry of oscillation (cylindrical and spherical [5]) and/or background density inhomogeneities (either fixed [5, 34]

or self-generated [29]). The idea of phase mixing of a wave in an inhomogeneous medium leading to dissipation of wave energy may serve as a possible model for coronal heating [35]. Thus from the above discussion we understand that a thorough understanding of wave breaking (via phase mixing) and the estimation of phase mixing time is a pertinent issue in nonlinear plasma physics and forms a concrete area of research. This area is explicitly explored in this thesis.

In this thesis, by performing analytical calculations and computer simulations, we present a thorough investigation and understanding on the formation, evolution and breaking [5,6] of variety of relativistically intense longitudinal electron plasma oscillations/waves that a homogeneous unmagnetized plasma can support. We restrict our study to the one-dimensional case *i.e.* the variation of physical quantities is only along the  $x$ -direction (direction of propagation). Throughout this thesis ions are considered as positively charged background of infinite mass and hence stationary during the fast time-scale. We start our study from relativistic cold plasma wave breaking via phase mixing and then gradually extend our attention to the relativistic warm plasma wave breaking physics [36–44] by including finite electron temperature.

This thesis is divided into 8 chapters. **Chapter - 1** provides an introduction to the breaking of nonlinear electron plasma oscillations/waves and their importance in context of current research interests. Different nonlinear effects which are the root cause of wave breaking in a cold as well as in a warm plasma are also discussed in this chapter.

**Chapter - 2** describes the simulation techniques that we have used in order to study the breaking of relativistically intense plasma waves. In this thesis, we have mainly used two in-house developed simulation tools *viz.* - Sheet Simulation [30–33]

and Particle-in-Cell (PIC) simulation [45–49]. To study the wave breaking physics in a cold plasma we have used Sheet Simulation code which is based on Dawson Sheet Model [5, 32] and wave breaking in warm plasmas have been studied using one dimensional PIC code.

In **Chapter - 3** we start our investigations by studying the space-time evolution of relativistically intense wave packets specified by their amplitudes ( $\delta$ ) and spectral widths ( $\Delta k$ ) in a cold plasma. Actually, in a typical laser/beam plasma interaction experiment a spectrum of relativistically intense waves with an arbitrary spread in  $\Delta k$  (and hence in phase velocity) is excited because of group velocity dispersion and nonlinear distortion of light pulse near the critical layer [50–53]. Such a wave packet exhibits phase mixing and eventually breaks at arbitrarily small amplitudes. In order to estimate the phase mixing time scale as a function of the amplitude ( $\delta$ ) and dimensionless spectral width ( $\Delta k/k$ ) of this wave packet, we first extend the Sheet Model proposed by Dawson into the relativistic regime and derive the relativistic equation of motion for the oscillating sheets. Then we solve this equation of motion in weakly relativistic limit by using Lindstedt-Poincaré [54] perturbation technique and find that the phase mixing time scale ( $t_{mix}$ ) crucially depends on the ratio of the amplitude of the wave packet ( $\delta$ ) and dimensionless spectral width ( $\Delta k/k$ ) of the wave packet. We further observe that for sharply peaked wave packets i.e  $\Delta k/k > 2\omega_p^2\delta^2/c^2k^2$ ,  $t_{mix}$  scales with  $\delta$  as  $1/\delta^3$  [30], while for broader wave packet i.e for  $\Delta k/k \leq 2\omega_p^2\delta^2/c^2k^2$ ,  $t_{mix}$  scales with  $\delta$  as  $1/\delta^5$ . Then we verify these theoretical results by a using a code based on Dawson Sheet Model discussed in chapter - 2.

Next, in **Chapter - 4** we bring our attention to the breaking of longitudinal Akhiezer - Polovin mode by using Dawson Sheet Model and derive an analytical

expression for the phase mixing time scale of this mode when it is subjected to an arbitrarily small longitudinal perturbation of amplitude  $\delta$ . As a longitudinal Akhiezer-Polovin wave is parametrized in terms of maximum fluid velocity ( $u_m$ , normalized to  $c$ ) and phase velocity ( $\beta_\phi = v_\phi/c$ ), we present analytical expression of phase mixing time as a function of  $u_m$ ,  $\beta_\phi$  and imposed perturbation  $\delta$ . First we construct longitudinal Akhiezer - Polovin travelling wave solutions from relativistic equation of motion of sheets and derive an expression for frequency ( $\omega_{ap}$ ) of a pure ( $\delta = 0$ ) longitudinal Akhiezer - Polovin mode. We observe that the expression for frequency for  $\delta = 0$  does not contain any spatial dependency. This is the reason for the fact that a pure longitudinal Akhiezer - Polovin mode does not exhibit phase mixing. Then we calculate an approximate expression for frequency  $[\Omega_{ap}(per)]$  upto first order in  $\delta$  for perturbed Akhiezer - Polovin mode in weakly relativistic limit. We show that, in this situation( *i.e.* after adding perturbation), the frequency  $[\Omega_{ap}(per)]$  indeed becomes an explicit function of the positions of the electron sheets constituting the wave, which results in wave breaking via phase mixing process. We also observe that as time progresses, density spikes arise in space and the structure eventually breaks in a time scale given by  $\sim \frac{2\pi\beta_\phi}{3\delta} \left[ \frac{1}{u_m^2} - \frac{1}{4} \right]$ . We also verify our analytical findings by Sheet simulation technique.

In **Chapter - 5**, another manifestation of breaking of nonlinear electron plasma oscillations via phase mixing has been observed by changing the geometry of the oscillations (from planar to cylindrical and spherical). Earlier it was mentioned that for nonrelativistic oscillations under planar geometry, the amplitude of the applied perturbation can not be increased beyond a certain value known as wave breaking limit [5,6]. Dawson in his paper [5] extended his nonrelativistic calculations by including geometrical effects. He assumed that the electrons are oscillating back

and forth along the radius either of a cylinder or of a sphere and found that even in nonrelativistic case, oscillations having cylindrical or spherical symmetry always exhibit phase mixing, at arbitrarily small amplitude of the applied perturbation. In this chapter we extend Dawson's earlier work [5] by including relativistic effects. We first derive the expressions for the fluid variables *viz.* electron density ( $n_e$ ), electric field ( $E$ ) and velocity ( $v$ ) by respectively using the principle of conservation of number of particles, Gauss's Law and Newton's Law. It is found that this method of deriving the fluid variables is easier compared to the derivation involving the definition of Lagrange coordinates used by other authors [55, 56]. Then we solve the equation of motion of the sheets in respective coordinate system by using Lindstedt-Poincaré [54] method and derive an expression for frequency of oscillation in the weakly relativistic limit upto third order in amplitude. We find that, for oscillations in cylindrical and spherical geometry, the frequency acquires spatial dependency which ultimately leads to wave breaking via phase mixing process. Analytical expressions for this phase mixing time scale as a function of the amplitude of the applied perturbation ( $\delta$ ) have been derived which show that for relativistic cylindrical and spherical oscillations, phase mixing time scale inversely with the cube of the amplitude of the applied perturbation. We observe that, for nonrelativistic case the phase mixing time scale follows the same scaling law. Inclusion of relativistic effects [55, 56] only hastens the phase mixing time (breaking time). We also verify our analytically obtained scaling law by Sheet Simulation code.

In the space-time evolution of the modes discussed in the previous chapters (chapter -3, 4 and 5), we observe that as time progresses the electron density becomes more and more spiky and eventually breaks via phase mixing. At breaking



point the electron density becomes singular ( $n_e \rightarrow \infty$ ). This singularity is an artefact of cold fluid plasma model. In fact when non-linear density perturbations are excited in a large amplitude plasma wave, thermal effects become important as the electron thermal pressure may not allow the density compression to build up as predicted by the simple cold plasma fluid model and in this situation a warm plasma theory is required.

In 1971, Coffey [36] first investigated the effect of electron temperature on the wave breaking limit for an Electron Plasma Wave in a warm plasma by using a “water-bag” [57] distribution for electrons. Unlike the cold plasma wave breaking which is defined by the crossing of the trajectories of the particles constituting the wave, Coffey defined wave breaking in a warm plasma as the trapping of the background plasma electrons at the upper boundary of the water-bag distribution (which is at electron sound speed  $s_0 = \sqrt{3k_B T_e/m}$ ) by the wave potential. The author also showed that maximum electric field amplitude explicitly depends on the initial electron temperature and decreases monotonically with increasing electron temperature. This limiting amplitude of electron plasma wave is known as Coffey’s limit [36, 39].

In 1988, Katsouleas and Mori [37, 39], extended the calculations carried out by Coffey by including relativistic effects. An analytical expression for the maximum electric field amplitude that can be sustained by a relativistically intense electron plasma wave was derived as a function of electron temperature and phase velocity of the wave in the ultrarelativistic regime, which is defined as  $\gamma_\phi^2 \lambda \gg 1$ , where  $\lambda = 3k_B T_e/mc^2$ . In the same year Rosenzweig [38] presented another expression for maximum electric field amplitude (in the limit  $v_\phi \rightarrow c$ ) as a function of electron temperature. Similar results were derived by Sheng and Meyer-ter-Vehn, using

a different set of equations [40]. Recently Schreoder *et. al.* [41, 42] proposed a new model of relativistic warm fluid theory and presented fundamentally different expressions for wave breaking amplitude in the limits  $\gamma_\phi^2 \lambda \gg 1$  and  $\gamma_\phi^2 \lambda \ll 1$  (laser wake field regime) respectively. Later Trines *et. al.* [43] extended the calculations of Katsouleas & Mori in the regime where  $\gamma_\phi^2 \lambda \ll 1$ . All these theoretical results [37–43] clearly indicate that, thermal effects significantly reduces the wave breaking limit from the cold plasma Akhiezer - Polovin limit. Physically it is expected, because the tendency of plasma density to increase to infinity is opposed by the pressure term and the inclusion of thermal velocity of the particles in the direction of wave propagation (positive  $x$  axis, in our case) enables them to get trapped at lower amplitude.

Considerable efforts have been made in this field over past two decades, mainly focusing on theoretical analysis by assuming the wave like solutions of the relativistic Vlasov-Maxwell's equations. However, there is no consensus on a correct model for studying the breaking of relativistically intense waves in a warm plasma. Therefore, it becomes imperative to conduct a numerical experiment on the space time evolution and breaking of large amplitude relativistically intense electron plasma waves in a warm plasma with a relativistically correct velocity distribution function (Jüttner-Synge distribution) [58].

Here we would like to note that in a cold plasma the phenomenon of wave breaking can be understood in terms of electron orbit crossing (as shown in Chapter -3, 4 and 5). But in a warm plasma the motion of the particles are random. As a result the wave breaking physics in a warm plasma (which includes particle trapping) is different and highly non trivial. Thus, in this situation, in order to enrich our understanding on the warm plasma wave breaking physics, we first study

the space time evolution and breaking of nonrelativistic electron plasma wave, because inclusion of relativistic effects would make the analysis more complex. Therefore in the next chapter we turn our attention to the space-time evolution and breaking of nonrelativistic electron plasma wave in a Maxwellian plasma.

In **Chapter - 6**, by using a 1D Particle-in-Cell (PIC) simulation code (discussed in chapter -2), we investigate the maximum electric field amplitude that can be sustained by a “self-consistent” freely running electron plasma wave (Langmuir wave) in a homogeneous warm plasma where electron’s velocity distribution is a Maxwellian and also study its stability towards a small amplitude longitudinal perturbation. Using a water-bag distribution for electrons, we first derive the initial conditions (initial positions, velocities for all the particles) required to excite a propagating wave in PIC code. In the PIC code, these initial conditions are then loaded along with a Maxwellian distribution. From simulation we observe that Coffey’s propagating wave solution [36], which was derived using a “water-bag” distribution for electrons; also represents a self-consistent propagating wave in a Maxwellian plasma, albeit with a lower amplitude. We show that if the amplitude of the initial perturbation exceeds Coffey’s wave breaking limit, within a few plasma periods the initialized wave self-consistently conforms itself with the background distribution and remains at an amplitude below Coffey’s limit for a large period of time ( $\sim 100$  plasma periods), provided the Landau damping rate is very weak. This final self-consistent wave amplitude does not increase even after increasing the perturbation amplitude and thus can be taken as maximum sustainable electric field amplitude in a Maxwellian plasma. By changing the initial electron temperature, we find that maximum electric field amplitude, that can be sustained by a self-consistent electron plasma wave follows a similar scaling given

by Coffey [36] but with slightly different coefficients.

Lastly in **Chapter - 7** we explore the physics of relativistically intense electron plasma waves in a warm plasma by conducting numerical experiments, using 1D PIC code. In order to study the space time evolution and stability of relativistically intense electron plasma waves towards a small amplitude longitudinal perturbation in a warm plasma, we first load Akhiezer - Polovin [27] type initial conditions in our PIC code. Along with this, we load a finite electron temperature (Jüttner - Synge distribution) on the background. We observe that without any perturbation the resultant structure propagates through the system for a long period of time provided the Relativistic Landau Damping rate [59] is small. We also find that in low amplitude limit it follows the relativistic warm plasma dispersion relation given by Pegoraro *et. al* [60] and many others [59,61–63]. Further it is demonstrated that for the phase velocities less than the velocity of light  $c$ , like cold plasma case in a warm plasma, relativistically intense waves also break via phase mixing at arbitrarily small amplitude when perturbed by a small amplitude longitudinal perturbation. This is far below the existing theoretical results on warm plasma wave breaking available in the literature [37–44]. Variations of phase mixing time for a wide range of input parameters have been studied.

Finally in **Chapter - 8**, we consolidate our work and enumerate the major tasks that can be undertaken for further research in this field.



2.1	Dawson Sheet Model . . . . .	17
2.2	Flow diagram of Particle-in-Cell Method . . . . .	21
3.1	Phase Mixing Time ( $\omega_p \tau_{mix}$ ) as a function of amplitude $\delta$ for $ \Delta k/k  =$ 0.1. . . . .	29
3.2	Phase Mixing Time ( $\omega_p \tau_{mix}$ ) as a function of amplitude $\delta$ for $ \Delta k/k  =$ 0.2. . . . .	30
3.3	Phase Mixing Time ( $\omega_p \tau_{mix}$ ) as a function of amplitude $\delta$ for $ \Delta k/k  =$ 0.5. . . . .	30
3.4	Phase Mixing Time ( $\omega_p \tau_{mix}$ ) as a function of amplitude $\delta$ for $ \Delta k/k  =$ 0. . . . .	31
4.1	Space-time evolution of the electron density (3D up, 2D down) for an Akhiezer - Polovin wave with velocity amplitude $u_m = 0.55$ and $\beta_\phi = 0.9995$ , without perturbation . . . . .	40
4.2	Space-time evolution of the electron density for an Akhiezer - Polovin wave with velocity amplitude $u_m = 0.55$ , $\beta_\phi = 0.9995$ and with per- turbation amplitude $\delta = 0.1$ . . . . .	41
4.3	Fourier spectrum of an Akhiezer - Polovin wave with velocity am- plitude $u_m = 0.55$ , $\beta_\phi = 0.9995$ and with perturbation amplitude $\delta$ $= 0.1$ at different time steps. . . . .	42
4.4	Momentum distribution of an Akhiezer - Polovin wave with velocity amplitude $u_m = 0.55$ , $\beta_\phi = 0.9995$ and with perturbation amplitude $\delta = 0.1$ at different time steps. . . . .	42

4.5	Analytical (solid) and numerical (circles) scalings of the phase mixing time for a finite amplitude Akhiezer - Polovin wave for $u_m = 0.20$ (4.5a), $0.55$ (4.5b) and $\beta_\phi = 0.9995$ as a function of perturbation amplitudes ( $\delta$ ) . . . . .	43
4.6	Analytical (solid) and numerical (circles) scalings of the phase mixing time as a function of the amplitude of Akhiezer - Polovin wave ( $u_m$ ) in the presence of a finite perturbation( $\delta$ ) = $0.01$ (4.6a), $0.1$ (4.6b) and $\beta_\phi = 0.9995$ . . . . .	43
4.7	Analytical (solid) and numerical (circles) scalings of the phase mixing time as a function of the phase velocity $\beta_\phi$ for a fixed amplitude of Akhiezer - Polovin wave $u_m = 0.2$ , $\delta = 0.01$ (4.7a) and $u_m = 0.1$ , $\delta = 0.1$ (4.7b) . . . . .	44
4.8	Analytical (solid) and numerical (circles) scalings of the phase mixing time as a function of the density amplitude of the Akhiezer - Polovin wave ( $\delta n/n_0 \sim \Delta n$ ) in the presence of a finite perturbation ( $\delta$ ) = $0.01$ (4.8a), $0.1$ (4.8b) and $\beta_\phi = 0.9995$ . . . . .	45
5.1	Cross-sectional view of Dawson Sheet Model in Cylindrical and Spherical Coordinates . . . . .	50
5.2	Snapshots of density profile of relativistic cylindrical oscillation at different time steps for amplitude $\Delta = 0.5$ . . . . .	56
5.3	Snapshots of electric field profile of relativistic cylindrical oscillation at different time steps for amplitude $\Delta = 0.5$ . . . . .	57
5.4	Variation of phase mixing time of relativistic cylindrical oscillation as a function of amplitude of applied perturbation $\Delta$ . . . . .	58

5.5	Variation of phase mixing time of nonrelativistic cylindrical oscillation as a function of amplitude of applied perturbation $\Delta$ . . . . .	58
5.6	Snapshots of density profile of relativistic spherical oscillation at different time steps for amplitude $\Delta = 0.5$ . . . . .	60
5.7	Snapshots of electric field profile of relativistic spherical oscillation at different time steps for amplitude $\Delta = 0.5$ . . . . .	60
5.8	Variation of phase mixing time of relativistic spherical oscillation as a function of amplitude of applied perturbation $\Delta$ . . . . .	61
5.9	Variation of phase mixing time of nonrelativistic spherical oscillation as a function of amplitude of applied perturbation $\Delta$ . . . . .	61
6.1	Potential energy vs position diagram . . . . .	70
6.2	Initial profile for $\beta = 0.1$ and $\Delta = 0.98$ . . . . .	72
6.3	Initial profile for $\beta = 0.2$ and $\Delta = 0.3$ . . . . .	73
6.4	Space-time evolution of electric field (3D up, 2D down) for $\beta = 0.1$ and $\Delta = 0.5$ without any perturbation [ $eE_{max}/m\omega_p v_\phi$ at $t = 0$ is below Coffey's limit (0.3155)]. . . . .	75
6.5	Space-time evolution of electric field (3D up, 2D down) for $\beta = 0.1$ and $\Delta = 0.5$ with a small amplitude perturbation [ $eE_{max}/m\omega_p v_\phi$ at $t = 0$ is below Coffey's limit (0.3155)]. . . . .	76
6.6	Space-time evolution of electric field (3D up, 2D down) for $\beta = 0.1$ and $\Delta = 0.98$ without any perturbation [ $eE_{max}/m\omega_p v_\phi$ at $t = 0$ is below Coffey's limit (0.3155)]. . . . .	77
6.7	Space-time evolution of electric field (3D up, 2D down) for $\beta = 0.1$ and $\Delta = 0.98$ with a small amplitude perturbation ( $eE_{max}/m\omega_p v_\phi$ at $t = 0$ is beyond Coffey's limit, 0.3155). . . . .	78



6.8	Snapshots of Fourier spectrum for $\beta = 0.1$ and $\Delta = 0.98$ without any perturbation [ $eE_{max}/m\omega_p v_\phi$ at $t = 0$ is below Coffey's limit (0.3155)]. . . . .	79
6.9	Snapshots of Fourier spectrum for $\beta = 0.1$ and $\Delta = 0.98$ with a small amplitude perturbation ( $eE_{max}/m\omega_p v_\phi$ at $t = 0$ is beyond Coffey's limit, 0.3155). . . . .	80
6.10	Space-time evolution of electric field (3D up, 2D down) for $\beta = 0.15$ and $\Delta = 0.965$ without any perturbation [ $eE_{max}/m\omega_p v_\phi$ at $t = 0$ is below Coffey's limit (0.2510)]. . . . .	81
6.11	Space-time evolution of electric field (3D up, 2D down) for $\beta = 0.15$ and $\Delta = 0.965$ with a small amplitude perturbation [ $eE_{max}/m\omega_p v_\phi$ at $t = 0$ is beyond Coffey's limit (0.2510)]. . . . .	82
6.12	Space-time evolution of electric field (3D up, 2D down) for $\beta = 0.2$ and $\Delta = 0.9455$ without any perturbation [ $eE_{max}/m\omega_p v_\phi$ at $t = 0$ is below Coffey's limit (0.2054)]. . . . .	83
6.13	Space-time evolution of electric field (3D up, 2D down) for $\beta = 0.2$ and $\Delta = 0.9455$ with a small amplitude perturbation ( $eE_{max}/m\omega_p v_\phi$ at $t = 0$ is beyond Coffey's limit, 0.2054). . . . .	84
6.14	$E_{max}$ as a function of $\beta$ . . . . .	85
6.15	Time evolution of electrostatic energy for $\beta = 0.35$ and $\Delta = 0.1$ . . . . .	86
7.1	Wave breaking limit as a function of $\lambda$ in laser wake field regime . . . . .	89
7.2	Wave breaking limit as a function of $\lambda$ in ultrarelativistic regime . . . . .	90
7.3	Time evolution of electrostatic energy at a fixed grid point for $\beta_\phi = 0.5$ , $u_m = 0.1$ , $\lambda = 3$ . . . . .	94

7.4	Parameter domains exhibiting relativistic Landau damping and wave breaking . . . . .	95
7.5	Space-time evolution of electric field for $\beta_\phi = 0.95$ , $u_m = 0.3$ , $\lambda = 5 \times 10^{-4}$ and $\delta = 0.0$ . . . . .	96
7.6	Space-time evolution of electric field for $\beta_\phi = 0.95$ , $u_m = 0.3$ , $\lambda = 10^{-2}$ and $\delta = 0.0$ . . . . .	97
7.7	Time evolution of electric field & density at a fixed grid point for $\beta_\phi = 0.95$ , $u_m = 0.3$ , $\lambda = 5 \times 10^{-4}$ and $\delta = 0.0$ . . . . .	97
7.8	Time evolution of electric field & density at a fixed grid point for $\beta_\phi = 0.95$ , $u_m = 0.3$ , $\lambda = 0.01$ and $\delta = 0.0$ . . . . .	98
7.9	$\Omega$ as a function of $\lambda$ , for $\beta_\phi = 0.95$ , $u_m = 0.10, 0.30$ , $\delta = 0.0$ . . . . .	98
7.10	$\Omega$ as a function of $k$ , for $u_m = 0.10, 0.30$ , $\delta = 0.0$ ( $\lambda$ is taken as 0.5) . . . . .	99
7.11	Space-time evolution of electric field for $\beta_\phi = 0.95$ , $u_m = 0.3$ , $\lambda = 5 \times 10^{-4}$ and $\delta = 0.05$ . . . . .	99
7.12	Space-time evolution of electric field for $\beta_\phi = 0.95$ , $u_m = 0.3$ , $\lambda = 10^{-2}$ and $\delta = 0.01$ . . . . .	100
7.13	Time evolution of electric field & density at a fixed grid point for $\beta_\phi = 0.95$ , $u_m = 0.3$ , $\lambda = 5 \times 10^{-4}$ and $\delta = 0.05$ . . . . .	101
7.14	Time evolution of electric field & density at a fixed grid point for $\beta_\phi = 0.95$ , $u_m = 0.3$ , $\lambda = 10^{-2}$ and $\delta = 0.01$ . . . . .	101
7.15	Frequency of the wave as a function of the position for $\beta_\phi = 0.95$ , $u_m = 0.3$ , $\lambda = 0.01$ and $\delta = 0.0$ . . . . .	102
7.16	Frequency of the wave as a function of the position for $\beta_\phi = 0.95$ , $u_m = 0.3$ , $\lambda = 0.01$ and $\delta = 0.01$ . . . . .	103

7.17	Fourier spectrum of electric field for $\beta_\phi = 0.95$ , $u_m = 0.3$ , $\lambda = 0.01$ and $\delta = 0.0$ (blue), $0.01$ (red) at different time steps . . . . .	104
7.18	Snapshots of phase space for $\beta_\phi = 0.95$ , $u_m = 0.3$ , $\lambda = 0.01$ and $\delta = 0.0$ at different time steps . . . . .	105
7.19	Snapshots of phase space for $\beta_\phi = 0.95$ , $u_m = 0.3$ , $\lambda = 0.01$ and $\delta = 0.01$ at different time steps . . . . .	106
7.20	Phase mixing time as a function of $\delta$ for $\lambda = 5 \times 10^{-3}$ and $10^{-2}$ . . .	107
7.21	Phase mixing time as a function of $\lambda$ for $\delta = 0.01$ and $0.02$ . . . . .	107
8.1	$\Omega/k$ as a function of $\lambda$ , for $\beta_\phi = 0.95$ , $u_m = 0.10, 0.30$ , $\delta = 0.0$ . . .	118
8.2	Space-time evolution of electric field for $\beta_\phi = 0.95$ , $u_m = 0.3$ , $\lambda =$ $0.90$ and $\delta = 0.0$ . . . . .	119
8.3	Snapshots of electron phase space for $\beta_\phi = 0.95$ , $u_m = 0.3$ , $\lambda = 0.90$ and $\delta = 0.0$ at different time steps . . . . .	120
8.4	Space-time evolution of electric field for $\beta_\phi = 0.95$ , $u_m = 0.3$ , $\lambda =$ $0.90$ and $\delta = 0.1$ . . . . .	120
8.5	Snapshots of electron phase space for $\beta_\phi = 0.95$ , $u_m = 0.3$ , $\lambda = 0.90$ and $\delta = 0.1$ at different time steps . . . . .	121

*The expert in anything was  
once a beginner.*

- Helen Hayes

# 1

## Introduction

The entire thesis presents a detailed study on the excitation, space-time evolution and breaking of a variety of longitudinal electron modes that a homogeneous unmagnetized plasma can support. In this chapter we give an overview of nonlinear plasma waves and discuss some basic aspects of wave breaking. At the outset, we introduce “nonlinear plasma waves” and the concept of “wave breaking”. In the next section we present a review of earlier works along the motivation for such studies where we discuss the open problems exist in this field. Finally we end this chapter with an outline of the remaining chapters of this thesis.

### 1.1 Nonlinear Plasma Waves and Wave Breaking (Overview)

Physicists have recognized that 99.999% of all the observable matter in the universe is in the plasma state which implies that plasmas are abundant in the universe. In general, it is thought that plasma is the fourth state of matter in order of solid, liquid, gas and finally plasma. This order is set by the ratio of the kinetic energy of the particles to the inter-particle potential energy. For a solid this ratio is  $\ll 1$ , as the temperature increases this ratio increases significantly. A plasma is an ensemble of charged (electrons and ions) and neutral particles which exhibits collective behaviour governed by the electromagnetic forces. Under equilibrium condition a plasma is macroscopically neutral or quasi-neutral *i.e.* it has an equal mix of electrons and ions (with some neutral particles, depending on the degree

of ionization) which are interacting via long range Coulomb force. Being a highly complex medium plasma can support an assortment of normal modes which are typically known as plasma waves [1–3]. These waves are often distinguished by their characteristic frequencies, the presence or absence of magnetic fields and the plasma temperature. Waves in plasmas can be respectively classified as electromagnetic or electrostatic according to whether or not there is an associated oscillating magnetic field. Under certain conditions, mixed modes can also exist. For plane waves, Faraday’s law of induction implies that an electrostatic wave in plasma must be longitudinal *i.e.* the self-consistent electric field is along the direction of propagation. In an unmagnetized plasma (no external magnetic field) two types of electrostatic normal modes can exist: (i) Electron Plasma Oscillations/Waves and (ii) Ion Acoustic Wave. The dynamics of electron plasma oscillation/wave depends on mass and temperature of the electrons in the plasma, where the ions are assumed to be infinitely massive and hence stationary. On the other side, the characteristics of an ion acoustic mode depends on the ion mass and electron temperature; electrons are assumed to be massless and hence follow the Boltzmann distribution. In response to a given perturbation, the acceleration of the electron will be much greater than that of an ion. For this reason, the characteristic frequency of electron motion is much higher than the ion. The reciprocals of the characteristic electron frequency and of the characteristic ion frequency determine the fast and slow time-scale respectively [4]. Depending on the strength of the applied perturbation (or the driver that excites the oscillation/wave) and pattern of motion (geometry of motion) of the oscillating species a variety of high frequency longitudinal electron modes can be excited in an unmagnetized homogeneous plasma.

The simplest electrostatic mode that describes the characteristics of a plasma is the plasma oscillation [5, 6] which arises when the quasi-neutrality condition of the plasma is disturbed. When the electrons are disturbed from their equilibrium positions, the resulting self-consistent electric field builds up to pull back the electrons in order to restore the quasi-neutrality condition. Because of inertia, the electrons overshoot their equilibrium positions and oscillate around their equilibrium positions with a characteristic frequency known as the plasma frequency which is given by  $\omega_p = \sqrt{4\pi n_0 e^2 / m}$ , where  $n_0$  is the equilibrium density of the electrons and  $e$  &  $m$  respectively are the charge and mass of an electron. Here, the necessary restoring force for oscillation is provided by the self-consistent electric

field generated due to the displacement of the electrons.

The theory of cold plasma oscillation does not take into account the random thermal motion of the electrons. If we let the electrons to have a finite (non-zero) temperature, then the electron pressure acts as a restoring force in addition to the self-consistent electric field and the oscillations propagate with a frequency higher than the cold plasma frequency ( $\omega_p$ ). This was reported first by Bohm & Gross [7] and known as Electron Plasma Wave or Langmuir Wave.

Such space charge oscillations/waves can generate very high electric field within a short distance and under certain conditions the work done by the self-consistent electric field  $E$  of the oscillation/wave over a distance of the order of wavelength ( $\lambda_p$ ) may approach the electron rest mass energy which mathematically can be expressed as *i.e*  $eE\lambda_p \sim mc^2$ . Under such conditions, the electrons quiver with a velocity close to the velocity of light in free space ( $c$ ) and the oscillations/waves are termed as relativistically intense oscillations/waves. Such kind of relativistically intense oscillations/waves are usually generated in laboratories by passing a high intensity laser pulse [8] ( $\sim 10^{18} \text{ Watt/cm}^2$  for a  $1\mu\text{m}$  wavelength laser ) or an ultrarelativistic electron beam pulse through an underdense plasma [9] (0.5 GeV, carrying 1 kA current, focussed to  $3\mu\text{m}$  spot size [30]).

Apart from its great academic interests in nonlinear plasma theory [10–13], the study of such kind of relativistically intense oscillations/waves has received a great deal of attention in a number of systems ranging from laboratory plasmas to astrophysical plasmas [14–16]. For instance, oscillations/waves with relativistic amplitudes are regularly encountered in laser assisted nuclear fusion [17–19] and particle acceleration experiments [8, 20–26]. In laser fusion experiments, an intense laser pulse falls on an overdense plasma and excites plasma waves through mode conversion [19] whereas in particle acceleration experiments, an intense laser/beam pulse propagating through an underdense plasma produces large amplitude wake-field through ponderomotive forces/electrostatic forces [8, 9]. A key feature of such waves is the ability to sustain very high self-consistent electric field within a short distance. As a result when a charged particle comes in resonance with these plasma waves, it perceives a very high DC electric field and gets accelerated to a very high energy within a very short distance [14–16]. The concept of generating energetic particles by trapping them in a large amplitude relativistically intense plasma wave has opened a new era in modern plasma physics. Recent

experiments [14, 16, 20–24, 26] indicate that plasma waves excited in the wake of a laser/beam pulse could generate accelerating gradients of the order of  $100\text{GV}/m$  in plasma-based accelerator experiments - this is as high as 1000 times stronger accelerating field as compared to conventional RF accelerators. Such highly energetic particles are useful in a wide variety of fields, ranging from medicine and biology to high-energy physics experiments. These energetic particles are also desirable for producing a hot spot to initiate ignition in an already compressed pellet for fast ignition applications of laser fusion [19]. But it is also reported by several authors that sometimes these high energetic electrons can prematurely heat the fuel in the capsule and make efficient implosions difficult in compression applications for inertial fusion.

Now, it is natural to expect that, larger the amplitude of the excited plasma wave, greater the acceleration would be. But, one can not increase the amplitude of a plasma oscillation/wave beyond a critical limit - known as “wave breaking limit”, discovered first by J. M. Dawson in 1959 for nonrelativistic cold plasma oscillations (where thermal velocity is negligible with respect to the quiver velocity of the electrons). By treating the electrons as oscillating sheets of charges (hereinafter referred as Dawson Sheet Model) Dawson clearly demonstrated that when the amplitude of a coherent plasma oscillation exceeds the so called “wave breaking limit”, the trajectories of the neighbouring electrons constituting the oscillation start crossing each other and the oscillation breaks within a period. This results in fine scale mixing of various parts of the oscillation which destroys the oscillation/wave.

Even without approaching the “wave breaking limit”, Dawson pictured a novel phenomenon where plasma oscillations start losing its periodicity gradually with time and eventually break at a particular time, provided that the frequency of oscillation for some physical reasons acquires a spatial dependency. This phenomenon is called “phase mixing”. In phase mixing, oscillations/waves break at arbitrarily small initial amplitude far below the corresponding “wave breaking limit”. Due to spatial dependency of the characteristic frequency, neighbouring particles gradually get out of phase and eventually cross causing the wave to break at arbitrarily small initial amplitude. Dawson derived a general expression for phase mixing time scale (wave breaking time) by using a physical reasoning (which is based on out of phase motion of neighbouring oscillators separated by a distance equal to

twice the amplitude of the oscillation/wave) and demonstrated that phase mixing can occur if there is a density inhomogeneity or the geometry of the oscillation changes from planar to cylindrical/spherical. However, later it has been shown by several authors that phase mixing can also take place when the oscillations/ waves become relativistically intense. We discuss all these works in detail in the next section.

## 1.2 Review of earlier works and Motivation

Starting from Dawson's work, which was carried out for a nonrelativistic cold plasma oscillation, we present here all the well-known theoretical and simulation works that has been contributed till date concerning wave breaking in cold and warm plasma theory (nonrelativistic and relativistic) for electron plasma oscillations/waves in an unmagnetized plasma. In order to present the earlier works according to the traditional practice and also for the sake of easy reading we divide this section in following four subsections; which are as follows:

### 1.2.1 Wave breaking in a nonrelativistic cold plasma

As mentioned earlier, the concept of wave breaking of nonlinear plasma oscillations for a cold plasma model was first introduced by Dawson [5]. Later in 1968 Davidson and Schram [6] obtained an exact solution of nonrelativistic cold fluid - Maxwell's equations by using Lagrange coordinates. These authors also demonstrated that if the minima of the normalized initial density crosses 0.5 at any point in space, it would break with in one plasma period. The above conclusion was derived with an initial condition where only a single well defined mode (sinusoidal mode) was excited. However in 2012, Verma *et. al.* [64] figured out that the addition of a very small perturbation to the second harmonic increases the wave breaking amplitude significantly. These results were also verified by particle-in-cell (PIC) simulations. Recently, Diver *et. al.* have derived an iterative analytical form for nonlinear plasma oscillations in a cold plasma from which one can compute the associated maximum density amplitude for a given value of density minimum [65].

Nonrelativistic oscillations can also break gradually via phase mixing if there is a density inhomogeneity (fixed or self-generated) and/or if the pattern of the oscil-



lation changes. The later case has been demonstrated by Dawson [5]. In 1973 Kaw *et. al.* [66] explained the phenomenon of phase mixing as mode coupling where energy gradually goes from longer to shorter and shorter wavelengths. Couple of years later Infeld *et. al.* [67] reported an exact space time dependent solution of nonlinear plasma oscillations in a cold plasma against a fixed ion background and concluded that all initial conditions ultimately lead to wave breaking via phase mixing, which was expected from Dawson's earlier work [5]. In 1999, Sengupta *et. al.* [29] considered the effect of ion motion (self-generated) on the space time evolution of nonlinear plasma oscillations in a cold plasma and found that the oscillations phase mix away at arbitrarily small amplitude of the applied perturbation. These authors [29] also derived an analytical expression for this phase mixing time scale and showed that phase mixing time scale depends on the mass ratio and the amplitude of the applied perturbation.

### 1.2.2 Wave breaking in a relativistic cold plasma

The analytical expression for maximum electric field amplitude that can be sustained by a relativistically intense non-linear wave in a cold plasma was first derived by Akhiezer and Polovin [27], before Dawson introduced the concept of “wave breaking” [5]. Using non-linear, relativistic, cold fluid equations in one dimension, Akhiezer and Polovin showed that, the maximum electric field amplitude ( $E_{max}$ ) that can be sustained by a relativistically intense travelling wave in a cold plasma is given by  $eE_{max}/m\omega_p c = \sqrt{2(\gamma_\phi - 1)}$ , where  $\gamma_\phi = 1/\sqrt{1 - \frac{v_\phi^2}{c^2}}$  is the Lorentz factor associated with the phase velocity  $v_\phi$  of the wave. However this Akhiezer - Polovin limit does not hold for arbitrary initial conditions. In 1976 Drake *et. al.* [68] showed that the inclusion of relativistic mass variation of the electrons create a spatial variation of the local frequency of the wave which leads to wave breaking. In 1989, Infeld and Rowlands [28] presented an exact space - time dependent solution of the relativistic cold plasma fluid- Maxwell equations in Lagrange coordinates [6]. The solution presented by them exhibits explosive behaviour for all initial conditions, except for the one which is needed to excite Akhiezer - Polovin waves. Physically this explosive behaviour arises due to the relativistic electron mass variation which causes the characteristic electron plasma frequency to acquire spatial dependency (as pointed out by Drake *et. al.* [68]), due to which neighbouring electrons gradu-

ally go out of phase and eventually cross causing the wave to break at arbitrarily small initial amplitude via phase mixing. An analytical expression for this phase mixing time scale as a function of the applied perturbation was first reported by Sengupta *et. al.* [30] in 2009. By studying the space-time evolution of two waves, separated by a wavenumber  $\Delta k$ , the authors [30] showed that the phase mixing time scale varies inversely with the cube of the amplitude of the wave (or applied perturbation). These authors [30] also verified their analytical results via computer simulation. However, later we explicitly show that in  $\Delta k \rightarrow 0$  limit, the analytical expression for phase mixing time presented by Sengupta *et. al.* [30] does not hold and requires revisiting. Moreover, in present day laser/beam-plasma acceleration experiments where  $E^2/8\pi nT_e \gg 1$ , it is natural to expect that the exciting mechanism *i.e.* laser, high energetic particle beam, electrical pulse etc. will in general excite a wave packet with energy distributed over several modes. Therefore the estimation of phase mixing time of such wave packets is essential from the point of view of particle acceleration.

The mechanism of wave breaking through gradual phase mixing is not exhibited by a pure Akhiezer - Polovin wave [27]. In fact, longitudinal Akhiezer - Polovin mode is a very special combination of frequency, wavenumber and their harmonics such that they propagate together as a coherent nonlinear structure with a constant phase velocity [32]. However, in 2012 Verma *et. al.* [69] obtained Akhiezer - Polovin wave solution from space time dependent solution of Infeld and Rowlands [28]. Same authors [33], by performing extensive numerical simulation, showed that even a longitudinal Akhiezer - Polovin wave breaks through the gradual process of phase mixing at an amplitude well below its wave breaking limit, when it is subjected to an arbitrarily small amplitude longitudinal perturbation. Recently it has also been observed by Bera *et. al.* [70,71] by performing fluid simulations that the wake wave generated by an ultrarelativistic electron beam in a cold plasma is nothing but longitudinal Akhiezer - Polovin mode which also breaks gradually via phase mixing. Still an analytical expression for the phase mixing time scale of this mode in terms of its parameters is yet to be discovered. Further, in relation to the particle acceleration experiments, it is known that wake waves cannot accelerate particles indefinitely, but give maximum acceleration only up to the dephasing length or dephasing time. It has been recently pointed out that [33] if the phase mixing time (wave breaking time) is shorter than the dephasing time of an electron

in the wake wave, then the maximum energy gain cannot be achieved as the wake wave gets damped because of phase mixing before the dephasing time is reached. Therefore the estimation of phase mixing time of a longitudinal Akhiezer - Polovin mode is very essential for Plasma wake wave acceleration (PWFA) mechanism in order to achieve maximum acceleration.

In addition to this, recently the space-time evolution of relativistically intense cylindrical and spherical waves have been respectively studied by Gorbunov [55] and Bulanov [56]. In the former case [55], the authors observed trajectory crossing of the neighbouring electrons which led to wave breaking via phase mixing. In the latter case [56], the authors observed that after some plasma period, the wave profile changes its direction of propagation which also occurs due to spatial dependency of the characteristic frequency of the wave. This time was termed as “turn-around time” [56]. But an analytical dependence of phase mixing time scale as a function of the applied perturbation for these cases has not been reported anywhere till date and thus forms an uncovered area of research which needs to be explored.

### 1.2.3 Wave breaking in a nonrelativistic warm plasma

In all the above works which we have discussed till now, thermal motions of the electrons were neglected. In 1971, Coffey [36] first showed that the inclusion of electron temperature ( $T_e$ ) significantly reduces the wave breaking limit for an electron plasma wave in a warm plasma. Using a “water-bag” [57] distribution for electrons Coffey [36] derived an analytical expression for the maximum electric field amplitude that can be sustained by an electron plasma wave propagating with a phase velocity  $v_\phi$  which can be written as  $\frac{eE_{max}}{m\omega_p v_\phi} = \left(1 - \frac{8}{3}\beta^{1/4} + 2\beta^{1/2} - \frac{\beta}{3}\right)^{1/2}$ , where  $\beta = \frac{3k_B T_e}{mv_\phi^2}$ ,  $T_e$  is the electron temperature and  $k_B$  is the Boltzmann’s constant. Unlike the cold plasma wave breaking which is defined by the crossing of the trajectories of the particles constituting the oscillation/wave [5], Coffey [36] defined wave breaking in a warm plasma as the trapping of background plasma electrons at the upper boundary of the water-bag distribution (which is at electron sound speed  $s_0 = \sqrt{3k_B T_e/m}$ ) by the wave potential. This limiting electric field amplitude of electron plasma wave is known as Coffey’s limit [36, 39]. Later Infeld and Rowlands [72] presented an exact space-time dependent solution of electron density for

nonlinear oscillations in a warm plasma by using Lagrange coordinates [6]. Later in 1995, Bauer *et. al.* [73] reported the experimental observation of wave breaking of electron plasma wave in a radio frequency afterglow plasma and observed that the onset of wave breaking conforms to the Coffey's wave breaking theory [36]. In 2012, by using 1-D PIC simulation method, Verma *et. al.* [74] have explored the physics beyond the breaking of nonrelativistic cold plasma oscillations [6] in a cold plasma. These authors [74] demonstrated that in contrast to the present understanding, after wave breaking all the initialized energy does not end up as the random kinetic energy of the particles, but some fraction always remains with two oppositely propagating coherent BGK [75] like modes with supporting trapped particle distributions and further demonstrated that the amplitude of this mode follows Coffey's limit [36]. Recently Trines [76] has presented an analytical expression for the maximum electric field amplitude sustained by a nonquasistatic oscillations in a warm plasma.

According to the cold plasma fluid theory, at the wave breaking amplitude, the density becomes singular [5, 6, 30, 33]. But in reality, the tendency of plasma density to increase to infinity at the wave crest is opposed by the plasma pressure and for large amplitude waves some electrons in the vicinity of the phase velocity get trapped by the wave potential and accelerated by the wave. A self-trapped electron is the one that already has initial velocity close to the phase velocity of the wave and thus can see a constant DC electric field for a sufficiently large time and get accelerated to high energies. Untrapped electrons are the slow electrons which move with their thermal speed in addition to taking part in the oscillation/wave. At the wave breaking a large number of electrons are brought into resonance with the wave which leads to a very strong irreversible damping of the wave and efficient acceleration of the electrons. Thus the study of maximum electric field amplitude that can be sustained by an electron plasma wave in a warm plasma is a key parameter of interest to other physicists studying topics in which wavebreaking is of importance.

Here we would like to note that, the verification of Coffey's limit for a resonantly excited wave in an inhomogeneous plasma has been attempted by several authors [77, 78]. These authors [78] observed that some particles get trapped even when there was no wave breaking and concluded that Coffey's limit can not be applied for a resonantly excited wave in an inhomogeneous plasma. However, the

verification of Coffey’s limit for a freely running propagating wave (for which the theoretical limit was derived using a water-bag distribution) in a warm plasma remains uncovered for distributions where all range of velocities exist naturally (Maxwellian). Therefore it will be interesting to study the validity of Coffey’s wave breaking criterion for a Maxwellian plasma over a wide range of initial electron temperature.

### 1.2.4 Wave breaking in a relativistic warm plasma

Finally we have reached to a point where we discuss the effect of finite electron temperature on the wave breaking limit for a relativistically intense wave in a warm plasma. In 1988, Katsouleas and Mori [37, 39], first extended the calculations carried out by Coffey [36] by including relativistic effects. An analytical expression for the maximum electric field amplitude that can be sustained by a relativistically intense electron plasma wave has been derived as a function of electron temperature and Lorentz factor in the ultrarelativistic regime which is defined as  $\gamma_\phi^2 \lambda \gg 1$ , where  $\lambda = 3k_B T_e / mc^2$ . In the same year Rosenzweig [38] presented another expression of maximum electric field amplitude (in the limit  $v_\phi \rightarrow c$ ) as a function of electron temperature. Similar results were derived by Sheng and Meyer-ter-Vehn [40], using a different set of equations [79–81]. Recently Schreoder *et. al.* [41, 42] proposed a new model of relativistic warm fluid theory and presented fundamentally different expressions for wave breaking amplitude in the limits  $\gamma_\phi^2 \lambda \gg 1$  and  $\gamma_\phi^2 \lambda \ll 1$  (laser wake field regime) respectively. Later Trines *et. al.* [43] extended the calculations of Katsouleas & Mori in the regime where  $\gamma_\phi^2 \lambda \ll 1$ .

Here we would like to note that the behaviour of a relativistically intense Langmuir wave (electron plasma wave) in a warm plasma after its breaking regime has been studied by Bulanov *et. al.* [82] and Anna Grassi *et. al.* [83], by carrying out a 2D PIC simulation. The former authors [82] observed that the density distribution in a breaking wave has a typical “peakon” form and behaviour of the wave is similar to the breaking water waves, when a symmetric Stokes profile evolves to a skewed wave [84–86]. The latter authors [83] studied the evolution of phase-space dynamics by using Vlasov simulation method. In addition to the above works, the effect of ion motion on relativistic strong plasma waves in a homogeneous plasma

has been studied by Khachatryan [87] in 1998. It has been shown that the wave breaking field weakly depends on the mass of the ions, but the wavelength changes significantly with the inclusion of ion motion.

The above discussion indicates that several theoretical models have been proposed till date to find the maximum electric field amplitude that can be sustained by a relativistically intense wave in a warm plasma. In addition to this, for relativistic warm plasma case all the theoretical limits [37–43] clearly indicate that, thermal effects significantly reduces the wave breaking limit from the cold plasma Akhiezer - Polovin limit and at  $\lambda \rightarrow 0$  limit, all the results approaches the cold plasma Akhiezer - Polovin limit. Later we will show that (in Chapter - 7) these results leads to different wave breaking limits even for same parameter domain which lead to inconclusive results. Therefore, by carrying out a computer simulation, it is essential to explore the effect of finite electron temperature on the cold plasma Akhiezer - Polovin limit [27] and to verify which of the above limits [37–43] hold in reality for studying the breaking of relativistically intense waves in a warm plasma. In addition to this, it is also very crucial to check whether the above limits hold in the presence of a small amplitude perturbations or do they phase mix like cold plasma Akhiezer - Polovin wave [33], as in a realistic experiment, there will always be some noises associated with the excited wave.

From the above review we understand that, the estimation of phase mixing time and the calculation of maximum electric field amplitude (wave breaking amplitude) that can be sustained by a relativistically intense plasma oscillation/wave in a cold and warm plasma is a topic of fundamental importance from several aspects. This topic is explicitly explored in this thesis.

### 1.3 Scope and outline of this thesis

This thesis explicitly presents a study on the excitation, space-time evolution and breaking (via phase mixing) of a variety of relativistically intense oscillations/waves in a cold and warm plasma which may throw some light on the aforementioned issues discussed in the previous section. From the previous discussions we also understand that, several unsolved issues exist in this field even where ions were taken as rest. Major problems in these areas need to be understood first and explored

explicitly. With this desire, throughout this thesis the ions will be considered as a immobile positively charged background. In this thesis attention has been given to the longitudinal oscillations/waves in 1-D only and we assume that plasma is homogeneous and there is no applied magnetic field. With these comments, we now end this chapter by providing a brief outline of the next chapters.

This thesis is organized as follows: Chapter - 2 describes the simulation techniques that we have used in order to study the breaking of relativistically intense plasma oscillations/waves. In this thesis, we have used two in-house developed simulation tools *viz.* - Sheet Simulation [30–33] and Particle-in-Cell (PIC) simulation [45–49]. To study the wave breaking physics in a cold plasma we have used Sheet Simulation code which is based on Dawson Sheet Model [5, 32] and wave breaking in a warm plasma has been studied using one dimensional PIC code.

In Chapter - 3 we start our investigations by studying the space-time evolution of a relativistically intense wave packet specified by its amplitude ( $\delta$ ) and spectral width ( $\Delta k$ ) in a cold plasma. Such a wave packet exhibits phase mixing and eventually breaks at arbitrarily small amplitudes. We find that the phase mixing time scale ( $t_{mix}$ ) crucially depends on the ratio of the amplitude of the wave packet ( $\delta$ ) and dimensionless spectral width ( $\Delta k/k$ ) of the wave packet. We observe that for sharply peaked wave packets i.e  $\Delta k/k > 2\omega_p^2\delta^2/c^2k^2$ ,  $t_{mix}$  scales with  $\delta$  as  $1/\delta^3$  [?], while for broader wave packet i.e for  $\Delta k/k \leq 2\omega_p^2\delta^2/c^2k^2$ ,  $t_{mix}$  scales with  $\delta$  as  $1/\delta^5$ . Then we verify these results by a using a code based on Dawson Sheet Model.

Next, in Chapter - 4, we shift our attention to the breaking of a special kind of wave *i.e.* longitudinal Akhiezer - Polovin mode by using Dawson Sheet Model and derive an analytical expression for the phase mixing time scale of this mode when it is subjected to an arbitrarily small longitudinal perturbation of amplitude  $\delta$ . As a longitudinal Akhiezer-Polovin wave is parametrized in terms of maximum fluid velocity ( $u_m$ , normalized to  $c$ ) and phase velocity ( $\beta_{ph}$ , normalized to  $c$ ), we present the phase mixing time as a function of  $u_m$ ,  $\beta_\phi$  and imposed perturbation  $\delta$ . We derive that the longitudinal Akhiezer - Polovin wave breaks in a time scale given by  $\sim \frac{2\pi\beta_\phi}{3\delta} \left[ \frac{1}{u_m^2} - \frac{1}{4} \right]$ . We also verify our analytical findings by Sheet simulation technique.

Another manifestation of breaking of nonlinear electron plasma oscillations via phase mixing is observed by changing the geometry or pattern of the oscillation



(from planar to cylindrical and spherical). This has been illustrated in [Chapter - 5](#). In this chapter we extend Dawson’s earlier work [\[5\]](#) by including relativistic effects. Analytical expressions for phase mixing time scales as a function of the amplitude of the applied perturbation ( $\delta$ ) have been derived which indicate that for relativistic cylindrical and spherical oscillations, phase mixing time scales inversely with the cube of the amplitude of the applied perturbation. We observe that, for nonrelativistic case the variation of phase mixing time with the amplitude of the applied perturbation follows the same scaling law. Inclusion of relativistic effects [\[55, 56\]](#) only hastens the phase mixing time but the scaling law remains unchanged. We also verify our analytically obtained scaling law by Sheet Simulation code.

Here we would like to note that in a cold plasma the phenomenon of wave breaking can be understood in terms of electron orbit crossing [\[5, 6, 29–32\]](#). But in a warm plasma the motion of the particles are random. As a result the wave breaking physics in a warm plasma (which includes particle trapping) is different and highly non trivial. Thus, in this situation, in order to enrich our understanding on the warm plasma wave breaking physics, we first study the space time evolution and breaking of nonrelativistic electron plasma wave, because inclusion of relativistic effects would undoubtedly make the analysis more complex. Therefore in the next chapter we turn our attention to the space-time evolution and breaking of nonrelativistic electron plasma wave in a Maxwellian plasma where we verify Coffey’s wave breaking limit [\[36\]](#) for a Maxwellian plasma.

In [Chapter - 6](#), by using a 1D Particle-in-Cell (PIC) simulation code, we numerically investigate the maximum electric field amplitude that can be sustained by a “self-consistent” freely running electron plasma wave (Langmuir wave) in a homogeneous warm plasma where electron’s velocity distribution is a Maxwellian. We also study the stability of this wave towards a small amplitude longitudinal perturbation. From simulation we observe that Coffey’s propagating wave solution [\[36\]](#), which was derived using a “water-bag” distribution for electrons, also represents a self-consistent propagating wave in a Maxwellian plasma albeit with a lower amplitude. We show that if the amplitude of the initial perturbation exceeds Coffey’s wave breaking limit, within a few plasma periods the initialized wave self-consistently conforms itself with the background distribution and remains at an amplitude below Coffey’s limit for a large period of time ( $\sim 100$  plasma periods) provided the Landau damping rate is very weak. This final self-consistent wave



amplitude does not increase even after increasing the perturbation amplitude and thus can be taken as maximum sustainable electric field amplitude. By changing the electron temperature, we find that maximum electric field amplitude that can be sustained by a self-consistent electron plasma wave follows a similar scaling given by Coffey [36] but with slightly different coefficients.

Lastly in Chapter - 7 we explore the effect of electron temperature on the space-time evolution of a relativistically intense electron plasma wave in a warm plasma by conducting numerical experiment using 1D PIC code. In order to study the space time evolution and stability of these waves towards a small amplitude longitudinal perturbation in a warm plasma, we first load Akhiezer - Polovin [27] type initial conditions in our PIC code. Along with this, we load a finite electron temperature (Jüttner-Synge [58]) into the background of the electrons. We first observe that for phase velocities for which  $\gamma_\phi \ll 1 + k_B T_e / mc^2$ , the wave damps within a few plasma period and essentially follows the relativistic Landau Damping rate given by Buti [59]. In the opposite regime we find that the wave propagates through the system for a long period of time and in small amplitude limit essentially follows the relativistic warm plasma dispersion relation [59–63]. Further we demonstrate that for the phase velocities less than the velocity of light  $c$ , like cold plasma case [33], in a warm plasma also relativistically intense waves break via phase mixing at arbitrarily small amplitude when perturbed by a small amplitude longitudinal perturbation. This amplitude is far below the existing theoretical results on warm plasma wave breaking available in the literature [37–44]. Variations of phase mixing time for a wide range of input parameters have been studied. Using our simulation results, we also show that the phase mixing time scale in a warm plasma can be interpreted using Dawson’s formula [5] for phase mixing time for a non-relativistic cold inhomogeneous plasma, which is based on out of phase motion of neighbouring oscillators constituting the wave.

Finally in Chapter - 8, we consolidate our work and enumerate the major tasks that can be undertaken for further research in this field.

*Everyone should learn how to  
code, it teaches you how to  
think.*

- Steve Jobs

# 2

## Overview of Sheet Simulations and Particle-in-Cell Simulations

This chapter gives a brief overview of the simulation techniques used to explore the objectives of this thesis as discussed in Chapter-1.

### 2.1 Why Simulations ?

Though 99.999% of all observable matter in the universe is in the plasma state, still the technologies required to confine and manipulate plasmas in a laboratory are very expensive and sometimes takes a long time to develop. In addition to this, being a highly nonlinear many body system where each particle undergoing electromagnetic interactions with each other, sometimes it is very difficult to study the dynamics of a plasma by analytical approach. Therefore, to study the behaviour of a plasma, one must find a easier way. Modern digital computers are one of the logical weapons to overcome the aforementioned issues. Now a days computer technologies and sophisticated algorithms with prodigious calculating speed are cheap and can be altered far more quickly than a physical equipment. Additionally, in a computer simulation it is very easy to develop certain diagnostics that would be difficult (and sometimes impossible) to install in a physical set up. Thus computer simulations can be utilised as an indispensable tool for exploring the physics as one wishes.

The most common methods of simulating plasmas are so called Particle-in-Cell (PIC) methods [10, 47, 48, 88], Molecular Dynamics (MD) methods [89, 90]

which treat plasmas as a collection of large number of charged particles, fluid simulations [91–93] which treat plasmas as a fluid and Vlasov simulations [48] where one solves the distribution functions in phase space. All the simulation methods are used successfully in studying different plasma physics problems at different spatio-temporal scales: at the smallest scales one can use the Particle-In-Cell method, or Vlasov simulations, while at large scales the MHD (fluid) approach can be applied. At intermediate scales the hybrid methods are often used. Besides the above, there also exists a simulation method which works only for 1-D problems and was introduced by Dawson by treating the electrons as oscillating sheets of charges - hereinafter referred as Sheet Simulation. Here, we first study the sheet simulation method and show that the algorithm of the sheet simulation is very easy to develop which also saves the time of computation. Later we demonstrate that Sheet simulation method have certain limitations which we overcome by using Particle-in-Cell simulation method. Therefore, in our study, we mainly use two in-house developed simulation codes based on two different techniques *viz.* (i) Sheet Simulation and (ii) Particle-in-Cell Simulation.

## 2.2 Brief overview of Sheet Simulations

The method of solving the problems of nonlinear oscillations in a cold plasma by treating electrons as oscillating sheet of charges was first introduced by Dawson [5]. Later this model has been taken up by several authors for solving different problems [30–33, 69] which exhibits the versatility of this model. In the following subsections we first discuss the electrostatic sheet model in planar geometry by including the relativistic mass variation effects and later extend it to cylindrical and spherical geometry [5].

### 2.2.1 Sheet Model in planar geometry

Fig-2.1 shows a schematic of Dawson Sheet Model in planar geometry. According to the sheet model description of a cold plasma, electrons are assumed to be infinite sheets of charges embedded in a cold immobile positive ion background. These sheets are constrained to move only along  $x$  axis. Evolution of any coherent mode can be studied in terms of oscillating motion of these charged sheets about their

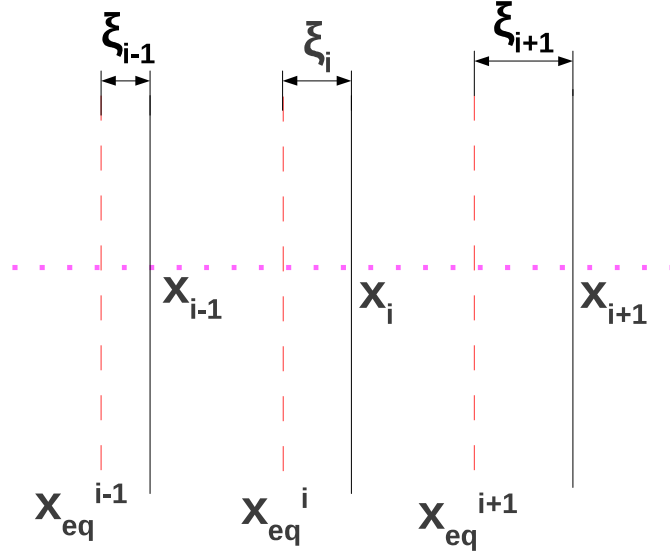


Figure 2.1: Dawson Sheet Model

equilibrium positions. Now following the above figure, let us assume that,  $\xi_i(x_{eq}^i, \tau)$  and  $\xi_{i+1}(x_{eq}^{i+1}, \tau)$  respectively be the displacement of the  $i$ -th and  $(i+1)$ -th electron sheet from their respective equilibrium positions  $x_{eq}^i$  and  $x_{eq}^{i+1}$ . Here,  $x_{eq}$  is the Lagrange coordinate (equilibrium coordinate) of a sheet and  $\tau$  is the Lagrange time, where,  $x = x_{eq} + \xi(x_{eq}, \tau)$  is the Euler position of the sheet and Euler time is given by  $t = \tau$ . Thus, one can easily write

$$\frac{\partial}{\partial x} = \left( \frac{1}{1 + \frac{\partial \xi}{\partial x_{eq}}} \right)^{-1} \frac{\partial}{\partial x_{eq}} \quad (2.1)$$

and

$$\frac{\partial}{\partial \tau} = \frac{\partial}{\partial t} + v \frac{\partial}{\partial x} \quad (2.2)$$

If  $n(x_{eq}, \tau)$  and  $n_0$  respectively represent the instantaneous density and equilibrium density, then from the conservation of the number of particles we can write,

$$n_0 (x_{eq}^{i+1} - x_{eq}^i) = n(x_{eq}, t) (x_{i+1} - x_i) \quad (2.3)$$

$$n(x_{eq}, \tau) = \frac{n_0}{1 + \frac{\xi_{i+1}(x_{eq}^{i+1}, t) - \xi_i(x_{eq}^i, t)}{(x_{eq}^{i+1} - x_{eq}^i)}} \quad (2.4)$$

Eq.(2.4) can be simplified as

$$n(x_{eq}, \tau) = \frac{n_0}{1 + \frac{\partial \xi}{\partial x_{eq}}} \quad (2.5)$$

Now using the Gauss's Law, the expression of the self-consistent electric field becomes

$$E(x_{eq}, \tau) = 4\pi en_0 \xi(x_{eq}, \tau) \quad (2.6)$$

Here we would like to mention that the similar expressions for density and electric field can also be derived from fluid equations by using the transformations given by Eqs.(2.1) and (2.2). Now, the relativistic equation of motion of an oscillating sheet can be written as

$$\frac{d}{d\tau} \frac{m\dot{\xi}}{\sqrt{1 - \frac{\dot{\xi}^2}{c^2}}} = -eE \quad (2.7)$$

Here, the dot sign represents the derivative *w.r.t* time. After putting the expression for electric field the above equation can be simplified as

$$\frac{\ddot{\xi}}{\left(1 - \frac{\dot{\xi}^2}{c^2}\right)^{3/2}} + \omega_p^2 \xi = 0 \quad (2.8)$$

This is the equation for a relativistic harmonic oscillator. Note that, in the non-relativistic limit ( $c \rightarrow \infty$ ) Eq.(2.8) transforms to the well known linear harmonic oscillator equation oscillating with frequency  $\omega_p$ . The above derived expressions for electric field and density can be expressed in terms of Euler coordinates  $(x, t)$  by using the transformations  $x = x_{eq} + \xi(x_{eq}, \tau)$  and  $t = \tau$ . Thus, for any given initial conditions, once the displacement  $\xi$  of a particular sheet is computed as a function of its equilibrium position  $x_{eq}$  and time  $\tau$ , by solving the sheet equation of motion given by Eq.(2.8), the problem of spatio-temporal evolution of the whole system is essentially solved in principle. In sheet simulation we essentially follow the same thing. First for a given set of initial conditions, Eq.(2.8) is solved using 4th order Runge-Kutta scheme. Then density is calculated from expression (2.5) by using the forward difference derivative scheme and electric field can then easily be found from Eq.(2.6) as it is directly proportional to  $\xi$ .

Here, we would like to note that, Eq.(2.8) can also be exactly solved analytically.

In fact, we also present an perturbative solution and an exact analytical solution of Eq.(2.8) in Chapter-3 and 4 respectively. However Sheet simulation method is used here to compare the analytically obtained phase mixing time (which is defined as the crossing of adjacent sheets) scales as to compute that one has to rely either on the weakly relativistic calculations or on the perturbative calculations. Moreover in the next subsection, we note that it is not possible to obtain exact analytical solution of the sheet equation (even nonrelativistic) in cylindrical and spherical geometries. Thus, under those circumstances sheet simulation method is required to study the evolution of a coherent mode.

### 2.2.2 Sheet Model in cylindrical and spherical geometry

From the above subsection, we understand that the algorithm of sheet simulation method is very easy to develop. In fact, it is also very easy to transform the sheet model into cylindrical and spherical geometries from the planar one. Here, we only write down the sheet equations and the expressions of the fluid variables *viz.* density, velocity and electric field in cylindrical and spherical geometries. However, in chapter-5, we give an explicit derivation of the fluid variables as given for planar case.

In cylindrical geometry, the equation of motion of a sheet (by including relativistic mass variation effects) can be written as

$$\frac{\ddot{R}}{(1 - \frac{\dot{R}^2}{c^2})^{3/2}} + \frac{\omega_p^2}{2} \left[ \frac{(r_0 + R)^2 - r_0^2}{(r_0 + R)} \right] = 0 \quad (2.9)$$

Here,  $r_0$  and  $R(r_0, t)$  respectively represent the equilibrium positions and displacement from the equilibrium positions of the electron sheets. So the Euler positions of the sheets can be written as  $r(r_0, t) = r_0 + R(r_0, t)$ .

The expressions for the fluid variables are as follows:

$$n(r_0, t) = \frac{n_0 r_0}{(r_0 + R)(1 + \frac{\partial R}{\partial r_0})} \quad (2.10)$$

$$v(r_0, t) = \dot{R}(r_0, t) \quad (2.11)$$

$$E(r_0, t) = 2\pi e n_0 \left[ \frac{(r_0 + R)^2 - r_0^2}{(r_0 + R)} \right] \quad (2.12)$$

In spherical geometry, the equation of motion of a sheet is given by

$$\frac{\ddot{R}}{(1 - \frac{\dot{R}^2}{c^2})^{3/2}} + \frac{\omega_p^2}{3} \left[ \frac{(r_0 + R)^3 - r_0^3}{(r_0 + R)^2} \right] = 0 \quad (2.13)$$

and the expressions for the fluid variables are

$$n(r_0, t) = \frac{n_0 r_0^2}{(r_0 + R)^2 (1 + \frac{\partial R}{\partial r_0})} \quad (2.14)$$

$$v(r_0, t) = \dot{R}(r_0, t) \quad (2.15)$$

$$E(r_0, t) = \frac{4\pi e n_0}{3} \left[ \frac{(r_0 + R)^3 - r_0^3}{(r_0 + R)^2} \right] \quad (2.16)$$

In contrast to the planar case, here Eq.(2.9) and Eq.(2.13) can not be solved exactly by analytical approach. We will present a perturbative solution of these equations by considering the weakly relativistic limit. In our simulation code, we solve these equations using 4th order Runge-Kutta method and compute the fluid variables for the cylindrical & spherical case by using the set of Eqs.(2.10) - (2.12) and Eqs.(2.14) - (2.16) respectively.

Now it is also worth mentioning that, although the algorithm for sheet simulation is very easy to develop in a modern computer and one can illustrate a number of properties [5, 30–33, 69] of 1-D plasma with this model, but it also has some limitations. As for example, after phase mixing the handling of sheet crossing becomes very complicated in sheet simulations. In a warm plasma there always particle crossing occurs due to the random motion of the particles. Therefore the study of nonlinear waves in a warm plasma by sheet simulations will complicate the picture. As we wish to explore the physics of wave breaking in a warm plasma also, therefore we carry out sheet simulations only for the cold plasma cases (Chapter -3, 4 and 5) and next, for finite temperature cases (Chapter -6 and 7), we use Particle-in-Cell (PIC) simulation method which is more versatile and advanced as compared to the sheet simulation method.

## 2.3 Brief overview of 1-D Particle-in-Cell Simulations

The Particle-in-Cell (PIC) method [10, 48, 88] is extensively used to study the nonlinear physics of classical electron-ion plasmas. A detailed description of a 1-D electrostatic PIC code has been given by Birdsall *et. al.* [48] and by Kruer [10]. Here we provide a very brief overview of this method without going into the details of numerical algorithms that have been used in this program.

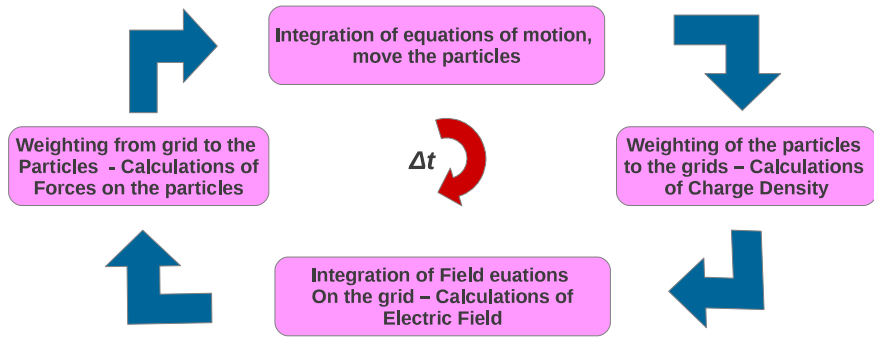


Figure 2.2: Flow diagram of Particle-in-Cell Method

Basically a particle code numerically solves the motions of a collection of charged particles in their self-consistent fields. The program can be summed up as the repetition of four main operations as illustrated in Fig-2.2. Here we simulate a 1-D plasma system; means that the variation of all the physical quantities are allowed only along one direction (here along the  $x$  direction). We assume that the plasma to be infinite in extent and use periodic boundary conditions. The length of the system (say,  $L$ ) is chosen to be equal to the wavelength of the lowest mode under consideration. The whole system is divided into  $NG$  cells of width  $\Delta x = L/NG$  using  $NG+1$  points, known as grid points. These points are taken at the centre of the cells. All the field quantities like electric field, potential, charge density etc. are evaluated at the grid points.

After discretizing the system into cells, particles are then loaded in the phase space according to given input density and velocity perturbations. As by using PIC method, we study the space-time evolution of electron plasma waves in warm



plasmas, a background electron temperature has also been added to the electrons. Velocity distribution with a specific input thermal speed has been loaded randomly in the phase space by using the “inversion of cumulative distributions” method as follows: Let us assume that, the initial velocity distribution is given by  $f_0(v, v_{th})$ , where  $v_{th}$  is the thermal speed. The cumulative distribution function can be written as

$$R_{qr} = F(v_s, v_{th}) = \frac{\int_0^{v_s} f_0(v, v_{th}) dv}{\int_0^\infty f_0(v, v_{th}) dv} \quad (2.17)$$

where  $R_{qr}$  are the quasi random numbers in the range  $-1 \leq R_{qr} \leq 1$ . Thus equating  $F(v_s, v_{th})$  to a quasi random distributions of numbers  $R_{qr}$ , will generate the  $v_s$  corresponding to the distribution  $f_0(v, v_{th})$  and a specific value of  $v_{th}$ . Using the positions and charges of all the particles charge densities are calculated on the grid points by using a weighting scheme. Weighting implies some form of interpolation from the particle positions to the grid points. In our cases, we use Cubic spline weighting scheme.

The next step is to solve the Poisson’s equation on the grids by using the charge on that grid. We use tridiagonal method to calculate the potential [46] and then use central difference scheme to evaluate the electric field on the grids. The program then uses a second weighting scheme (same as the first one) to map the electric field from the grid on to the particles and hence the forces on the particles are calculated.

In the next step, the forces calculated on the particles are used to push the particles to a new position by solving the equation of motion (here, the Newton’s equation of motion). We use the standard leap-frog scheme for this purpose. After this the above cycle is repeated for several time steps (as per the requirements) with a time step small enough to resolve the highest frequency in the problem.

*Mathematics is the language  
in which God has written the  
universe.*

- Galileo Galilei

# 3

## Breaking of Large Amplitude Relativistically Intense Wave Packets in a Cold Plasma

This chapter presents a study on the breaking of a large amplitude relativistically intense wave packet in a cold plasma. By using Dawson Sheet Model, it has been found that the phase mixing time ( $\tau_{mix}$ ) of this wave packet crucially depends on the relative magnitude of the amplitude  $\delta$  and the dimensionless spectral width  $\Delta k/k$  of the wave packet; for  $\Delta k/k \leq 2\omega_p^2\delta^2/c^2k^2$ ,  $\tau_{mix}$  scales with  $\delta$  as  $1/\delta^5$  and for  $\Delta k/k > 2\omega_p^2\delta^2/c^2k^2$ ,  $\tau_{mix}$  scales with  $\delta$  as  $1/\delta^3$ . We have also verified our theoretical results using a simulation code which is based on Dawson Sheet Model.

### 3.1 Introduction

Study of relativistically intense plasma waves and their space-time evolution is an area of intense research in plasma physics because of its application to a broad range of physical problems related to laser plasma interaction, astrophysical plasmas and inertial confinement thermonuclear fusion.

Now, in a typical laser/beam plasma interaction experiment, a spectrum of relativistically intense plasma waves with an arbitrary spread in wave number ( $\Delta k$ , and hence in  $v_\phi$ ) is excited because of group velocity dispersion and nonlinear distortion of light pulse near the critical layer. Moreover, in present day laser/beam-plasma experiments where  $E^2/8\pi nT_e \gg 1$ , it is natural to expect that the exciting

mechanism *i.e.* laser, high energetic particle beam, electrical pulse etc. will in general excite a wave packet with energy distributed over several modes. Such a kind of excitation of wave packets has also been seen in the simulations presented by several authors [50–53, 94]. Therefore, from the viewpoint of experiments and simulations both, it is of utmost importance to study the spatio-temporal evolution of a wave packet, where the initial electrostatic energy is distributed over multiple modes.

Now it is expected that, such an arbitrary wave packet will exhibit phase mixing [5, 28–33, 68] and ultimately break at arbitrarily small amplitude. By studying the space-time evolution of two relativistically intense waves of amplitude  $\delta$  and having wave numbers separated by an amount  $\Delta k$ , authors in Ref. [30] showed that, in general a wave packet having amplitude  $\delta$  and spectral width  $\Delta k$  will phase mix and break in a time scale given by  $\omega_p \tau_{mix} \sim \left\{ \frac{3}{64} (3\omega_p^2 \delta^3 / c^2 k^2) [|\Delta k/k| / (1 + \Delta k/k)] \right\}^{-1} \times (1 + 1/|1 + \Delta k/k|)^{-1}$ . This expression shows that in the limit  $\Delta k/k \rightarrow 0$ ,  $\omega_p \tau_{mix} \rightarrow \infty$  *i.e.* a sinusoidal wave will not undergo phase mixing. This is contrary to present understanding that relativistically intense plasma waves in a cold homogeneous plasma with immobile ions always phase mixes and breaks [28, 68] at an arbitrary low amplitude; except for the case of longitudinal Akhiezer-Polovin mode [27] whose amplitude is limited to  $\frac{eE_{WB}}{m\omega_p c} \sim \sqrt{2}(\gamma_\phi - 1)^{1/2}$  as mentioned in the introduction.

In order to resolve this anomaly, in the present chapter we extend the calculations of ref. [30] and show that phase mixing occurs even in the limit  $\Delta k/k \rightarrow 0$ . In fact, we clearly delineate the regimes where the phase mixing formula presented in Ref. [30] holds.

In Ref. [30], the relativistic equation of motion of an electron was derived using Dawson sheet model [5, 30, 32] and solved in the weakly relativistic limit using Krylov-Bogoliubov method of averaging [95]. The relativistically correct frequency of oscillation was obtained upto second order in wave amplitude “ $\delta$ ”. The expression for frequency thus derived, because of relativistic mass variation effects, clearly exhibits spatial dependency, which is a signature of phase mixing. As noted in the previous paragraph, the spatial dependency in the expression of frequency derived in Ref. [30] vanishes in the limit  $\Delta k/k \rightarrow 0$ , indicating that a sinusoidal wave does not phase mix. To resolve this, in section 3.2 of this chapter, we extend the calculations of Ref. [30] and derive an expression for frequency

correct upto fourth order in oscillation amplitude “ $\delta$ ” using Lindstedt - Poincaré perturbation method [54]. This improved calculation of frequency exhibits spatial dependency even in the limit of  $\Delta k/k \rightarrow 0$ . Using this modified expression of frequency and using Dawson’s argument [5], phase mixing time is estimated, both in small and large  $\Delta k/k$  limit. In section 3.3, we verify the analytically derived scalings of phase mixing time on amplitude “ $\delta$ ” for different values of  $\Delta k/k$ , using numerical simulations based on Dawson sheet model [5, 96] as described in the previous chapter. Finally in section 3.4, we present a summary of this work.

## 3.2 Equation of Motion and its Solution

From Dawson Sheet Model, the relativistic equation of motion of an oscillating sheet, in normalized form, can be written as

$$\frac{\ddot{\xi}}{(1 - \dot{\xi}^2)^{3/2}} + \xi = 0 \quad (3.1)$$

Here, we have used the following normalization:  $\tau \rightarrow \omega_p \tau$ ,  $\xi \rightarrow \frac{\omega_p \xi}{c}$ ,  $\dot{\xi} \rightarrow \frac{\dot{\xi}}{c}$ ,  $E \rightarrow \frac{eE}{m\omega_p c}$ . An exact analytical solution of Eq.(3.1) will be presented in the next chapter. Here, we will solve it in weakly relativistic limit. In weakly relativistic limit, Eq.(3.1) transforms to

$$\ddot{\xi} + \xi - \frac{3}{2}\xi\dot{\xi}^2 + \frac{3}{8}\xi\dot{\xi}^4 \approx 0 \quad (3.2)$$

Now we solve Eq.(3.2) using Lindstedt - Poincaré Preturbation Technique [54] by expanding the displacement  $\xi(x_{eq}, \tau)$  and the oscillation frequency  $\Omega(x_{eq})$  in series as:  $\xi = \xi_0 + \xi_1 + \xi_2 + \dots$  and  $\Omega^2 = 1 + \omega_1^2 + \omega_2^2 + \dots$  [54], where  $x_{eq}$  is the equilibrium positions of the sheets. Initial conditions required to excite a wave packet are [30]

$$n_e(x, 0) = n_0 \left[ 1 + \delta \cos \left( \frac{\Delta k}{2} x \right) \cos \left( k + \frac{\Delta k}{2} \right) x \right] \quad (3.3)$$

and

$$v_e(x, 0) = \frac{\omega_p \delta}{2} \left[ \frac{1}{k} \cos(kx) + \frac{1}{k + \Delta k} \cos(k + \Delta k)x \right] \quad (3.4)$$

The ions are infinitely massive and provide a homogeneous neutralizing background. The zero-th order solution to Eq.(3.2) is  $\xi_0 = \xi(x_{eq})\cos[\Omega t + \phi_0(x_{eq})]$  with  $\xi(x_{eq})$  being the oscillation amplitude.  $\xi(x_{eq})$  and  $\phi_0(x_{eq})$  are respectively given by

$$\xi(x_{eq}) = \frac{\omega_p \delta}{2ck} \left[ 1 + \frac{k^2}{(k + \Delta k)^2} + \frac{2k}{(k + \Delta k)} \cos(\Delta k x_l) \right]^{1/2} \quad (3.5)$$

and

$$\phi_0(x_{eq}) = \tan^{-1} \left\{ \frac{\left[ \frac{\cos(kx_l)}{k} + \frac{\cos(k+\Delta k)x_l}{(k+\Delta k)} \right]}{\left[ \frac{\sin(kx_l)}{k} + \frac{\sin(k+\Delta k)x_l}{(k+\Delta k)} \right]} \right\} \quad (3.6)$$

where  $x_l = x_{eq} + \xi(x_{eq}, 0)$ , the initial position of a sheet at  $\tau = 0$ , after adding the perturbation.

The solution to Eq.(3.2) correct upto  $\xi_1(x_{eq}, \tau)$  can be written as (for complete derivation see Appendix -A)

$$\begin{aligned} \xi(x_{eq}, \tau) = & \xi(x_{eq})\cos(\Omega\tau + \phi_0) + \frac{3\xi(x_{eq})^3}{16}\cos(\Omega\tau + 2\phi_0) \\ & - \frac{\xi(x_{eq})^3}{16}\cos(\Omega\tau - 2\phi_0) - \frac{\xi(x_{eq})^3}{8}\cos 2(\Omega\tau + \phi_0) \end{aligned} \quad (3.7)$$

The frequency  $\Omega(x_{eq})$  is determined from the condition that there are no secular resonant terms in the equations for  $\xi_1, \xi_2, \dots$ . We find that the oscillation frequency correct upto the fourth order of the oscillation amplitude  $\delta$  is given by (for complete derivation see Appendix -A)

$$\begin{aligned} \Omega(x_{eq}) \approx & 1 - \frac{3\omega_p^2 \delta^2}{64c^2} \left[ \frac{1}{k^2} + \frac{1}{(k + \Delta k)^2} + \frac{2\cos(\Delta k x_l)}{k(k + \Delta k)} \right] - \frac{3\omega_p^4 \delta^4}{1024c^4} \times \\ & \left[ 3 \left\{ \frac{\cos(kx_l)}{k} + \frac{\cos(k + \Delta k)x_l}{(k + \Delta k)} \right\}^4 - \left\{ \frac{1}{k^2} + \frac{1}{(k + \Delta k)^2} + \frac{2\cos(\Delta k x_l)}{k(k + \Delta k)} \right\}^2 \right] \end{aligned} \quad (3.8)$$

As derived in the appendic A, here the term  $3 \left\{ \frac{\cos(kx_l)}{k} + \frac{\cos(k + \Delta k)x_l}{(k + \Delta k)} \right\}^4$  comes from the second order correction in the Lindstedt- Poincaré series due to the term  $-(3/2)\xi\dot{\xi}^2$  in Eq.(3.2) and the other term  $\left\{ \frac{1}{k^2} + \frac{1}{(k + \Delta k)^2} + \frac{2\cos(\Delta k x_l)}{k(k + \Delta k)} \right\}^2$  comes from to the first order correction in the Lindstedt- Poincaré series due to the next higher order term in the series expansion of  $\xi(1 - \dot{\xi}^2)^{3/2}$ , which is  $(3/8)\xi\dot{\xi}^4$  in Eq.(3.2).

The expression for frequency clearly shows spatial dependency (dependence on

initial position of the sheet) for arbitrary values of  $\Delta k/k$ . As  $\Delta k/k \rightarrow 0$ , the first correction term becomes independent of sheet positions whereas the second correction term (“ $\delta^4$ ” term) still retains its spatial dependence. Because of this space dependence different “pieces” of the wave packet slowly go out of phase as time progresses, resulting in the phenomenon of phase mixing. Dawson argued that [5] the time required for this phase mixing is roughly the length of time it takes for two neighbouring sheets separated by twice the amplitude of oscillation to become half a period out of phase. Using this argument [5], the general expression for phase mixing time, to lowest order in the amplitude, can be written as

$$\tau_{mix} \sim \frac{\pi}{2} \frac{1}{\xi_{max} \frac{d\Omega(x_{eq})}{dx_{eq}}} \quad (3.9)$$

where  $d\Omega/dx_{eq}$  [calculated from Eq.(3.8)] is given by

$$\begin{aligned} \frac{d\Omega}{dx_{eq}} = \frac{3\omega_p^2 \delta^2}{64c^2} \left\{ \frac{2\sin(\Delta k x_l) \Delta k}{k(k + \Delta k)} \right\} + \frac{36\omega_p^4 \delta^4}{1024c^4} \left\{ \frac{\cos(k x_l)}{k} + \frac{\cos(k + \Delta k) x_l}{(k + \Delta k)} \right\}^3 \\ \times \{ \sin(k x_l) + \sin(k + \Delta k) x_l \} \end{aligned} \quad (3.10)$$

In the above expression the small term of order  $(\delta^2 \Delta k/k)^2$  is neglected. Taking  $\xi_{max} = \frac{\omega_p \delta}{2c} [1/k + 1/(k + \Delta k)]$  [from Eq.(3.3)], calculating the maximum value of  $\frac{d\Omega}{dx_{eq}}$  and putting them in Eq.(3.9), the final expression for phase mixing time ( $\tau_{mix}$ ) stands as

$$\tau_{mix} = \frac{\pi}{2} \left[ \frac{3\omega_p^2 \delta^3}{64c^2 k^2} \left\{ 1 + \frac{1}{(1 + \Delta k/k)} \right\} \right]^{-1} \left[ \frac{\Delta k/k}{1 + \Delta k/k} + \frac{9\sqrt{3}\omega_p^2 \delta^2}{8c^2 k^2} \right]^{-1} \quad (3.11)$$

It is clear from above expression, that for  $\Delta k/k > 2\omega_p^2 \delta^2 / c^2 k^2$ , upto leading order, the phase mixing time is given by

$$\tau_{mix} = \frac{\pi}{2} \left[ \frac{3\omega_p^2 \delta^3}{64c^2 k^2} \left\{ 1 + \frac{1}{(1 + \Delta k/k)} \right\} \left\{ \frac{\Delta k/k}{1 + \Delta k/k} \right\} \right]^{-1} \quad (3.12)$$

This is as same expression as Eq.(19) of Ref. [30]. This shows for  $\Delta k/k > 2\omega_p^2 \delta^2 / c^2 k^2$ ,  $\tau_{mix}$  scales with “ $\delta$ ” as  $1/\delta^3$ . For  $\Delta k/k \leq 2\omega_p^2 \delta^2 / c^2 k^2$ , upto leading

order, the phase mixing time is given by

$$\tau_{mix} = \frac{\pi}{2} \left[ \frac{27\sqrt{3}\omega_p^4\delta^5}{512c^4k^4} \left\{ 1 + \frac{1}{(1 + \Delta k/k)} \right\} \right]^{-1} \quad (3.13)$$

which shows that for broadly spread wave packets (since  $\Delta k$  is small), the phase mixing time  $\tau_{mix}$  scales with “ $\delta$ ” as  $1/\delta^5$ . In the next section, we verify these scalings using a code based on Dawson sheet model [5,30,32,96].

### 3.3 Results from Sheet Simulations

Using a code based on Dawson sheet model (as discussed in chapter 2), in this section we numerically verify the process of phase mixing of a large amplitude longitudinal wave packet, described by it's two parameters, amplitude  $\delta$  and spectral width  $\Delta k/k$ . For this purpose we have used a one - dimensional (1D) sheet code based on Dawson Sheet Model of a 1D plasma. In this code we have followed the motion of an array of  $\sim 10000$  electron sheets. Using initial conditions given by Eqs. (3.3), (3.4) and using periodic boundary conditions, the equation of motion for each sheet is then solved using fourth order Runge-Kutta scheme. Density and electric field have been calculated by using the following expressions  $n(x_{eq}, t) = n_0/(1 + \frac{\partial \xi}{\partial x_{eq}})$  and  $E(x_{eq}, t) = 4\pi en_0\xi$  respectively (as derived in chapter -2).

Moreover, to obtain the exact phase mixing time (wave breaking time), at each computational time step, the ordering of sheets is checked for sheet crossing (electron trajectory crossing) [96]. If the algorithm finds that such a crossing has taken place, it displays the time of crossing and stops running further. Phase mixing time is measured as the time taken by any two adjacent sheets to cross over. We terminate our code at this time because the expression for self-consistent electric field ( $E = 4\pi en_0\xi$ ) used in equation of motion becomes invalid beyond this point [5,30,32,96]. Now we verify the phase mixing time obtained from simulation data with our analytical prediction which has been derived in weakly relativistic limit.

Figs. 3.1 - 3.3 respectively show the dependence of phase mixing time with amplitude  $\delta$  for three different values of  $|\Delta k/k|$ ;  $|\Delta k/k| = 0.1, 0.2$  and  $0.5$ . In all

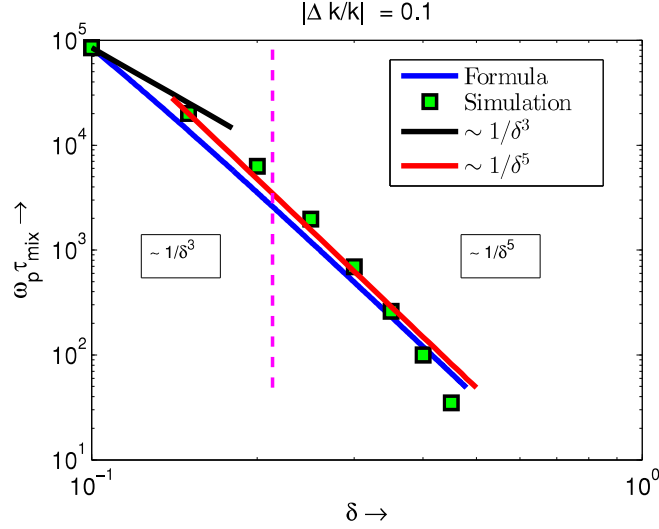


Figure 3.1: Phase Mixing Time ( $\omega_p \tau_{mix}$ ) as a function of amplitude  $\delta$  for  $|\Delta k/k| = 0.1$ .

the figures points represent the simulation results and the blue line is the complete formula given by Eq.(3.11). Comparing figure 3.3 with figure 10 in ref [30], we note that the improved formula [Eq.(3.11)] shows a much better fit to the simulation results. The vertical dashed magenta line separates the two regimes viz.  $\Delta k/k > 2\omega_p^2\delta^2/c^2k^2$  and  $\Delta k/k < 2\omega_p^2\delta^2/c^2k^2$ . In the regime  $\Delta k/k > 2\omega_p^2\delta^2/c^2k^2$ , the dependence of phase mixing time on  $\delta$  is predominantly  $\sim 1/\delta^3$  (black line) whereas the regime  $\Delta k/k \leq 2\omega_p^2\delta^2/c^2k^2$ , the dependence of phase mixing time on  $\delta$  is predominantly  $\sim 1/\delta^5$  (red line). We observe, that as  $|\Delta k/k|$  increases, the vertical dashed line shifts towards the right as expected from theoretical analysis. For sinusoidal case ( $|\Delta k/k| = 0$ ), the phase mixing time scale is given by  $\tau_{mix} = \frac{\pi}{2} \left[ \frac{27\sqrt{3}\omega_p^4\delta^5}{256c^4k^4} \right]^{-1}$ , obtained by putting  $|\Delta k/k| = 0$  in Eq.(3.13). In Fig.3.4 we have shown the variation of phase mixing time scale as a function of  $\delta$  for  $|\Delta k/k| = 0$ . Here the points are simulation results and the continuous line represents the scaling obtained from Eq.(3.13). In this case phase mixing time scale is always proportional to  $1/\delta^5$ . In all the cases shown above, the analytical expressions presented by Eqs.(3.11) and (3.13) are showing a good fit to the observed numerical results, thus vindicating our analytical results.



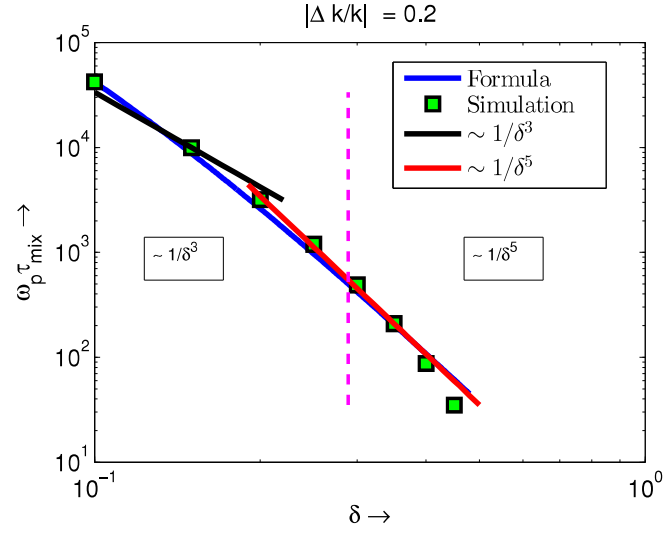


Figure 3.2: Phase Mixing Time ( $\omega_p \tau_{mix}$ ) as a function of amplitude  $\delta$  for  $|\Delta k/k| = 0.2$ .

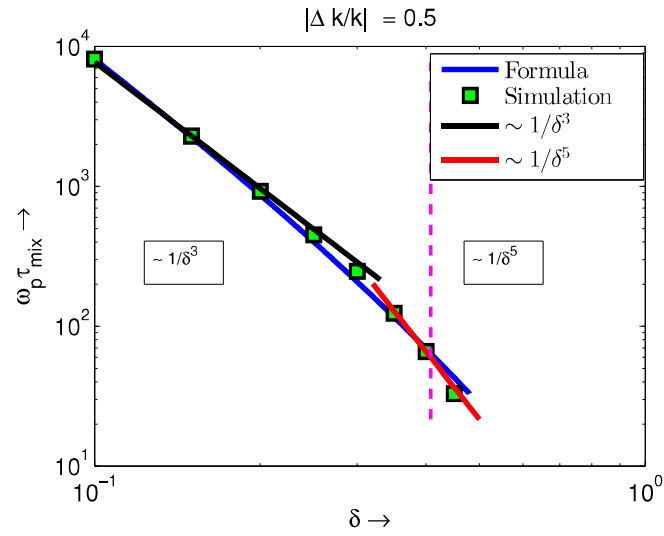


Figure 3.3: Phase Mixing Time ( $\omega_p \tau_{mix}$ ) as a function of amplitude  $\delta$  for  $|\Delta k/k| = 0.5$ .

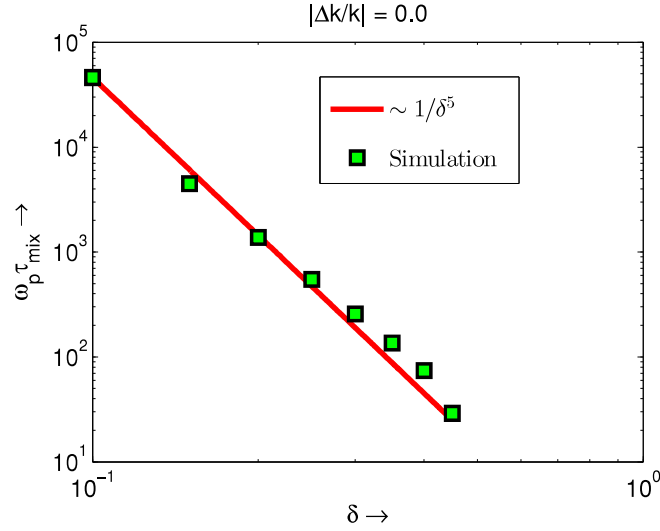


Figure 3.4: Phase Mixing Time ( $\omega_p \tau_{mix}$ ) as a function of amplitude  $\delta$  for  $|\Delta k/k| = 0$ .

### 3.4 Summary

The breaking of relativistically intense longitudinal wave packets in a cold plasma has been studied. It is shown that the phase mixing time scale  $\tau_{mix}$  crucially depends on the relative magnitude of the amplitude of the wave packet  $\delta$  and dimensionless spectral width of the wave packet  $|\Delta k/k|$ . It is found that, for broadly spread wave packets i.e for  $\Delta k/k \leq 2\omega_p^2 \delta^2 / c^2 k^2$ ,  $\tau_{mix}$  scales with  $\delta$  as  $1/\delta^5$ . For a sharply peaked wave packet i.e for  $\Delta k/k > 2\omega_p^2 \delta^2 / c^2 k^2$ ,  $\tau_{mix}$  scales with  $\delta$  as  $1/\delta^3$ .



*Everything is theoretically  
impossible, until it is done.*

- Robert A. Heinlein

# 4

## Analytical Estimate of Phase Mixing Time of Longitudinal Akhiezer - Polovin Wave

This chapter presents a study on the breaking of a very special kind of wave - the Akhiezer - Polovin mode [27]. It is mentioned in chapter -1, that a longitudinal Akhiezer - Polovin mode have a very special combination of frequency, wave-number and their harmonics such that they propagate together as a coherent nonlinear structure with a constant phase velocity. The electric field amplitude of this wave is limited by the wave breaking limit given by  $\frac{eE_{WB}}{m\omega_p c} = \sqrt{2}(\gamma_\phi - 1)^{1/2}$ . In this chapter, it has been shown that, a longitudinal Akhiezer - Polovin mode can break via the process of phase mixing at an amplitude which is far below its wave breaking limit, when it is perturbed by a small amplitude longitudinal perturbation [33]. Using Dawson Sheet Model [5, 32], an analytical expression for the phase mixing time has been derived. It has been found that, the phase mixing time scales with maximum fluid velocity ( $u_m$ ) and phase velocity ( $\beta_\phi$ ) as  $\omega_p \tau_{mix} \sim \frac{2\pi\beta_\phi}{3\delta} \left[ \frac{1}{u_m^2} - \frac{1}{4} \right]$ ; where  $\delta$  is the amplitude of the applied velocity perturbation (here  $u_m$ ,  $\beta_\phi$  and  $\delta$  all are normalized to the velocity of light  $c$ ). This numerical dependence of phase mixing time on  $u_m$ ,  $\beta_\phi$  and  $\delta$  has been verified using a code based on Dawson Sheet Model [96].

## 4.1 Introduction

In 1956, Akhiezer and Polovin [27] obtained an exact one-dimensional longitudinal travelling wave solution in a cold plasma, including relativistic mass effects of electrons. The authors [27] demonstrated that the maximum electric field amplitude ( $E_{WB}$ ) that can be sustained by this wave is limited by the wave breaking limit which is given by  $\frac{eE_{WB}}{m\omega_p c} = \sqrt{2}(\gamma_\phi - 1)^{1/2}$  [11]. However this Akhiezer-Polovin limit does not hold for arbitrary initial conditions. In 1989, Infeld and Rowlands [28] presented an exact space - time dependent solution of the relativistic cold plasma fluid- Maxwell equations in Lagrange coordinates [3,6]. The solution presented by them [28] shows explosive behaviour for all initial conditions except for the one which are needed to excite Akhiezer - Polovin waves. Physically, this explosive behaviour arises due to relativistic variation of electron mass [68], which causes the characteristic electron plasma frequency to acquire a spatial dependency. Due to this neighbouring electrons gradually move out of phase and eventually cross, causing the wave to break, a phenomenon known as phase mixing [29–33]. This process of wave breaking through gradual phase mixing is not exhibited by a pure Akhiezer - Polovin wave.

Recently Verma *et al.* [69] constructed a longitudinal Akhiezer - Polovin travelling wave solution from the exact space time dependent solution of Infeld and Rowlands [28], using appropriate choice of initial conditions. It was further shown by the same authors [33], by performing extensive numerical simulations [96], that even a longitudinal Akhiezer - Polovin wave breaks through the gradual process of phase mixing at an amplitude well below its wave breaking limit, when it is subjected to arbitrarily small longitudinal perturbations. It was observed through simulations that phase mixing time decreases with increasing  $u_m$ ( for a fixed  $\delta$  ) and increasing  $\delta$ ( for a fixed  $u_m$  ), where  $u_m$  and  $\delta$  are respectively the maximum fluid velocity of the Akhiezer - Polovin wave and the amplitude of the applied perturbation.

In this chapter we present a weakly relativistic calculation which analytically brings out the dependence of phase mixing time of a longitudinal Akhiezer - Polovin mode on it's parameters and the amplitude of velocity perturbation  $\delta$ . We further verify the analytically obtained scaling numerically, using a code based on Dawson sheet model [30,32,33,96].

In section 4.2, we construct a longitudinal Akhiezer - Polovin travelling wave solution using Dawson Sheet Model [32, 69]. Section 4.3 is devoted to weakly relativistic calculations which are required for an estimation of phase mixing time of longitudinal Akhiezer - Polovin wave subjected to a small amplitude sinusoidal perturbation. In section 4.4 analytical predictions are compared with numerical findings. Finally section 4.5 contains a discussion and a summary of this work.

## 4.2 Relativistic Travelling Wave Solution

Like the previous problem, here also we use the same normalisations and start from the relativistic equation of motion of an oscillating sheet which is given by,

$$\frac{\ddot{\xi}}{(1 - \dot{\xi}^2)^{3/2}} + \xi = 0 \quad (4.1)$$

In the previous chapter we have given a perturbative solution of Eq.(4.1). Here we give an exact analytical solution of the above equation in the following way : Multiplying Eq.(4.1) by  $\dot{\xi}$ , we get

$$\frac{1}{(1 - \dot{\xi}^2)^{1/2}} + \frac{\xi^2}{2} = a(x_{eq}) \quad (4.2)$$

Here “ $a(x_{eq})$ ” corresponds to the total energy of a sheet. Substituting

$$\xi = \sqrt{2(a - 1)} \sin \alpha \quad (4.3)$$

in Eq.(4.2), solution of Eq.(4.3) becomes

$$\tau = \frac{2}{r'} E(\alpha, r) - r' F(\alpha, r) + \Phi(x_{eq}) \quad (4.4)$$

which gives  $\alpha$  as an implicit function of  $\tau$  and  $x_{eq}$ , where  $r = [(a - 1)/(a + 1)]^{1/2}$  and  $r' = \sqrt{1 - r^2}$ .  $E(\alpha, r)$  and  $F(\alpha, r)$  are incomplete elliptic integrals of second and first kind [97] respectively and  $\phi(x_{eq})$  is an integration constant. Eq.(4.3) along with Eq.(4.4) describes the motion of an electron sheet about its equilibrium position for a given set of initial conditions  $\Phi(x_{eq})$  and  $r(x_{eq})$ . Frequency  $\Omega$  of

an electron sheet is obtained by integrating Eq.(4.2) between two turning points ( $\dot{\xi} = 0$ ) and is given by

$$\Omega = \frac{\pi}{2} \frac{r'}{[2E(r) - r'K(r)]} \quad (4.5)$$

where  $E(r)$  and  $K(r)$  are complete elliptic integrals of second and first kind [97] respectively. It is evident from Eq.(4.5) that for arbitrary set of initial conditions, “ $\Omega$ ” is in general a function of “ $x_{eq}$ ”. Since any coherent mode is made up of a large number of electron sheets oscillating about their equilibrium positions, this spatial dependency of  $\Omega$  causes the neighbouring electron sheets to gradually go out of phase with time [5, 30–32, 68], which eventually leads to crossing of electron sheet trajectories resulting in singularities in the electron density profile. This is the phenomenon of phase mixing leading to wave breaking [5, 28–32, 68]. For a sinusoidal initial density profile and for wave like initial conditions, the phenomenon of phase mixing leading to wave breaking is convincingly demonstrated in the previous chapter and in references [28, 30, 31, 68].

As stated in the previous section, in Ref. [69] it is shown that it is possible to choose a special set of initial conditions which excites a propagating solution with phase velocity  $\beta_\phi$ , which does not phase mix and break. This propagating solution is nothing but a longitudinal Akhiezer - Polovin wave [27]. Absence of phase mixing implies, from Eq.(4.5), that “ $a$ ”(energy of an oscillating sheet) should be independent of “ $x_{eq}$ ” and propagation with a fixed phase velocity  $\beta_\phi$  fixes the functional form of  $\Phi(x_{eq})$  as  $\Phi(x_{eq}) = x_{eq}/\beta_\phi$ . This form of  $\Phi(x_{eq})$  is obtained by choosing  $\xi$  ( hence  $\alpha$  ) to be entirely a function of  $\psi = \Omega(t - x/\beta_\phi)$ . Thus the initial conditions for exciting a longitudinal Akhiezer - Polovin wave are

$$\xi_{ap}(x_{eq}, 0) = \frac{2r}{r'} \sin \alpha \quad (4.6)$$

$$\dot{\xi}_{ap}(x_{eq}, 0) = \frac{2r \cos \alpha \sqrt{1 - r^2 \sin^2 \alpha}}{r'^2 \left( 1 + \frac{2r^2}{r'^2} \cos^2 \alpha \right)} \quad (4.7)$$

along with  $\alpha(x_{eq}, 0)$  implicitly given by

$$\frac{2}{r'} E(\alpha, r) - r' F(\alpha, r) = -\frac{x_{eq}}{\beta_\phi} \quad (4.8)$$

Following Akhiezer - Polovin’s work [27], we now choose  $u_m$ (maximum fluid veloc-

ity) and  $\beta_\phi$  as independent parameters instead of  $a$ (or  $r$ ) and  $\beta_\phi$ .  $a$  and  $u_m$  are related to each other through Eq.(4.1) and Eq.(4.2) as  $a = 1/\sqrt{1-u_m^2}$ . In the next section we add a small perturbation to  $\xi_{ap}(x_{eq}, 0)$  and  $\dot{\xi}_{ap}(x_{eq}, 0)$  which leads to phase mixing and subsequent breaking of longitudinal Akhiezer - Polovin wave.

### 4.3 Estimation of Phase Mixing Time

Adding a small amplitude sinusoidal perturbation with velocity amplitude  $\delta$  and wavelength  $k_{ap}$  (same as the longitudinal Akhiezer - Polovin wave) to  $\xi_{ap}$  and  $\dot{\xi}_{ap}$ , we get

$$\xi_{per} = \xi_{ap} - \frac{\delta}{\omega_{ap}} \sin(k_{ap}x_{eq}) \quad (4.9)$$

$$\dot{\xi}_{per} = \dot{\xi}_{ap} + \delta \cos(k_{ap}x_{eq}) \quad (4.10)$$

where  $\xi_{ap}$  and  $\dot{\xi}_{ap}$  are the required initial conditions for exciting a longitudinal Akhiezer-Polovin wave [69] and  $\xi_{per}$ ,  $\dot{\xi}_{per}$  are the initial conditions after adding the perturbation. Here  $\omega_{ap}$  is the frequency (normalized to nonrelativistic plasma frequency  $\omega_p$ ) of the Akhiezer - Polovin wave. The perturbed initial conditions are equivalent to adding a small amplitude sinusoidal density perturbation propagating with phase velocity  $\beta_\phi$ , to longitudinal Akhiezer - Polovin wave. In the weakly relativistic limit, keeping terms linear in  $\delta$ , the energy associated with an electron sheet becomes

$$a_{per} \approx a + \left[ -\frac{\xi_{ap}\delta}{\omega_{ap}} \sin(k_{ap}x_{eq}) + \delta \dot{\xi}_{ap} \cos(k_{ap}x_{eq}) \right] \quad (4.11)$$

where  $a \approx 1 + \xi^2/2 + \dot{\xi}^2/2$ . This in turn gives

$$r_{per}^2 = \frac{a_{per} - 1}{a_{per} + 1} \approx r^2 - \frac{2r^2}{a^2 - 1} \delta \left[ \frac{\xi_{ap}}{\omega_{ap}} \sin(k_{ap}x_{eq}) - \dot{\xi}_{ap} \cos(k_{ap}x_{eq}) \right] \quad (4.12)$$

Now using Eq.(4.5), and expanding the complete elliptic integrals upto order  $\sim r_{per}^2$ , the frequency of oscillation in the perturbed case can be approximately written as

$$\omega_{per} \approx 1 - \frac{3r_{per}^2}{4} \quad (4.13)$$



Finally substituting  $r_{per}^2$  in the above equation, the frequency of oscillation in the weakly relativistic limit stands as

$$\omega_{per} \approx 1 - \frac{3r^2}{4} + \frac{3r^2}{2(a^2 - 1)} \delta \left[ \frac{\xi_{ap}}{\omega_{ap}} \sin(k_{ap}x_{eq}) - \dot{\xi}_{ap} \cos(k_{ap}x_{eq}) \right] \quad (4.14)$$

It is clear from the above expression that the frequency of the wave is dependent on the equilibrium position of the electrons which leads to the phenomena of phase mixing as shown in Ref. ([33]). Following Dawson's argument [5], the phase mixing time ( $\tau_{mix}$ ) depends on the spatial derivative of frequency as  $\tau_{mix} \approx \pi/2\xi_{max}(d\omega_{per}/dx_{eq})$ . Differentiating Eq.(4.14) w.r.t  $x_{eq}$  we get

$$\begin{aligned} \frac{d\omega_{per}}{dx_{eq}} = & \frac{3r^2}{2(a^2 - 1)} \delta \left[ \frac{1}{\omega_{ap}} \frac{d\xi_{ap}}{dx_{eq}} \sin(k_{ap}x_{eq}) - \frac{d\dot{\xi}_{ap}}{dx_{eq}} \cos(k_{ap}x_{eq}) \right] \\ & + \frac{3r^2}{2(a^2 - 1)} \delta \left[ \frac{\xi_{ap}}{\beta_{\phi}} \cos(k_{ap}x_{eq}) + k_{ap}\dot{\xi}_{ap} \sin(k_{ap}x_{eq}) \right] \end{aligned} \quad (4.15)$$

Now respectively using Eqs.(4.6), (4.7), the derivatives  $d\xi_{ap}/dx_{eq}$ ,  $d\dot{\xi}_{ap}/dx_{eq}$  become

$$\frac{d\xi_{ap}}{dx_{eq}} = \frac{2r}{r'} \cos \alpha \frac{d\alpha}{dx_{eq}} \quad (4.16)$$

$$\frac{d\dot{\xi}_{ap}}{dx_{eq}} = -\frac{2r}{r'} \sin \alpha \frac{(1 - r^2 \sin^2 \alpha)^{1/2}}{(1 + \frac{2r^2}{r'^2} \cos^2 \alpha)} \frac{d\alpha}{dx_{eq}} \left[ 1 + \frac{r^2 \cos^2 \alpha}{(1 - r^2 \sin^2 \alpha)} - \frac{4r^2}{r'^2} \frac{\cos^2 \alpha}{(1 + \frac{2r^2}{r'^2} \cos^2 \alpha)^2} \right] \quad (4.17)$$

The derivative  $d\alpha/dx_{eq}$  can be calculated by using Eq.(4.8)

$$\frac{d\alpha}{dx_{eq}} = \frac{\beta_{\phi}^{-1}}{\left\{ \frac{r'}{(1 - r^2 \sin^2 \alpha)^{1/2}} - \frac{2}{r'} (1 - r^2 \sin^2 \alpha)^{1/2} \right\}} \quad (4.18)$$

Now, using Eqs.(4.16), (4.17) and (4.18) in Eq.(4.15), the maximum value of  $d\omega_{per}/dx_{eq}$  (at  $\alpha \sim \pi/2$ ) can be written as

$$\frac{d\omega_{per}}{dx_{eq}} \approx \frac{6\delta}{\beta_{\phi}} \frac{r^3}{r'} \frac{1}{a^2 - 1} \quad (4.19)$$

Finally substituting the above expression in Dawson formula and using  $\xi_{max} = 2r/r'$  in Eq.(4.19), (at  $\alpha \sim \pi/2$ ), the formula for phase mixing time ( $\tau_{mix}$ ), correct

upto order  $\sim u_m^2$ , stands as,

$$\tau_{mix} \approx \frac{2\pi\beta_\phi}{3\delta} \left[ \frac{1}{u_m^2} - \frac{1}{4} \right] \quad (4.20)$$

It is clear from the above expression that phase mixing time scales directly with  $\beta_\phi$ , inversely with  $\delta$  and has a  $u_m^{-2}$  dependence on  $u_m$ .

In the next section we verify these predictions numerically using Dawson sheet simulation.

## 4.4 Results from Sheet Simulations

Using a code based on Dawson sheet model (as described in chapter -2), in this section we numerically verify the process of phase mixing of a large amplitude Akhiezer - Polovin wave perturbed by a small amplitude sinusoidal perturbation. We first load Akhiezer - Polovin type initial conditions with a sinusoidal perturbation of velocity amplitude  $\delta$  in a one-dimensional relativistic sheet code [30,32,33,96] containing  $\sim 10000$  electron sheets. Using these initial conditions and using periodic boundary conditions, the equation of motion for each sheet is then solved using fourth order Runge-Kutta scheme. At each time step, ordering of sheets is checked for sheet crossing (electron trajectory crossing). Phase mixing time is measured as the time taken by any two adjacent sheets to cross over as mentioned in the previous chapter.

Figs 4.1 and 4.2 respectively show the space time evolution of the electron density profile of an Akhiezer - Polovin wave without and with perturbation. From Fig-4.2 we observe that as time progresses, the density profile becomes more and more spiky as energy is irreversibly transferred to higher and higher harmonics. Due to longitudinal perturbation, the energy which was initially loaded on the Akhiezer - Polovin mode goes to higher harmonics, then partially returns to the original mode, again goes to higher harmonics and so on. This partial back-and-forth sloshing of energy between different harmonics eventually results in accumulation of energy at higher harmonics. But such phenomenon does not occur in Fig-4.1 (without perturbation) and the amplitude does not change even after several plasma periods. A manifestation of this process is also seen in the Fourier

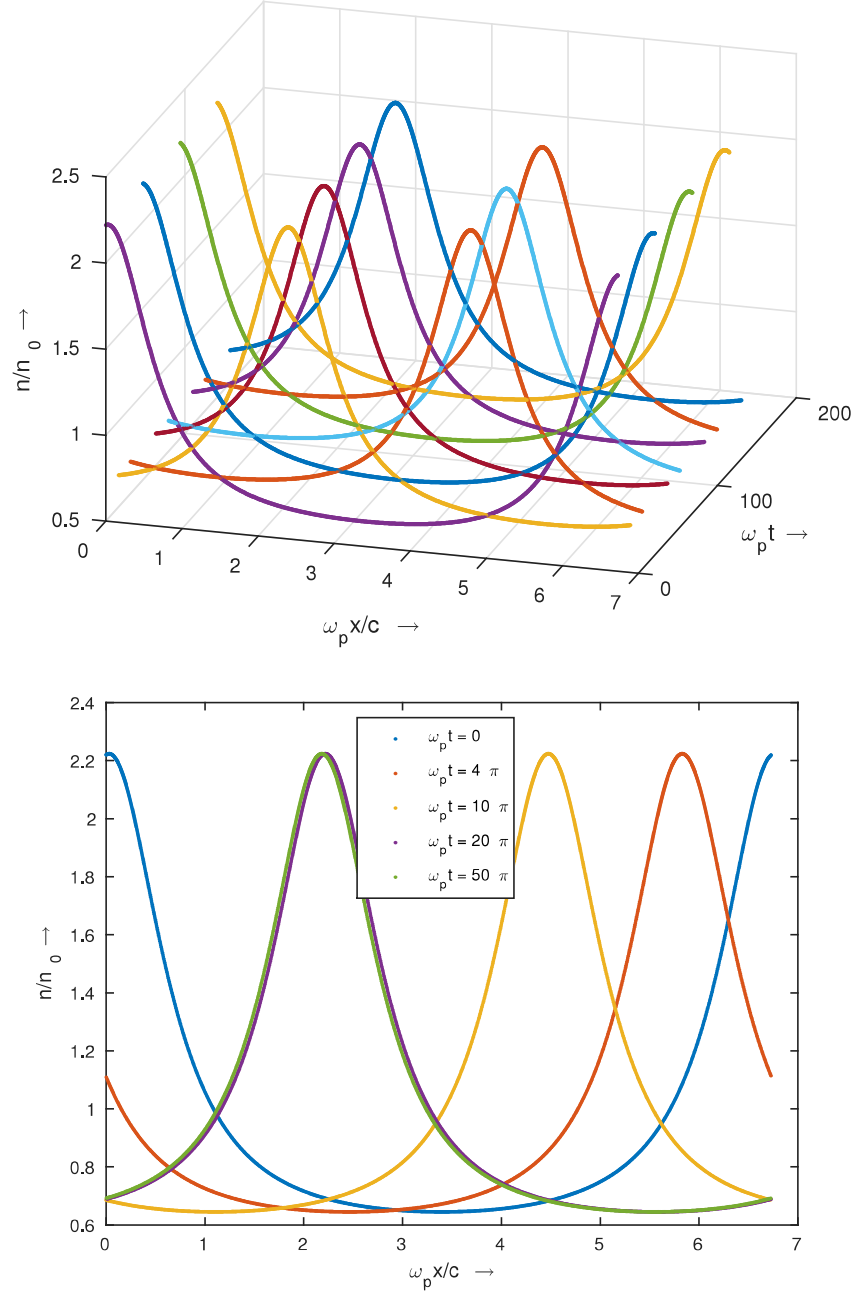


Figure 4.1: Space-time evolution of the electron density (3D up, 2D down) for an Akhiezer  
- Polovin wave with velocity amplitude  $u_m = 0.55$  and  $\beta_\phi = 0.9995$ , without perturbation

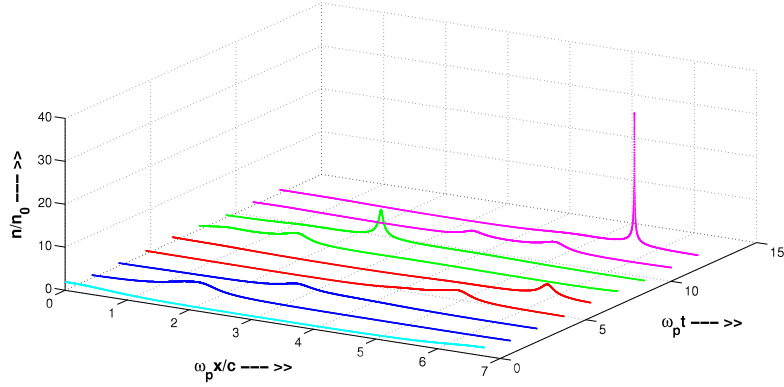


Figure 4.2: Space-time evolution of the electron density for an Akhiezer - Polovin wave with velocity amplitude  $u_m = 0.55$ ,  $\beta_\phi = 0.9995$  and with perturbation amplitude  $\delta = 0.1$

spectrum where we see a broadening of the spectrum as time progresses (Fig-4.3, here the  $k_L$  is the mode number corresponding to longest wavelength supported by the simulation box size). Thus the energy which was loaded in the primary mode eventually distributes over higher modes. Interaction of these high “ $k$ ” modes with the particles (sheets) accelerates the particles, causing the initial delta-function momentum distribution to spread. Fig-4.4 shows that as time progresses, the momentum distribution function gradually spreads generating multi-stream flow; a clear indication of phase mixing leading to breaking. Figures. 4.5 - 4.7 respectively show the variation of phase mixing time with respect to  $\delta$ ,  $u_m$  and  $\beta_\phi$  for fixed values of the other two parameters. In all the cases points represent the simulation results and the solid line represents our scaling obtained from Eq.(4.20).

We note here that our analytical expression for phase mixing time has been derived in the limit of weak relativistic effects. As a result we have kept terms which are linear in  $\delta$  and in addition have neglected terms which are of order higher than  $u_m^2$ . Thus the expression for phase mixing time is approximate in  $\delta$  and  $u_m$ , but exact in  $\beta_\phi$ . Therefore the numerical results in Fig. 4.5 (variation of  $\tau_{mix}$  with  $\delta$ ) for small values of  $\delta$  (upto  $\sim 0.12$ ) and in Fig. 4.7 (variation of  $\tau_{mix}$  with  $\beta_\phi$ ) fit the analytical expression quite well, whereas the numerical result in Fig. 4.6 matches the analytical expression reasonably upto  $u_m \sim 0.4$ . Hence in all the cases, the analytical expression [Eq.(4.20)] shows a reasonably good fit to the observed numerical results, thus vindicating our weakly relativistic calculation.

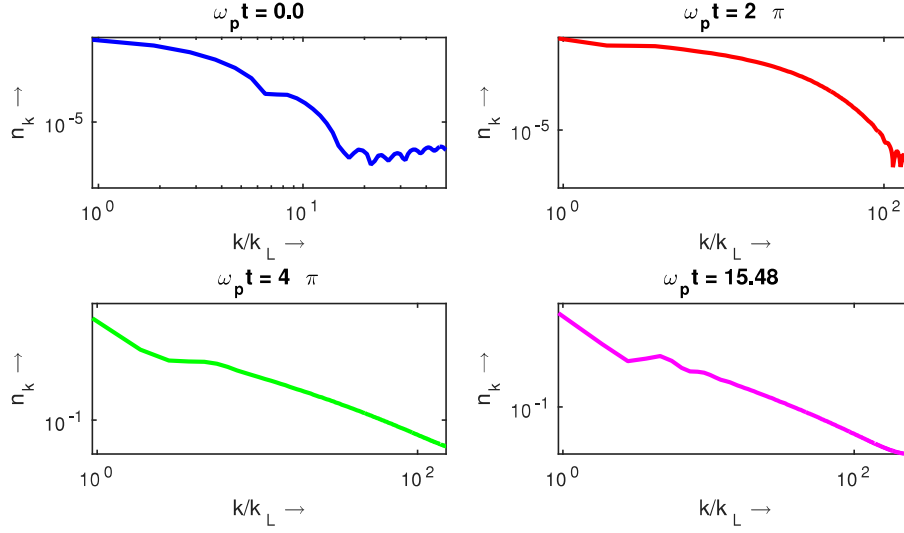


Figure 4.3: Fourier spectrum of an Akhiezer - Polovin wave with velocity amplitude  $u_m = 0.55$ ,  $\beta_\phi = 0.9995$  and with perturbation amplitude  $\delta = 0.1$  at different time steps.

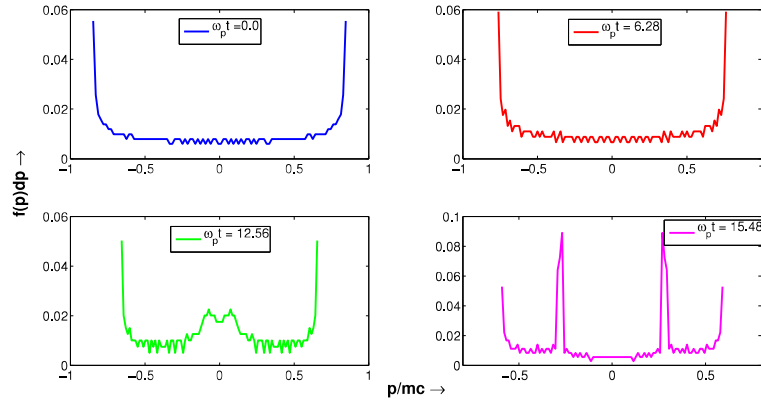


Figure 4.4: Momentum distribution of an Akhiezer - Polovin wave with velocity amplitude  $u_m = 0.55$ ,  $\beta_\phi = 0.9995$  and with perturbation amplitude  $\delta = 0.1$  at different time steps.

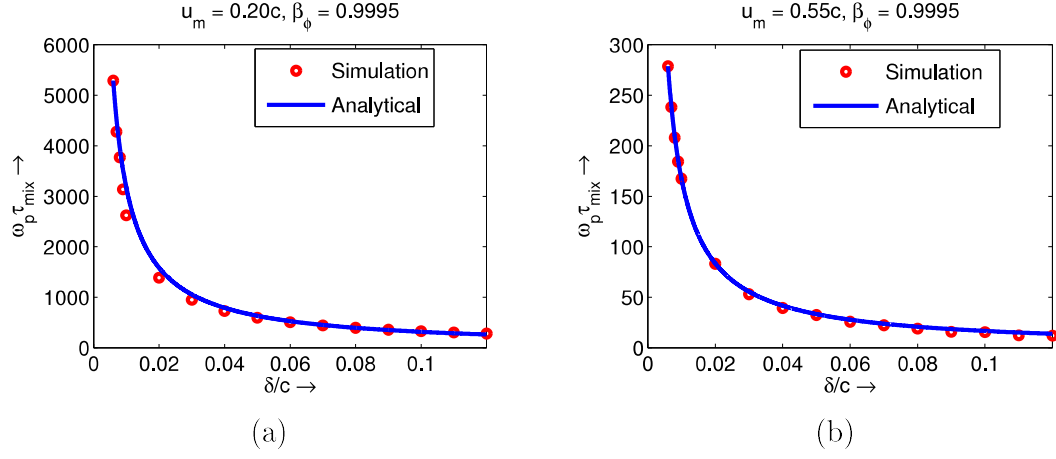


Figure 4.5: Analytical (solid) and numerical (circles) scalings of the phase mixing time for a finite amplitude Akhiezer - Polovin wave for  $u_m = 0.20$ (4.5a),  $0.55$ (4.5b) and  $\beta_\phi = 0.9995$  as a function of perturbation amplitudes ( $\delta$ )

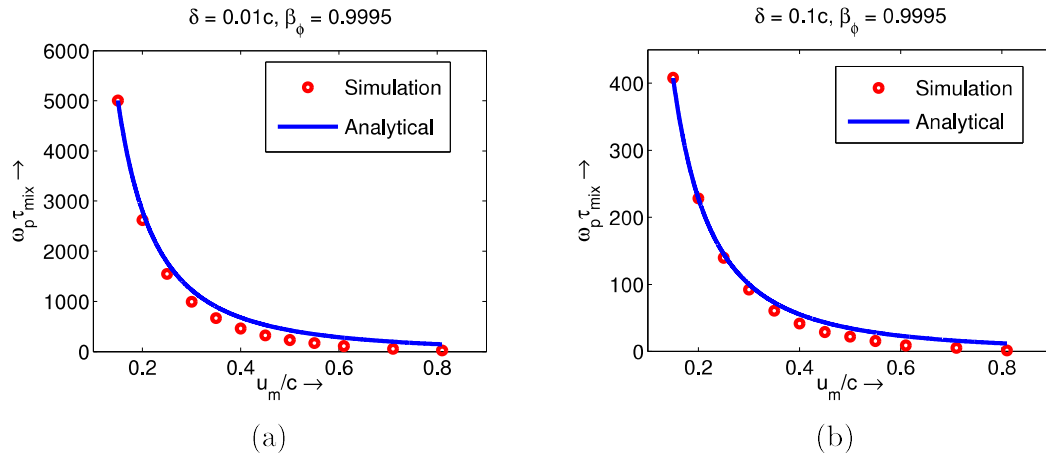


Figure 4.6: Analytical (solid) and numerical (circles) scalings of the phase mixing time as a function of the amplitude of Akhiezer - Polovin wave ( $u_m$ ) in the presence of a finite perturbation( $\delta$ ) =  $0.01$ (4.6a),  $0.1$ (4.6b) and  $\beta_\phi = 0.9995$ .

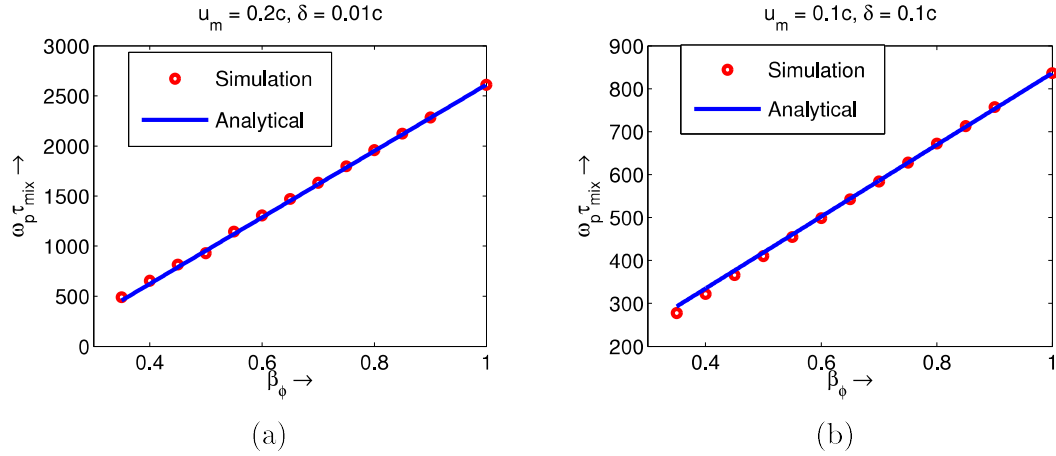


Figure 4.7: Analytical (solid) and numerical (circles) scalings of the phase mixing time as a function of the phase velocity  $\beta_\phi$  for a fixed amplitude of Akhiezer - Polovin wave  $u_m = 0.2$ ,  $\delta = 0.01$ (4.7a) and  $u_m = 0.1$ ,  $\delta = 0.1$ (4.7b)

## 4.5 Discussion and Summary

The phenomenon of phase mixing is a manifestation of spatially-dependent plasma frequency [30]. It is well known that a large amplitude longitudinal Akhiezer - Polovin wave breaks via the process of phase mixing at an amplitude well below the breaking amplitude for Akhiezer - Polovin wave ( $\sqrt{2}\sqrt{\gamma_\phi - 1}$ ), when subjected to an arbitrarily small longitudinal perturbation [33]. We have derived an expression for phase mixing time which brings out its dependence on  $u_m$ ,  $\beta_\phi$  and  $\delta$ . Our weakly relativistic calculation indicates that the phase mixing time scales linearly with  $\beta_\phi$ , inversely with  $\delta$  and has  $1/u_m^2$  dependence on  $u_m$ . We have verified this scaling using numerical simulations. We note here that, the dependence of phase mixing time on density amplitude  $\Delta$  [ $(\delta n/n_0)_{max} = (n/n_0 - 1)_{max}$ ] can be obtained from Eq.(4.20) as  $\tau_{mix} \approx \frac{2\pi\beta_\phi}{3\delta} \left[ \left( \frac{1+\Delta}{\beta_\phi\Delta} \right)^2 - \frac{1}{4} \right]$  by eliminating  $u_m$  using  $n = n_0\beta_\phi/(\beta_\phi - v)$ . This shows that for  $\Delta \gg 1$ ,  $\tau_{mix}$  is essentially independent of  $\Delta$  and for  $\Delta \ll 1$ ,  $\tau_{mix}$  scales as  $\sim 1/\beta_\phi\delta\Delta^2$ . Fig- shows the dependence of phase mixing time on  $\Delta$ . We emphasize here that for  $\Delta \ll 1$ , for a given  $\beta_\phi$  and  $\delta \sim \Delta$ , our expression for phase mixing time exhibits  $\sim 1/\Delta^3$  scaling, in conformity with the results presented in references [30, 55].

Some evidences of our analytical results have also seen in the simulation results

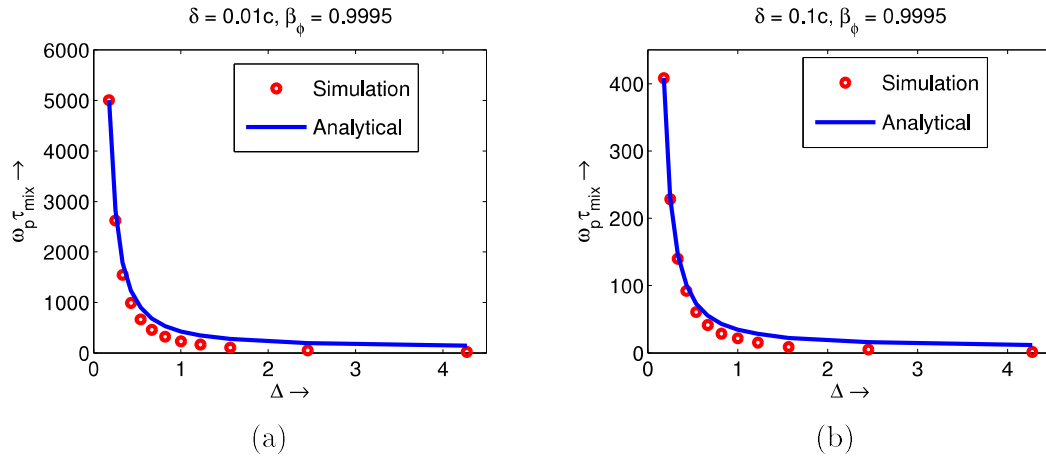


Figure 4.8: Analytical (solid) and numerical (circles) scalings of the phase mixing time as a function of the density amplitude of the Akhiezer - Polovin wave ( $\delta n/n_0 \sim \Delta n$ ) in the presence of a finite perturbation ( $\delta$ ) = 0.01(4.8a), 0.1(4.8b) and  $\beta_\phi = 0.9995$

obtained by Bera *et. al.* [70, 71] In their numerical experiment the space-time evolution of a relativistic electron beam driven wake-field in a cold, homogeneous plasma is studied using 1D-fluid simulation techniques. It is observed that the wake wave gradually evolves and eventually breaks, exhibiting sharp spikes in the density profile and sawtooth like features in the electric field profile. It is demonstrated that the excited wakefield is a longitudinal Akhiezer-Polovin mode which breaks via phase mixing. By changing the beam density and beam velocity, the variation of phase mixing time is studied for a wide range of input parameters and it is observed that, the breaking time scale follows the scaling given by Eq.(4.20).





*He needs "space" and  
"time," as if this were  
physics and not a human  
relationship.*

- Robert A. Heinlein

# 5

## Nonlinear Dynamics of Relativistically Intense Plasma Waves in Cylindrical and Spherical Geometry

This chapter presents the study on the space-time evolution and the breaking of relativistically intense cylindrical and spherical plasma oscillations via phase mixing process [5, 28–33, 68]. Analytical expressions for phase mixing time scales as a function of the amplitude of the applied perturbation have been derived for relativistically intense cylindrical and spherical oscillations which indicate that phase mixing time scales inversely with the cube of the amplitude of the applied perturbation. We also observe that, for nonrelativistic case the variation of phase mixing time scale follows the same scaling law. Inclusion of relativistic effects only hastens the phase mixing time but the scaling law remains unchanged. We also verify our analytically obtained scaling law by Sheet Simulation code [96] by extending it to cylindrical and spherical geometry.

### 5.1 Introduction

It is well known that Dawson [5] was the first to discover the fact that for a nonrelativistic cold plasma, oscillations in a slab/planar geometry would be stable below a critical amplitude called wave breaking limit given by  $eE/m\omega_p v_\phi = 1$ . Beyond this limit multi-stream flow or fine scale mixing develops which destroys the collective motion of the plasma electrons.

Dawson [5] further extended his nonrelativistic calculations by changing the pattern of motion such that electrons are oscillating back and forth along the radius of either a cylinder or a sphere and demonstrated that in nonrelativistic case, oscillations having cylindrical or spherical symmetry always break at arbitrarily small amplitude of the applied perturbation. This breaking occurs via phase mixing [5, 28–33, 68]. Later it has been shown by several authors that plasma oscillations/waves in a slab geometry can also break in the similar fashion, if the electron’s quiver velocity becomes relativistic [28, 30–33, 68] and/or there exists background density inhomogeneities (either fixed [67] or self-generated [29]). In the later case, the authors [29] have found that phase mixing time scale crucially depends on the amplitude of the applied perturbation as shown in the previous two chapters.

In the last few years much attention has been paid to the study of relativistically intense cylindrical and spherical plasma oscillations/waves, both theoretically [55, 56, 98] and experimentally [99, 100]. For example, Gorbunov *et. al.* [55] and Bulanov *et. al.* [56] respectively studied the evolution of cylindrical and spherical plasma waves analytically by using Lagrange coordinates [3, 6]. These authors respectively derived the equation of motion of an electron oscillating along the radius of a cylinder [55] and sphere [56]. The frequency of oscillation correct upto second order in oscillation amplitude were derived for cylindrical and spherical case, which turned out to be same. In the former case [55], the authors observed trajectory crossing of the neighbouring electrons which leads to wave breaking via phase mixing. In the later case [56], the authors observed that after some plasma period, the wave profile changes it’s direction of propagation which also occurs due to spatial dependency of the characteristic frequency of the wave. This time was termed as “turn-around time” [56]. But, an analytical expression for phase mixing time as a function of the amplitude of the applied perturbation for cylindrical and spherical plasma oscillations/waves were not presented. Though Gorbunov *et. al.* [55] attempted to predict a phase mixing time by using Dawson’s argument [5], still the verification of their prediction was never shown explicitly. Therefore the space time evolution of relativistically intense cylindrical/spherical plasma oscillations/waves, estimation of phase mixing time and their variation with the amplitude of the applied perturbation has been explicitly explored in this chapter.

In this chapter we extend Dawson's earlier work [5] by including relativistic effects. An important feature of cylindrical and spherical oscillations is that its parameters vary only with the distance from the source i.e they depend only on the radial coordinate of the oscillating electrons. Therefore we limit our study to one dimensional case only. In section 5.2 we extend Dawson Sheet Model from planar to cylindrical and spherical geometry and also include the relativistic mass variation effects. We first derive the expressions for the fluid variables *viz.* density ( $n$ ), electric field ( $E$ ) and velocity ( $v$ ) by respectively using the principle of conservation of number of particles, Gauss's Law and Newton's Law. We find that this method of deriving the fluid variables is easier compared to the derivation involving the definition of Lagrange coordinates used by other authors [55,56]. Then we solve the equation of motion in respective coordinate system by using Lindstedt-Poincaré perturbation method [54] and derive an approximate expression for frequency of oscillation in the weakly relativistic limit upto fourth order in oscillation amplitude. We observe that in general the expressions for frequencies acquire spatial dependency which ultimately lead to breaking via phase mixing [5,28-33,68]. In section 5.3 we study the dynamics of cylindrical and spherical plasma oscillation and derive analytical expressions for (cylindrical and spherical) phase mixing time scales as a function of the amplitude of the applied perturbation by using Dawson's argument [5], for all the cases under consideration. Further, we verify this scaling by performing numerical simulations, using a code based on Dawson Sheet Model [96] by extending it to cylindrical and spherical geometry. Finally in section 5.4 we summarize this work.

## 5.2 Governing Equations

According to Dawson Sheet Model, cylindrical and spherical oscillations arise respectively due to cylindrical and spherical sheet of charges [Fig-(5.1)] oscillating about their equilibrium positions. These sheet of charges are embedded in a homogeneous background of immobile ions. Unlike the slab geometry, in these cases the electric field gets tweaked by the geometrical effects and for same displacement amplitude the electric field amplitude becomes different for different equilibrium positions of the sheets which in turn makes the frequency of oscillation space de-

pendent. This is reason why phase mixing and wave breaking in these cases is an inherent phenomena, arising due to geometry of the problem.

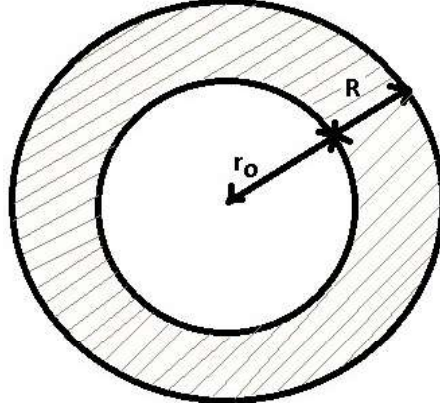


Figure 5.1: Cross-sectional view of Dawson Sheet Model in Cylindrical and Spherical Coordinates

In the following subsections we separately derive the expressions for the fluid variables and derive the equation of motion for cylindrical & spherical oscillations considering relativistic mass variation effect of the electrons. Let  $r_0$  and  $R(r_0, t)$  respectively be the equilibrium positions and displacement from the equilibrium positions of the electron sheets. So the Euler positions of the sheets can be written as  $r(r_0, t) = r_0 + R(r_0, t)$ .

### 5.2.1 Fluid Variables in Cylindrical Geometry

In cylindrical geometry, the conservation of the number of particle yields

$$2\pi n_0 r_0 dr_0 = 2\pi n r dr$$

where,  $n_0$  and  $n$  be the equilibrium and instantaneous density respectively.

$$n(r_0, t) = \frac{n_0 r_0}{(r_0 + R)(1 + \frac{\partial R}{\partial r_0})} \quad (5.1)$$

Now using Gauss's Law in cylindrical geometry, we have

$$\frac{1}{r} \frac{\partial}{\partial r} (rE) = 4\pi e(n_0 - n)$$

Substituting the value of  $n$ , from Eq.(5.1), the electric field stands as

$$E(r_0, t) = 2\pi en_0 \left[ \frac{(r_0 + R)^2 - r_0^2}{(r_0 + R)} \right] \quad (5.2)$$

Now the relativistically correct equation of motion of electron sheet can be written as

$$m \frac{d}{dt} \left[ \frac{\dot{R}}{(1 - \frac{\dot{R}^2}{c^2})^{1/2}} \right] = -eE$$

putting the value of  $E$  from Eq.(5.2), we get

$$\frac{\ddot{R}}{(1 - \frac{\dot{R}^2}{c^2})^{3/2}} = -\frac{\omega_p^2}{2} \left[ \frac{(r_0 + R)^2 - r_0^2}{(r_0 + R)} \right] \quad (5.3)$$

Here  $\omega_p = 4\pi n_0 e^2/m$  is the nonrelativistic plasma frequency. Taking  $R/r_0 = \rho$ , Eq.(5.3) modifies as

$$\frac{\ddot{\rho}}{(1 - \frac{r_0^2 \dot{\rho}^2}{c^2})^{3/2}} + \frac{\omega_p^2}{2} \left[ \frac{(1 + \rho)^2 - 1}{(1 + \rho)} \right] = 0 \quad (5.4)$$

In nonrelativistic limit ( $c \rightarrow \infty$ ), we get the same Eq. obtained by Dawson [5]

$$\ddot{\rho} + \frac{\omega_p^2}{2} \left[ \frac{(1 + \rho)^2 - 1}{(1 + \rho)} \right] = 0$$

Here *dot* sign represents the derivative w.r.t time. In the weakly relativistic limit and small amplitude oscillations Eq.(5.4) can be simplified as [55] (expanded upto the third order of  $\rho$  and second order of  $\dot{\rho}$ )

$$\ddot{\rho} - \frac{3}{2} \frac{r_0^2 \omega_p^2}{c^2} \rho \dot{\rho}^2 + \omega_p^2 \rho - \frac{\omega_p^2}{2} \rho^2 + \frac{\omega_p^2}{2} \rho^3 = 0 \quad (5.5)$$

Now, by using Lindstedt - Poincare perturbation method [54], the expression for frequency correct upto the fourth order of oscillation amplitude can be written as [derivation given in Appendix-(B)]

$$\Omega_{cy}(rel) = \omega_p \left[ 1 - \frac{3\omega_p^2}{16} \frac{r_0^2 \rho_0 (r_0)^2}{c^2} + \frac{\rho_0 (r_0)^2}{12} + \frac{\rho_0 (r_0)^4}{512} \right] \quad (5.6)$$

Here  $\rho_0(r_0)$  is the displacement amplitude of the electrons, which in general depends on their equilibrium positions  $r_0$ . In nonrelativistic limit  $c \rightarrow \infty$ , Eqs.(5.5) and (5.6) respectively become

$$\ddot{\rho} + \frac{\omega_p^2}{2} [2\rho - \rho^2 + \rho^3] = 0 \quad (5.7)$$

and

$$\Omega_{cy}(nonrel) = \omega_p \left[ 1 + \frac{\rho_0(r_0)^2}{12} + \frac{\rho_0(r_0)^4}{512} \right] \quad (5.8)$$

### 5.2.2 Fluid Variables in Spherical Geometry

Now following the same procedure in spherical geometry the same fluid variables can be penned as

$$n(r_0, t) = \frac{n_0 r_0^2}{(r_0 + R)^2 (1 + \frac{\partial R}{\partial r_0})} \quad (5.9)$$

$$\begin{aligned} \frac{1}{r^2} \frac{\partial(r^2 E)}{\partial r} &= 4\pi e(n_0 - n) \\ E(r_0, t) &= \frac{4\pi e n_0}{3} \left[ \frac{(r_0 + R)^3 - r_0^3}{(r_0 + R)^2} \right] \end{aligned} \quad (5.10)$$

Now the relativistically correct equation of motion of an electron oscillating sheet along the radius of a sphere is given by,

$$\frac{\ddot{R}}{(1 - \frac{\dot{R}^2}{c^2})^{3/2}} + \frac{\omega_p^2}{3} \left[ \frac{(r_0 + R)^3 - r_0^3}{(r_0 + R)^2} \right] = 0 \quad (5.11)$$

In nonrelativistic limit, the above Eq. transforms to [5]

$$\ddot{R} + \frac{\omega_p^2}{3} \left[ \frac{(r_0 + R)^3 - r_0^3}{(r_0 + R)^2} \right] = 0$$

In terms of  $\rho$ , Eq.(5.11) becomes

$$\frac{\ddot{\rho}}{(1 - \frac{r_0^2 \dot{\rho}^2}{c^2})^{3/2}} + \frac{\omega_p^2}{3} \left[ \frac{(1 + \rho)^3 - 1}{(1 + \rho)^2} \right] = 0 \quad (5.12)$$

In weakly relativistic limit and small amplitude oscillation, the above Eq. takes the form [56]

$$\ddot{\rho} - \frac{3}{2} \frac{r_0^2 \omega_p^2}{c^2} \rho \dot{\rho}^2 + \omega_p^2 \rho - \omega_p^2 \rho^2 + \frac{4\omega_p^2}{3} \rho^3 = 0 \quad (5.13)$$

And frequency of oscillation stands as [derivation given in Appendix-(B)]

$$\Omega_{sph}(rel) = \omega_p \left[ 1 - \frac{3\omega_p^2}{16} \frac{r_0^2 \rho_0(r_0)^2}{c^2} + \frac{\rho_0(r_0)^2}{12} + \frac{\rho_0(r_0)^4}{72} \right] \quad (5.14)$$

In non relativistic limit, the equation of motion for small amplitude oscillation becomes [5]

$$\ddot{\rho} + \frac{\omega_p^2}{3} [3\rho - 3\rho^2 + 4\rho^3] = 0 \quad (5.15)$$

And the frequency of oscillation inclines as

$$\Omega_{sph}(nonrel) = \omega_p \left[ 1 + \frac{\rho_0(r_0)^2}{12} + \frac{\rho_0(r_0)^4}{72} \right] \quad (5.16)$$

Here we want to note that Eqs.(5.5) and (5.13) respectively are the same equation derived by Gorbunov [55] and Bulanov [56]. In the expressions of  $\Omega_{cy}(rel)$  and  $\Omega_{sph}(rel)$  the second term represents correction due to the relativistic effects and other terms represent additional anharmonicity introduced by cylindrical and spherical geometry respectively. In addition to this, it should be noted from the expressions of the electric field [Eqs.(5.2) and (5.10)] that, even for the same displacement amplitude, the electric field depends explicitly on the equilibrium positions of the electrons (unlike the planar geometry case) which results in a position dependent restoring force. Therefore the frequency of oscillation depends on the equilibrium positions of the sheets which leads to wave breaking via phase mixing. In the next section we present a scaling law for this phase mixing time.



### 5.3 Dynamics of Nonlinear Cylindrical & Spherical Plasma Oscillations and Calculation of Phase Mixing Time

In this section we describe the dynamics of relativistically intense cylindrical and spherical plasma oscillations and calculate their phase mixing time. In order to study the space-time evolution and breaking of cylindrical and spherical oscillations, we first load the initial conditions needed to excite axisymmetric cylindrical and spherical oscillations respectively in one dimensional (along the radius) sheet code (based on Dawson Sheet Model) containing  $\sim 10000$  cylindrical and spherical surfaces of charges. In this code the density and electric field are respectively calculated from Eqs.(5.1) & (5.2) (for cylindrical oscillations) and from Eqs.(5.9) & (5.10) (for spherical oscillations) (as mentioned in chapter -2).

Now for cylindrical and spherical oscillations, its parameters depend only on the radial coordinate of the oscillating species (here the electron sheets) *i.e.* they are radially symmetric in nature. As Bessel functions and Spherical Bessel functions [97] respectively form a complete orthogonal set (basis functions) in cylindrical and spherical coordinate systems, then any arbitrary radial perturbation imposed in these systems can be written as a superposition of these basis functions (Fourier Bessel Series) in their respective coordinate system [101, 102]. Therefore to excite an oscillation in cylindrically and spherically symmetric system we respectively use Bessel functions and Spherical Bessel functions as an initial perturbation. Here, we want to note that, the structure and propagation of nonrelativistic axisymmetrical waves in linear and nonlinear regime using such type of initial conditions has been studied first by Travelpiece & Gould [103] for a cylindrical plasma column and later continued by several authors [104–106]. Using these type of initial conditions the equation of motion for each electron sheet is solved using fourth order Runge-Kutta scheme. At each time step, ordering of the sheets are checked for sheet crossing. Phase mixing time is measured as the time taken by any two of the adjacent sheets to cross over (similar to previous two cases).

In the following subsections we study the space-time evolution & derive the expressions for phase mixing time as a function of the amplitude of the applied

perturbation for cylindrical and spherical plasma oscillations respectively.

### 5.3.1 Breaking of Cylindrical Plasma Oscillations

The relativistic equation of motion of an electron sheet along the radius of a cylinder is given by Eq.(5.3). This equation can be solved numerically with the help of two initial conditions  $R(r_0, t = 0)$  and  $\dot{R}(r_0, t = 0)$ . Here we consider plasma oscillations localized in space in the vicinity of the axis  $r = 0$  [55]. We assume that electron velocity at  $t = 0$  is zero :  $\dot{R}(r_0, t = 0) = 0$ . We also assume that at  $t = 0$  the oscillations are excited by an electric field of the form [104–106]

$$\bar{E}(r_0, t = 0) = \frac{eE(r_0, t = 0)}{m\omega_p^2 X} = \Delta J_n \left[ \frac{\alpha_{nm} r(r_0, 0)}{R_0} \right] \quad (5.17)$$

where  $X$  is given by  $R_0/\alpha_{nm}$ ,  $J_n$  is  $n$ -th order Bessel function and  $\alpha_{nm}$  is the  $m$ -th zero of  $n$ -th order Bessel function [101, 102].  $\Delta$  is the amplitude of applied electric field perturbation and  $R_0$  is the maximum value of the radius of the cylindrical system under consideration. We consider that at initial time, the electric field  $E(r_0, 0)$  at the boundaries of the simulation are zero i.e  $E(r_0 = 0, t = 0) = 0$  and  $E(r_0 = R_0, t = 0) = 0$ .

In the above scenario satisfied by the all initial conditions the lowest order mode is  $n = 1$  and  $m = 1$  (As  $E$  is zero on the axis at  $t = 0$  so  $n = 0$  cannot be taken as lowest order mode as  $J_0(\alpha_{01}r/R_0) \neq 0$  at  $r = 0$ ). Therefore, here we study the space-time evolution of the lowest order mode  $\Delta J_1(\alpha_{11}r/R_0)$ . The length of the system  $R_0$  is taken upto the first zero of the Bessel function.

To solve Eq.(5.3) we first numerically calculate the initial profile of  $R(r_0, t = 0)$  in the following way: At initial instant of time  $t = 0$ , the electrons are at their equilibrium position  $r_0$  and radially displaced by an amount  $R(r_0, 0)$  by adding the perturbation given by Eq.(5.17). So the Euler positions of the electrons at  $t = 0$  become  $r(r_0, 0) = r_0 + R(r_0, 0)$ . All the particles at their initial position produce an electric field of the form  $\bar{E}(r_0, t = 0) = \Delta J_1[\alpha_{11}r(r_0, 0)/R_0]$ . On the other hand from Gauss's Law the electric field  $E(r_0, 0)$  is given by

$$E(r_0, 0) = 2\pi en_0 \frac{[r_0 + R(r_0, 0)]^2 - r_0^2}{[r_0 + R(r_0, 0)]} \quad (5.18)$$

Comparing Eqs.(5.17) and (5.18) we can find  $R(r_0, 0)$  for given values of  $r_0$ .

Based on the scheme described above, numerical computations have been carried out and the spatial variation of electric field and electron density with time have been shown. The results of relevant simulations are illustrated in Figs-5.2 and 5.3. Figs- 5.2 and 5.3 respectively show the snapshots of the electron density and electric field profiles for the value  $\Delta = 0.5$ . Fig-5.2 shows that, as time progresses, the density maxima increases gradually and shows a high spike at  $\omega_p t = 314.2221$  which is a signature of wave breaking via the process of phase mixing [5, 28–33, 68]. From Fig- 5.3 we observe that, as time goes on, the radial profile of electric field becomes steeper and acquires a jump at the off-axis radial point, where electron density spikes.

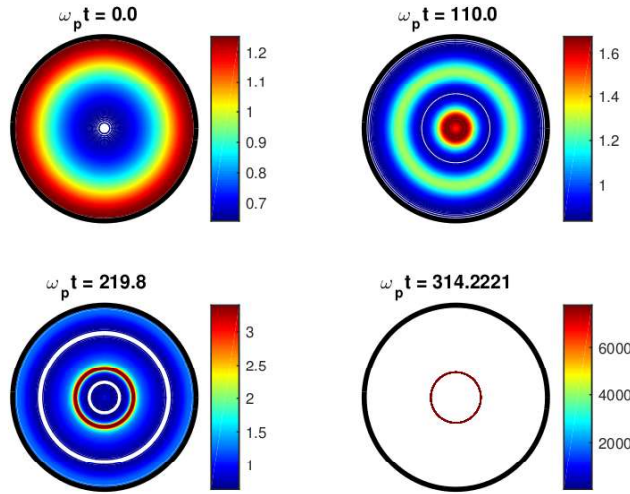


Figure 5.2: Snapshots of density profile of relativistic cylindrical oscillation at different time steps for amplitude  $\Delta = 0.5$ .

Now we present a scaling for phase mixing time scale in the following way: Equating the electric field given by Eq.(5.17) with Eq.(5.18) and in the small amplitude limit  $\Delta \ll 1$ , we can write

$$\frac{r_0}{X} \rho_0(r_0) \sim \Delta J_1 \left[ \alpha_{11} \frac{r_0}{R_0} \right] \quad (5.19)$$

Now putting the value of  $\rho_0(r_0)$  from above, the expression for frequency of relativistic cylindrical plasma oscillation [from Eq.(5.6)] modifies to (correct upto

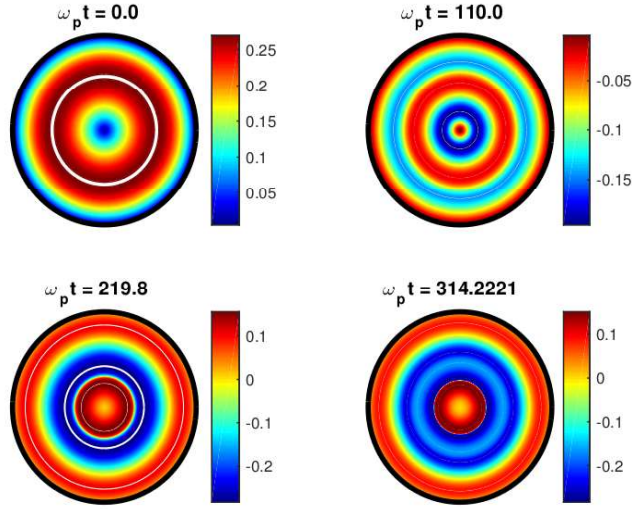


Figure 5.3: Snapshots of electric field profile of relativistic cylindrical oscillation at different time steps for amplitude  $\Delta = 0.5$ .

$\Delta^2$ )

$$\Omega_{cy}(rel) \sim \omega_p \left[ 1 - \frac{3}{16} \frac{\omega_p^2 X^2 \Delta^2}{c^2} J_1^2 \left\{ \alpha_{11} \frac{r_0}{R_0} \right\} + \frac{X^2 \Delta^2}{12 r_0^2} J_1^2 \left\{ \alpha_{11} \frac{r_0}{R_0} \right\} \right] \quad (5.20)$$

According to Dawson's argument, the phase mixing time ( $\omega_p \tau_{mix}$ ) depends on the spatial derivative of frequency as  $\omega_p \tau_{mix} \sim \pi / [2 R_{max} (d\Omega/dr_0)]$ . Differentiating Eq.(5.20) w.r.t  $r_0$  and noting  $R_{max}$  is proportional to  $\Delta$ , the phase mixing time scale can be written as

$$\omega_p \tau_{mix} \sim \frac{1}{\Delta^3} \quad (5.21)$$

Here, we have omitted the proportionality constant which is a function of  $r_0$ . This proportionality constant only gives the position of breaking, which generally depends on the profile of the initial perturbation and is not of general interest. In the similar manner using Eq.(5.8), we can find that, for nonrelativistic cylindrical oscillations also, phase mixing time scale follows the same scaling law given by Eq.(5.21).

In order to verify this scaling expressed by Eq.(5.21) we repeat our numerical experiment for different values of  $\Delta$ . The variation of phase mixing time as function of the amplitude of applied perturbation are shown in Figs-5.4 and 5.5

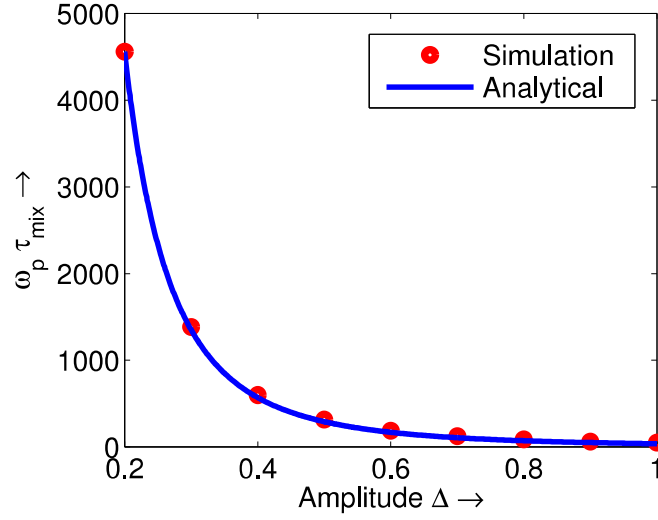


Figure 5.4: Variation of phase mixing time of relativistic cylindrical oscillation as a function of amplitude of applied perturbation  $\Delta$ .

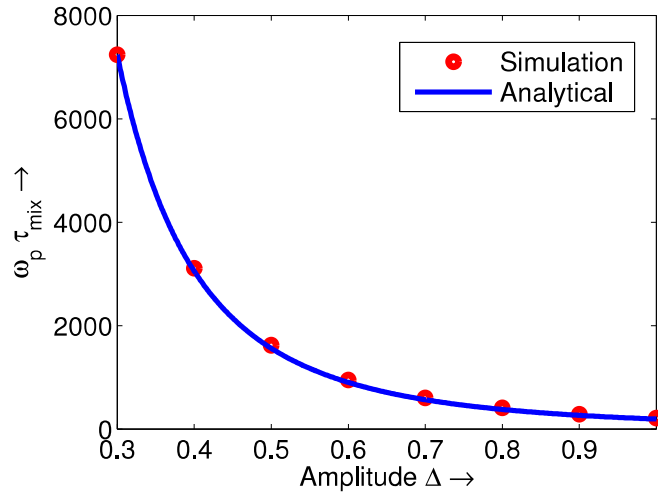


Figure 5.5: Variation of phase mixing time of nonrelativistic cylindrical oscillation as a function of amplitude of applied perturbation  $\Delta$ .

respectively for relativistic and nonrelativistic cases. In the figures points represent the simulation results and the solid line represents our theoretical scaling obtained from Eq.(5.21). By comparing these two figures, we understand that for a fixed value of the applied perturbation, relativistic effects hastens the phase mixing time, which is expected. Here for cylindrical oscillations, the controlling parameter is  $X\omega_p/c$ , which is respectively zero for nonrelativistic case and chosen to be  $\sim 1$  for relativistic case.

### 5.3.2 Breaking of Spherical Plasma Oscillations

In this subsection we present the space-time evolution of spherical plasma oscillations and estimate the phase mixing time in the similar fashion described in the above subsection.

Here the spherical oscillations have been excited by electric field  $E(r_0, t)$  of the form

$$\bar{E}(r_0, t = 0) = \frac{eE(r_0, t = 0)}{m\omega_p^2 Y} = \Delta j_\nu \left[ \frac{\beta_{\nu m} r(r_0, 0)}{R_0} \right] \quad (5.22)$$

where  $Y$  is given by  $R_0/\beta_{\nu m}$  and  $j_\nu(x)$  is the Spherical Bessel function of order  $\nu$  and defined as  $j_\nu(x) = \sqrt{\pi/2x} J_{\nu+1/2}(x)$ .  $\beta_{\nu m}$  is the  $m$ -th zero of  $\nu$ -th order Spherical Bessel function [101, 102]. We have computed the value of  $R(r_0, 0)$  by comparing Eq.(5.10) and (5.22) in the similar fashion described in the previous subsection. Here we have taken the lowest order mode  $\Delta j_1(\beta_{11}r/R_0)$  and the length of the system  $R_0$  is taken upto the first zero of the Spherical Bessel function. Then we have solved Eq.(5.11) numerically and calculated the density and electric field profile respectively from the expressions 5.9 and 5.10. The snapshots of density and electric field profile at different time steps have been shown in Figs-5.6 and 5.7 respectively. Like cylindrical waves here also it is observed that phase mixing leading to wave breaking is manifested by a density burst and a sharp gradient in the electric field profile.

Now to present a scaling law for this spherical oscillation, we again follow the same fashion. For a small amplitude perturbation  $\Delta \ll 1$ ,  $\frac{r_0}{Y}\rho_0(r_0) \sim \Delta j_1[\beta_{11}\frac{r_0}{R_0}]$  and the frequency of spherical oscillation correct upto second order in  $\Delta$  for rela-

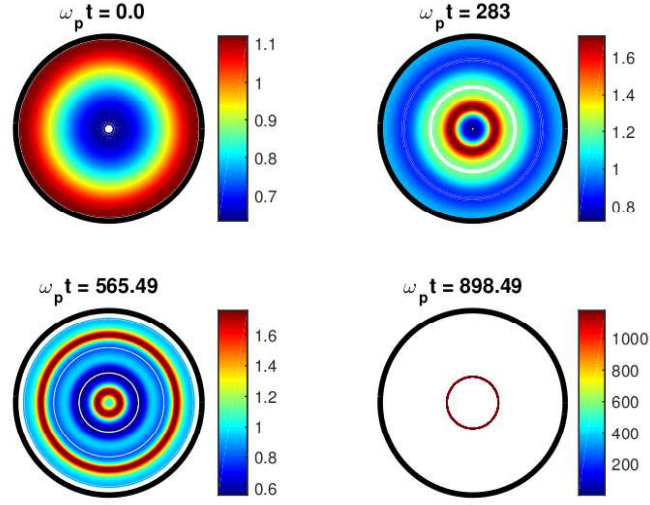


Figure 5.6: Snapshots of density profile of relativistic spherical oscillation at different time steps for amplitude  $\Delta = 0.5$ .

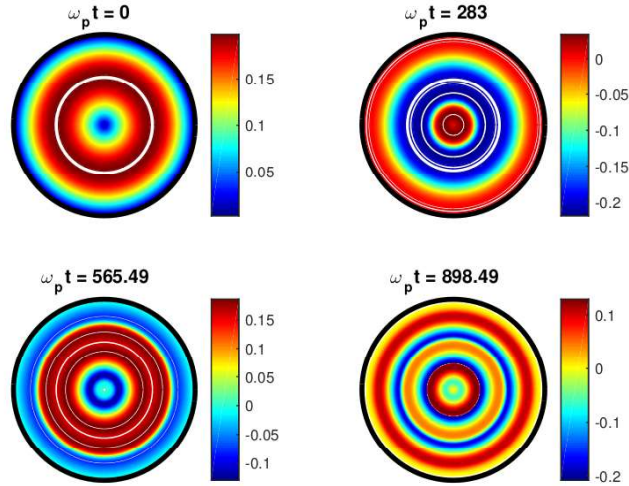


Figure 5.7: Snapshots of electric field profile of relativistic spherical oscillation at different time steps for amplitude  $\Delta = 0.5$ .

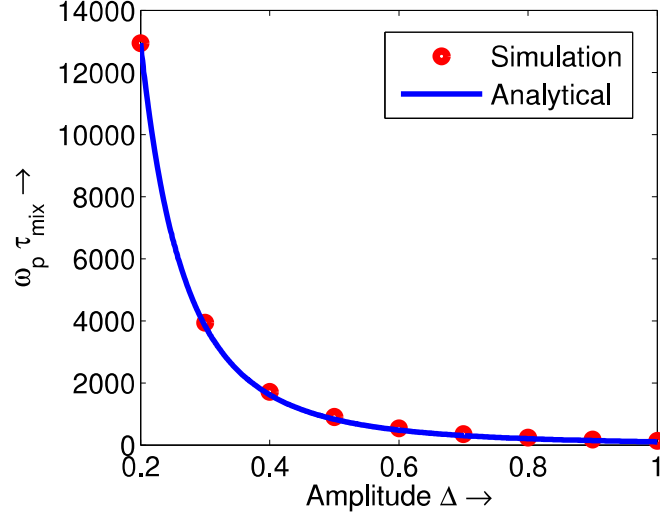


Figure 5.8: Variation of phase mixing time of relativistic spherical oscillation as a function of amplitude of applied perturbation  $\Delta$ .

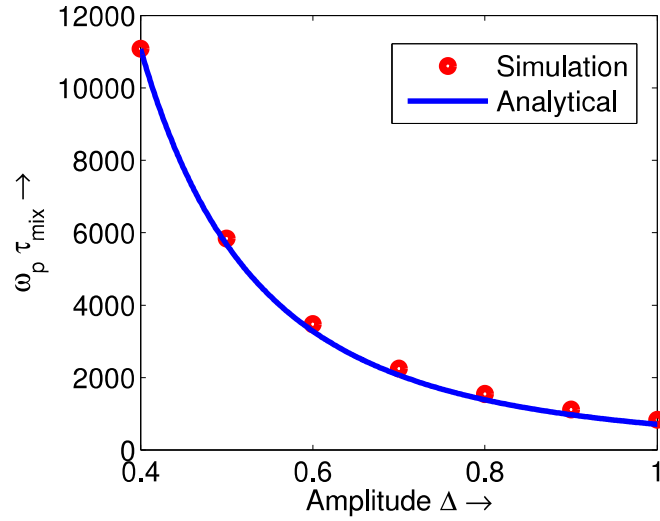


Figure 5.9: Variation of phase mixing time of nonrelativistic spherical oscillation as a function of amplitude of applied perturbation  $\Delta$ .



tivistic & nonrelativistic case respectively can be written as,

$$\Omega_{sph}(rel) \sim \omega_p \left[ 1 - \frac{3}{16} \frac{\omega_p^2 Y^2 \Delta^2}{c^2} j_1^2 \left\{ \beta_{11} \frac{r_0}{R_0} \right\} + \frac{Y^2 \Delta^2}{12 r_0^2} j_1^2 \left\{ \beta_{11} \frac{r_0}{R_0} \right\} \right] \quad (5.23)$$

and

$$\Omega_{sph}(non - rel) \sim \omega_p \left[ 1 + \frac{X^2 \Delta^2}{12 r_0^2} j_1^2 \left\{ \beta_{11} \frac{r_0}{R_0} \right\} \right] \quad (5.24)$$

Again following Dawson's argument, one can easily arrive at the same scaling law given by Eq.(5.21) for both relativistic and nonrelativistic case. The variation of phase mixing time ( $\tau_{mix}$ ) as a function of applied amplitude  $\Delta$  for relativistic and nonrelativistic spherical oscillations are respectively shown in Figs-5.8 and 5.9. In the figures numerical results have been displayed by dotted lines and the solid lines representing the scaling given by Eq.(5.21). Like cylindrical oscillations here the controlling parameter is  $Y\omega_p/c$  which is respectively zero for nonrelativistic case and chosen to be  $\sim 1$  for relativistic case.

In all these cases we observe that, the analytical scaling law given by Eq.(5.21) shows a very good fit to the observed numerical results, thus vindicating our weakly relativistic calculations.

## 5.4 Summary

In this chapter, we have demonstrated analytically and numerically the behaviour of nonlinear and relativistically intense cylindrical and spherical plasma oscillation using Dawson sheet model. Initial conditions are taken in terms of Bessel functions and Spherical Bessel functions to excite cylindrical and spherical oscillations respectively. This is because, as Bessel functions and Spherical Bessel functions are respectively the normal modes in cylindrical and spherical coordinate systems, thus any arbitrary perturbation in these systems can be written as a superposition of these basis functions in their respective coordinate systems. Fluid variables have been derived in a very straightforward way. The expressions for frequencies are given for both the cases and is found to be an explicit function of the equilibrium positions of the electron sheets. By performing numerical simulations it has been shown that the radial electron density of cylindrical and spherical plasma oscillations grows sharply with time and after some periods the density shows explosive

behaviour due to the crossing of neighbouring electron sheets which leads to wave breaking via phase mixing. Analytical expression for the phase mixing time scale has been derived and it is observed that for both cases (cylindrical and spherical) phase mixing time scales with the cube of the amplitude of the applied perturbation which indicates that “in general scaling of phase mixing time with amplitude is independent of geometry of oscillation”. Further we have found that inclusion of relativistic effects does not change the scaling of phase mixing time with amplitude of perturbation; it only hasten the process as compared to the nonrelativistic case.



*Nothing ever becomes real  
till it is experienced.*

- John Keats



# Wave Breaking Amplitude of a Self-consistent Electron Plasma Wave in a Maxwellian Plasma

In 1971 using a “water-bag” distribution for electrons, Coffey [36] showed that the wave breaking amplitude of an electron plasma wave in a warm plasma explicitly depends on the electron temperature. In this chapter, we revisit Coffey’s criterion and test its applicability for a Maxwellian plasma using a 1-D Particle-in-Cell (PIC) simulation code. We find that Coffey’s propagating wave solution, which was derived using a “water-bag” distribution for electrons, also represents a self-consistent propagating wave in a Maxwellian plasma, albeit with a lower amplitude. Moreover, we find that the maximum electric field amplitude that can be sustained by a self-consistent electron plasma wave in a Maxwellian plasma follows a similar scaling with temperature as given by Coffey but with slightly different coefficients.

## 6.1 Introduction

In the previous chapters we have seen that oscillations/waves break via phase mixing (except pure Akhiezer - Polovin wave) at amplitudes far below their wave-breaking limit when the electrons quiver with a speed close to  $c$  (velocity of light in vacuum) and/or the geometry of the oscillation changes. In such cases breaking occurs gradually with time and follows the time scale presented in earlier chapters. Moreover we have observed that, as time progress density spikes arise in space and

at the breaking point density becomes singular. Actually, this density singularity is an artefact of cold fluid plasma model. In fact, for non-linear density perturbations associated with a large amplitude plasma wave, electron pressure (as pressure  $P \sim n^3$ ) and hence thermal effects become important as the electron thermal pressure will not allow the density compression to build up to such high values as predicted by the simple cold plasma fluid model. Therefore, under this condition a warm plasma theory is required.

In 1971, Coffey [36] investigated the phenomenon of wave breaking for an electron plasma wave (nonrelativistic) in a warm plasma by using the simplest distribution *i.e.* “water-bag” distribution [39, 57] for electrons. Unlike the cold plasma wave breaking which is defined by the crossing of the trajectories of the oscillating particles constituting the wave, Coffey defined wave breaking in a warm plasma as the trapping of oscillating background plasma electrons which are at the upper boundary of the water-bag distribution (which is at electron sound speed  $v_0 = \sqrt{3k_B T_e / m}$ ) by the wave potential and showed that maximum electric field amplitude explicitly depends on the electron temperature and decreases monotonically with increasing electron temperature. This limiting amplitude of electron plasma wave is known as Coffey’s limit.

Verification of this effect of electron temperature in reducing the wave breaking amplitude had been attempted by Kruer [77] and Bergmann *et al.* [78, 107], using 1D Vlasov simulations, for resonantly driven plasma waves in an inhomogeneous plasma. The results presented by Bergmann *et al.* [78] clearly show that, when a small fraction of electrons are trapped in the wave potential, the periodic structure of the wave is still unaffected and wave does not break. This periodicity dies out when a large number of particles are get trapped. The authors in Ref. [78] concluded that Coffey’s limit can not be applied for resonantly excited waves. Here we emphasize that Coffey’s limit was derived for a freely running propagating wave in a homogeneous plasma, and to the best of our knowledge verification of Coffey’s limit for a freely running electron plasma wave in a homogeneous plasma where electron velocity distribution is Maxwellian has never been attempted.

In this present chapter, we revisit Coffey’s criteria for a freely running electron plasma wave in a Maxwellian plasma. First, in section 6.2 we derive an equation for an electron plasma wave in its own rest frame by considering water-bag distribution for electrons. We also derive an expression for maximum electric field

amplitude ( $E_{max}$ ) as a function of electron temperature ( $T_e$ ) using particle trapping condition. Next, in first portion of section 6.3 we compute the initial conditions needed to excite a propagating wave in a warm plasma from the equation of motion. In the second portion of section 6.3 we observe that Coffey's propagating wave solution, which was derived using a "water-bag" distribution for electrons, also represents a self-consistent propagating wave in a Maxwellian plasma, albeit with a lower amplitude. By adding an external perturbation we further show that if the initial resultant amplitude of the wave exceeds Coffey's wave breaking limit, within a few plasma periods the initialized wave self-consistently conforms itself with the background Maxwellian distribution and settles down to an amplitude below Coffey's limit and propagates for a large period of time ( $\sim 100$  plasma periods) provided the Landau damping rate is very weak. We found that the final self-consistent wave amplitude does not increase even after increasing the perturbation amplitude and thus can be taken as maximum sustainable electric field amplitude. By varying the initial electron temperature, we show that maximum electric field amplitude that can be sustained by a self-consistent electron plasma wave in a Maxwellian plasma follows a similar scaling given by Coffey but with slightly different coefficients. Finally we summarize in section 6.4.

## 6.2 Theoretical Model (Using "Water-Bag")

In this section we derive an expression for maximum electric field amplitude that can be sustained by a electron plasma wave using the framework of coupled Vlasov-Maxwell equations which can be written as

$$\frac{\partial f}{\partial t} + v \frac{\partial f}{\partial x} - \frac{eE}{m} \frac{\partial f}{\partial v} = 0 \quad (6.1)$$

$$\frac{\partial E}{\partial x} = 4\pi e(n_0 - n) \quad (6.2)$$

where the symbols have their usual meaning. An exact analytical solution of the above equations using a Maxwellian distribution for electrons is mathematically complicated. Therefore, here we start from a water-bag distribution  $[f(x, v)]$  as used in the Refs. [36,39]. According to the water-bag model, electron distribution function is constant in a bounded region ( $-v_0 \leq v \leq v_0$  at  $t = 0$ ,  $v_- \leq v \leq v_+$

at  $t \neq 0$ ) of phase space and is zero outside this region. Therefore it is sufficient to solve the equations for the boundaries of the phase space. The constant value of  $f$  is determined by  $\int_{-\infty}^{\infty} f dv = n_0$ , which gives  $f = n_0/2v_0$  and the value of  $v_0$  is determined by requiring that the second order moment of water-bag distribution be same as that for a Maxwellian distribution *i.e*  $\left[ \int_{-\infty}^{\infty} v^2 f dv \right]_{water-bag} = \left[ \int_{-\infty}^{\infty} v^2 f dv \right]_{Maxwellian}$  which yields,  $v_0 = \sqrt{3k_B T_e/m}$ . Now the electron density and fluid velocity at any instant are respectively given by [39]

$$n(x, t) = \int_{-\infty}^{\infty} f dv = \frac{n_0}{2v_0}(v_+ - v_-) \quad (6.3)$$

$$u(x, t) = \frac{\int_{-\infty}^{\infty} f v dv}{\int_{-\infty}^{\infty} f dv} = \frac{(v_+ + v_-)}{2} \quad (6.4)$$

Solving Eqs.(6.3) and (6.4),  $v_+$  and  $v_-$  can be written in terms of fluid velocity  $u$  and density  $n$  as [39]

$$v_{\pm} = u \pm v_0 \frac{n}{n_0}$$

The evolution equations satisfied by  $n$  and  $u$  are obtained by taking the zero-th and first order moment of the Vlasov equation which respectively give [39]

$$\frac{\partial n}{\partial t} + \frac{\partial}{\partial x}(nu) = 0 \quad (6.5)$$

$$\frac{\partial u}{\partial t} + u \frac{\partial u}{\partial x} = -\frac{eE}{m} - \frac{k_B T_e}{mn} \frac{\partial}{\partial x} \frac{n^3}{n_0^2} \quad (6.6)$$

For a water-bag distribution the heat flux is zero [3] so that there is a closure to the hierarchy of the moments of the Vlasov equation. From the above equation it is clear that pressure  $P = k_B T_e n^3/n_0^2$ . So the adiabatic equation of state is valid here. As we are looking for wavelike solutions, all fluid variables viz. density( $n$ ), fluid velocity( $u$ ) and electric field( $E$ ) are functions of a single variable  $\psi = t - x/v_\phi$ , where  $v_\phi$  is the phase velocity of the wave. Substituting  $\partial/\partial x = -(1/v_\phi)d/d\psi$  and  $\partial/\partial t = (d/d\psi)$  in Eqs. (6.5), (6.6) and (6.2) the continuity, momentum equation and Gauss's Law respectively become,

$$n = \frac{1}{(1 - u)} \quad (6.7)$$

$$\frac{d}{d\psi} \left[ u - \frac{u^2}{2} - \frac{\beta}{2} \frac{1}{(1-u)^2} \right] = -E \quad (6.8)$$

and

$$\frac{dE}{d\psi} = \frac{u}{1-u} \quad (6.9)$$

where we have used the normalizations,  $n \rightarrow n/n_0$ ,  $\psi \rightarrow \omega_p \psi$ ,  $u \rightarrow u/v_\phi$ ,  $E \rightarrow eE/m\omega_p v_\phi$  and  $\beta = \frac{3k_B T_e}{mv_\phi^2} = \frac{v_0^2}{v_\phi^2}$ , where the expression for  $n$  has been used in the momentum equation and Gauss's Law. Differentiating the above Eq.(6.8) and using Gauss's Law, we get

$$\frac{d^2 \chi}{d\psi^2} = -\frac{u}{1-u} \quad (6.10)$$

where  $\chi = \left[ u - \frac{u^2}{2} - \frac{1}{2} \frac{\beta}{(1-u)^2} \right]$ . This equation [39] describes the electron plasma wave in its own rest frame when the electron distribution is taken as water-bag distribution. This equation can not be solved analytically. The numerical solution of this equation with proper choice of initial conditions is presented in the next section.

Now multiplying both side of Eq.(6.10) by  $\chi'$  and using  $\chi' = -E$  (where  $'$  represents the derivative *w.r.t*  $\psi$ ), we get

$$\frac{1}{2} \frac{dE^2}{d\psi} = \left[ -u + \frac{\beta u}{(1-u)^4} \right] \frac{du}{d\psi} \quad (6.11)$$

Integrating Eq.6.11, the expression for electric field  $E$  as a function of  $u$  can be written as

$$E^2 = -u^2 - \frac{\beta}{(1-u)^2} + \frac{2\beta}{3} \frac{1}{(1-u)^3} + C_1 \quad (6.12)$$

Here  $C_1$  is the integration constant which we find out by using particle trapping condition in the following way:

Using  $E = -\chi'$ , the wave potential may be written as

$$\Phi = -\chi + C_2 \quad (6.13)$$

where,  $\Phi \rightarrow e\Phi/mv_\phi^2$  and  $C_2$  is another integration constant.

Now from the definition, when a particle at the upper boundary of the water-bag distribution gets trapped by the wave potential (*i.e.* particle at the “water-bag” boundary with velocity  $v_0$  at the crest of the wave potential reaches  $v_\phi$  at the trough



of the wave potential [Bauer *et. al.* [73]], the wave breaks [as shown in Fig.(6.1)]. Now following the Fig.(6.1) the energy conservation can be written as

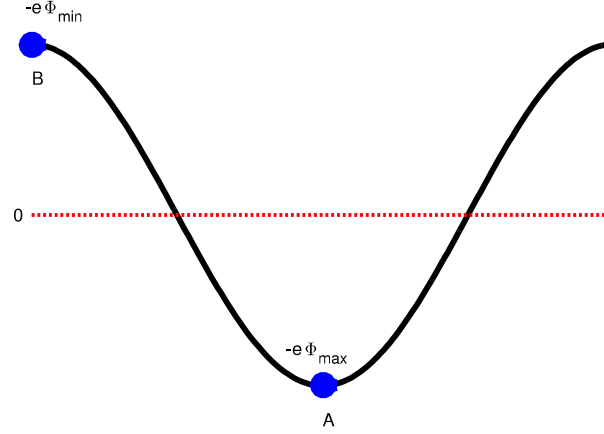


Figure 6.1: Potential energy vs position diagram

$$\frac{m}{2}(v_A - v_\phi)^2 - e\Phi_{max} = \frac{m}{2}(v_B - v_\phi)^2 - e\Phi_{min} \quad (6.14)$$

Mathematically in unnormalised unit, the above equation can be simplified as (in our case  $v_A = v_0$  and  $v_B = v_\phi$ )

$$\frac{1}{2}(v_0 - 1)^2 = -(\Phi_{min} - \Phi_{max}) \quad (6.15)$$

At  $u = 0$ ,  $\Phi = \Phi_{max} = \frac{\beta}{2} + C_2$ , and at  $u = u_m$  (maximum value of the oscillating fluid velocity),  $\Phi = \Phi_{min} = -\left[u_m - \frac{u_m^2}{2} - \frac{1}{2} \frac{\beta}{(1-u_m)^2}\right] + C_2$ . Now substituting the values of  $\Phi_{min}$  and  $\Phi_{max}$  in Eq.(6.15), the expression for the maximum value of the fluid velocity required to trap the particles which are at the boundary of the water-bag distribution stands as

$$u_m = 1 - \beta^{1/4} \quad (6.16)$$

Now, noting that, at  $u = u_m$ ,  $\Phi$  reaches its extreme value and thus  $E = 0$ . Using

this condition in Eq.6.12, the final form of electric field  $E$  as a function of  $u$  becomes

$$E = \left[ -u^2 - \frac{\beta}{(1-u)^2} + \frac{2}{3} \frac{\beta}{(1-u)^3} + (1 - \beta^{1/4})^2 + \beta^{1/2} - \frac{2}{3} \beta^{1/4} \right]^{1/2} \quad (6.17)$$

Now, from Gauss's Law  $E$  is maximum when  $u = 0$ . Therefore,

$$E_{max} = \left( 1 - \frac{8}{3} \beta^{1/4} + 2\beta^{1/2} - \frac{\beta}{3} \right)^{1/2} \quad (6.18)$$

which is Coffey's wave breaking limit.

## 6.3 Particle-In-Cell Simulation

Here we carry out a 1D PIC simulation with periodic boundary conditions in order to study the maximum electric field amplitude that can be sustained by a large amplitude freely running electron plasma wave in a Maxwellian plasma.

### 6.3.1 Simulation Model

Before starting simulation, in this section, we first compute the initial profiles needed to excite a freely running electron plasma wave in a Maxwellian plasma. As mentioned in the previous section, the equation representing the evolution of electron plasma wave in its own rest frame is given by

$$\frac{d^2 \chi}{d\psi^2} = -\frac{u}{1-u} \quad (6.19)$$

To solve Eq.(6.19) two initial conditions *i.e*  $\chi|_{\psi=0}$  and  $\chi'|_{\psi=0}$  are required. We compute these two values by respectively substituting  $u = 0$  (at  $\psi = 0$ ) in the expressions for  $\chi$  and  $\chi'$  (*i.e*  $E$ ). These two values respectively can be written as  $\chi|_{\psi=0} = -\frac{\beta}{2}$  and  $\frac{d\chi}{d\psi}|_{\psi=0} = -\Delta E_{max}$ . Here,  $\Delta = E/E_{max}$  decides the initial amplitude of the wave. As expected from Coffey's theory [36,39], the wave should propagate without any damping or distortion for all values of  $\Delta \leq 1$ . By using these two initial conditions, Eq.(6.19) has been solved numerically for different values of  $\Delta$  and  $\beta$ . Once  $\chi$  and  $\chi'$  are solved, all the fluid variables *viz.*  $u$ ,  $E$  and  $n$  can be computed by respectively using the expression for  $\chi$ ,  $\chi'$  and Eq.(6.7).

As for example, in Figs.(6.2) and (6.3) we have presented the profile of the fluid variables for two different values of  $\Delta$  and  $\beta$  as a function of  $\psi$  upto one wavelength ( $L_p$ , here the wavelength  $L_p$  has been found by measuring the distance between two consecutive peaks in the density amplitude). For a known  $\Delta$  ( $\leq 1$ ) and  $\beta$  value, we load these initial density and velocity profile in our PIC code. Here the wavelength  $L_p$  explicitly depends on  $\Delta$  and  $\beta$ . Thus by changing the values of  $\beta$  and  $\Delta$  different initial profiles required to excite a freely running large amplitude electron plasma wave in a warm plasma have been generated. In the next subsection we load these profiles along with a Maxwellian distribution (with same  $\beta$  value) in our code. We note that although this method of initialization loads a wave that is consistent with the water-bag distribution, we find that within a wave period the wave self-consistently conforms itself with the background Maxwellian distribution supported by trapped and untrapped particle distributions. Further, we also study

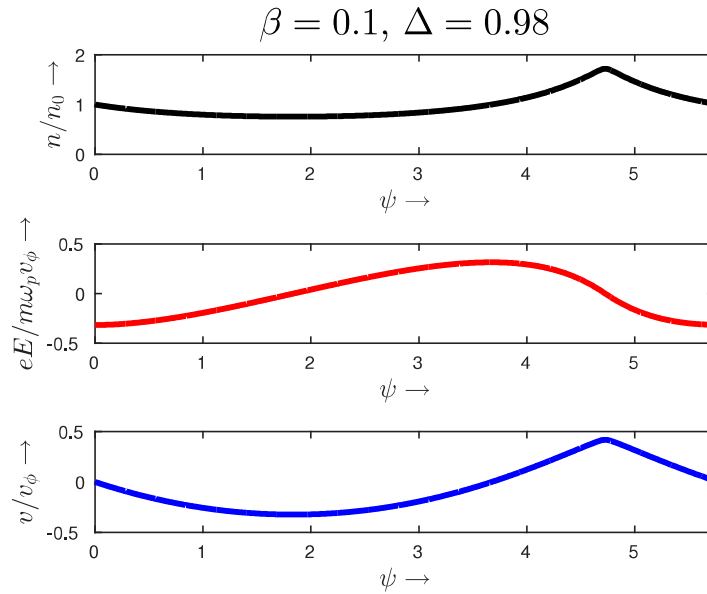


Figure 6.2: Initial profile for  $\beta = 0.1$  and  $\Delta = 0.98$

the stability of these waves (even increasing their initial amplitude beyond Coffey's limit) towards a small amplitude longitudinal perturbation given by

$$E_{per} = \delta \cos(k_{pr}x) \quad (6.20)$$

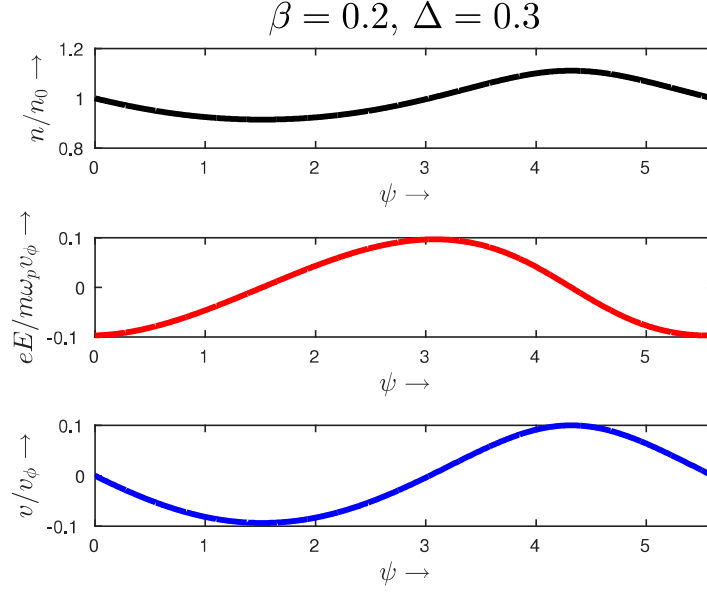


Figure 6.3: Initial profile for  $\beta = 0.2$  and  $\Delta = 0.3$

Here,  $k_{pr}$  is the primary wave number (which contains the highest amplitude) of the initialized wave and  $\delta$  is the amplitude of the applied perturbation of order  $\delta/\Delta \sim 10^{-2}$  to  $10^{-1}$ . This method of studying the stability by using a small amplitude sinusoidal perturbation only to the primary wave number has also been used by other authors [33].

Our simulation parameters are as follows: total number of particles  $N_p = 40000$ , number of grid points  $N_G = 500$ , time step  $\delta t = \pi/160$  and system length  $L = L_p$ , wavelength of the system, which depends on both  $\Delta$  and  $\beta$ . Here we use periodic boundary conditions. The normalisations are chosen to be  $x \rightarrow x\omega_p/v_\phi$ ,  $t \rightarrow \omega_p t$ ,  $n \rightarrow n/n_0$ ,  $v \rightarrow v/v_\phi$ ,  $v_{th} \rightarrow v_{th}/v_\phi$ ,  $E \rightarrow eE/m\omega_p v_\phi$  and  $\Phi \rightarrow e\Phi/mv_\phi^2$ .

### 6.3.2 Results from Simulation and Its Interpretation

In this subsection, we verify Coffey's wave breaking limit in a Maxwellian plasma by loading the initial profile as computed above.

In Figs. 6.4 - 6.7 we have shown the space time evolution of electric field of a freely running electron plasma wave in a Maxwellian plasma for different values of  $\Delta$  for a long period of time by keeping  $\beta$  fixed at 0.1. In Figs. 6.4 and 6.6

the values of  $\Delta$  are respectively taken as 0.5 and 0.98. Their response to a small amplitude longitudinal perturbation given by Eq.(6.20) are respectively presented in Figs. 6.5 and 6.7. In these figures, the electric field profile at  $t = 0$  without perturbation is presented by the blue line and red lines are showing the electric field profile with perturbation.  $\delta$  is taken as 0.05. The Figs. 6.4 - 6.7 clearly show that the wave is propagating without any breaking and losing periodicity throughout the system for a large period of time ( $\sim 100$  plasma periods) even after adding perturbation. From all these figures, we observe that, the maximum amplitude of the initialized wave at  $t = 0$  decreases by a small fraction from its initial value. This is due to the fact that, the initial conditions that we have used in order to carry our numerical experiment to study the evolution of electron plasma wave, are consistent with water-bag distribution. Therefore the initial perturbation takes some time ( $\sim$  few plasma period) to get adjusted with the background Maxwellian distribution. Now, for the value of  $\Delta = 0.5$ , though the wave is perturbed by a small amplitude longitudinal perturbation, the maximum electric field amplitude after adding perturbation remains below the Coffey's limit ( $eE_{max}/m\omega_p v_\phi = 0.3155$  from Eq.6.11), as for example,  $eE_{max}/m\omega_p v_\phi = 0.2564$  (measured from Fig. 6.5, at  $t = 0$ ). But, in Fig. 6.7 the response to a small amplitude perturbation for  $\Delta = 0.98$  shows that, even the maximum electric field amplitude after adding the perturbation becomes greater than Coffey's limit at  $t = 0$  ( $eE_{max}/m\omega_p v_\phi = 0.3649$ , measured from Fig. 6.7), within  $\sim 1$  plasma periods the wave self-consistently adjusts itself by reducing the maximum electric field amplitude below Coffey's limit and propagates through the system. After adjustment, the amplitude of the maximum electric field amplitude changes hardly with time. This can be observed explicitly in Figs. 6.8 and 6.9, where we have shown the time evolution of Fourier spectrum of the electric field for  $\Delta = 0.98$  without and with perturbation respectively at the same instants. The figures clearly indicate that, there is hardly any differences between them after the time  $\omega_p t = 2\pi$  and the maximum amplitude remains nearly constant. We have verified our results by changing the amplitude  $\delta$  from 0.05 to 0.1. It is observed that after adding perturbation at  $t = 0$ , the amplitude of the initialized wave may go beyond the Coffey's limit, but after  $\sim 1$  plasma period the amplitude goes below the Coffey's limit and saturates at an amplitude which does not increase even after increasing the amplitude of the applied perturbation  $\delta$ . This amplitude is strictly

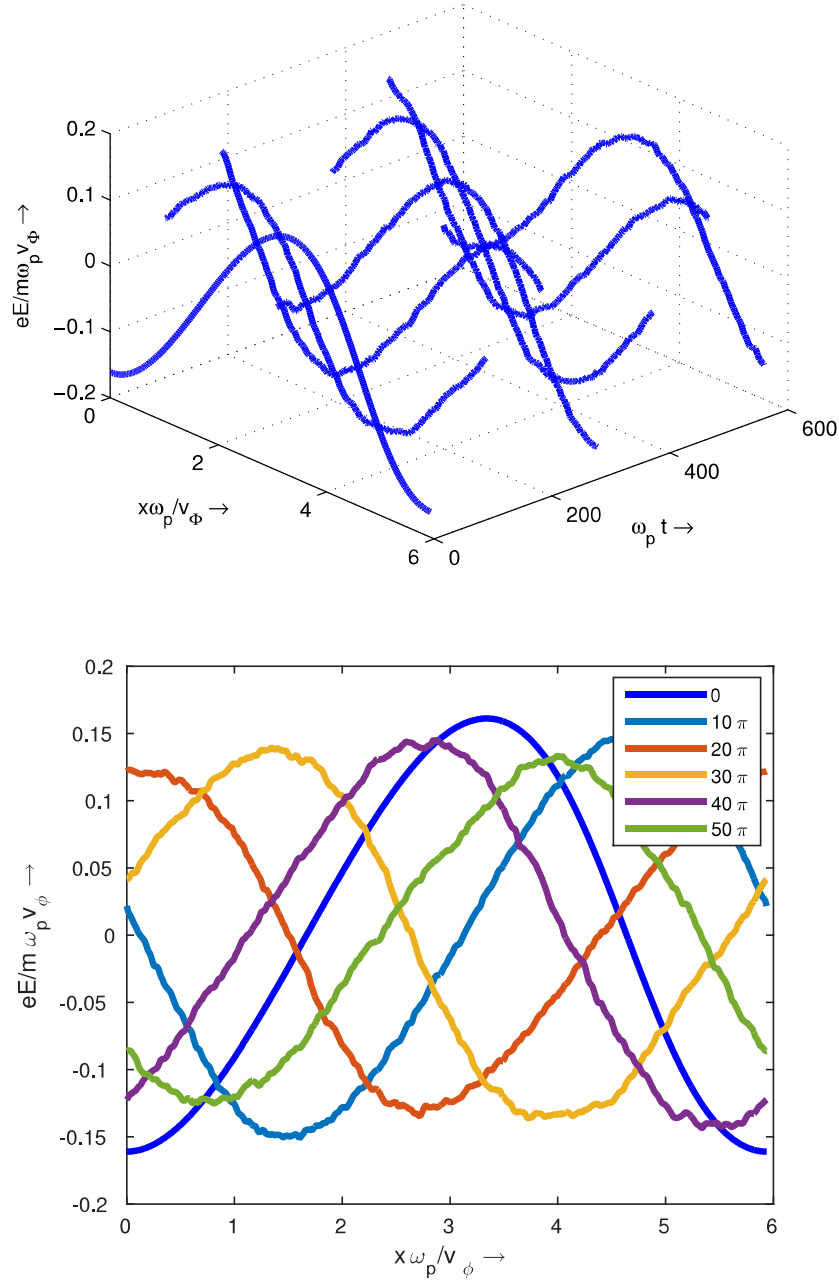


Figure 6.4: Space-time evolution of electric field (3D up, 2D down) for  $\beta = 0.1$  and  $\Delta = 0.5$  without any perturbation [ $eE_{max}/m\omega_p v_\phi$  at  $t = 0$  is below Coffey's limit (0.3155)].

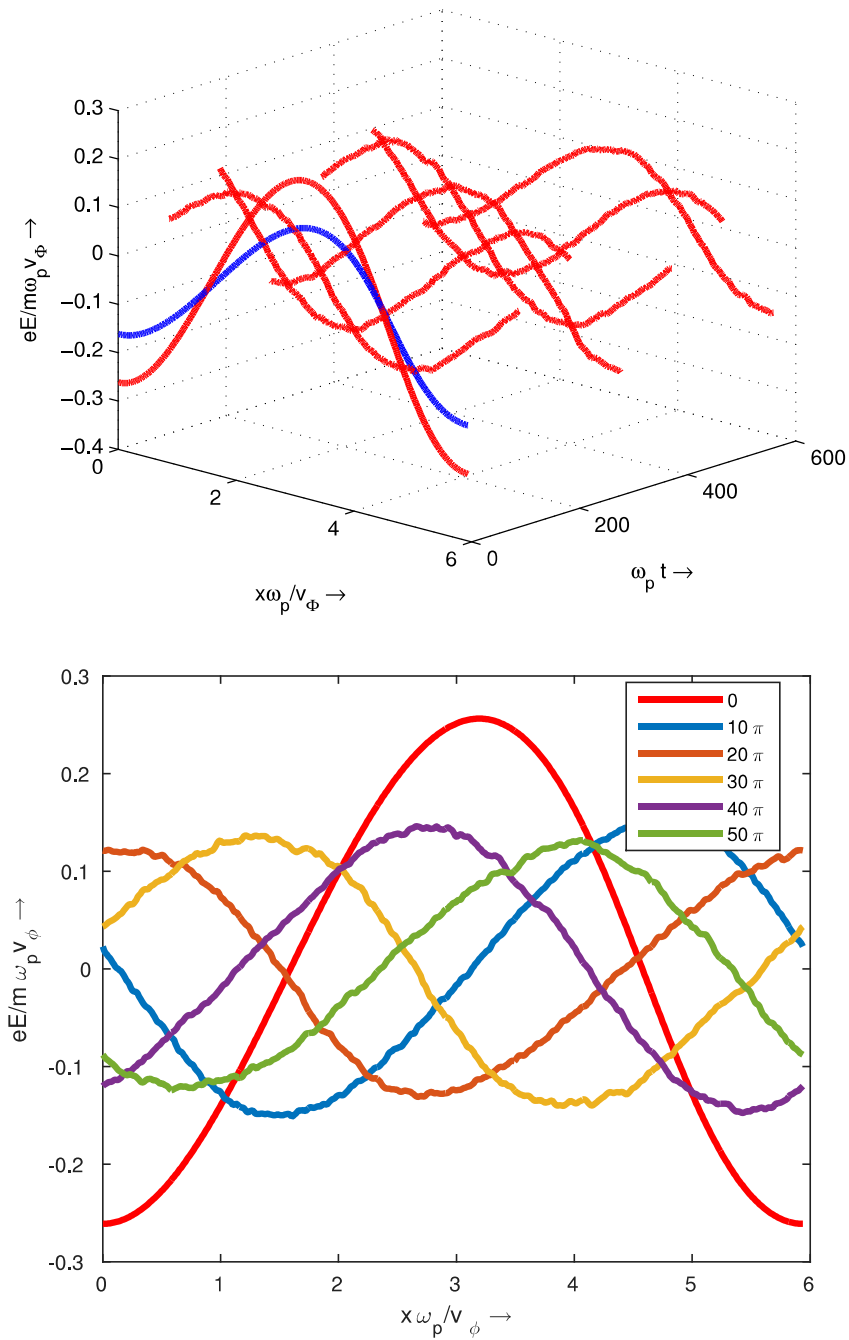


Figure 6.5: Space-time evolution of electric field (3D up, 2D down) for  $\beta = 0.1$  and  $\Delta = 0.5$  with a small amplitude perturbation [ $eE_{max}/m\omega_p v_\phi$  at  $t = 0$  is below Coffey's limit (0.3155)].

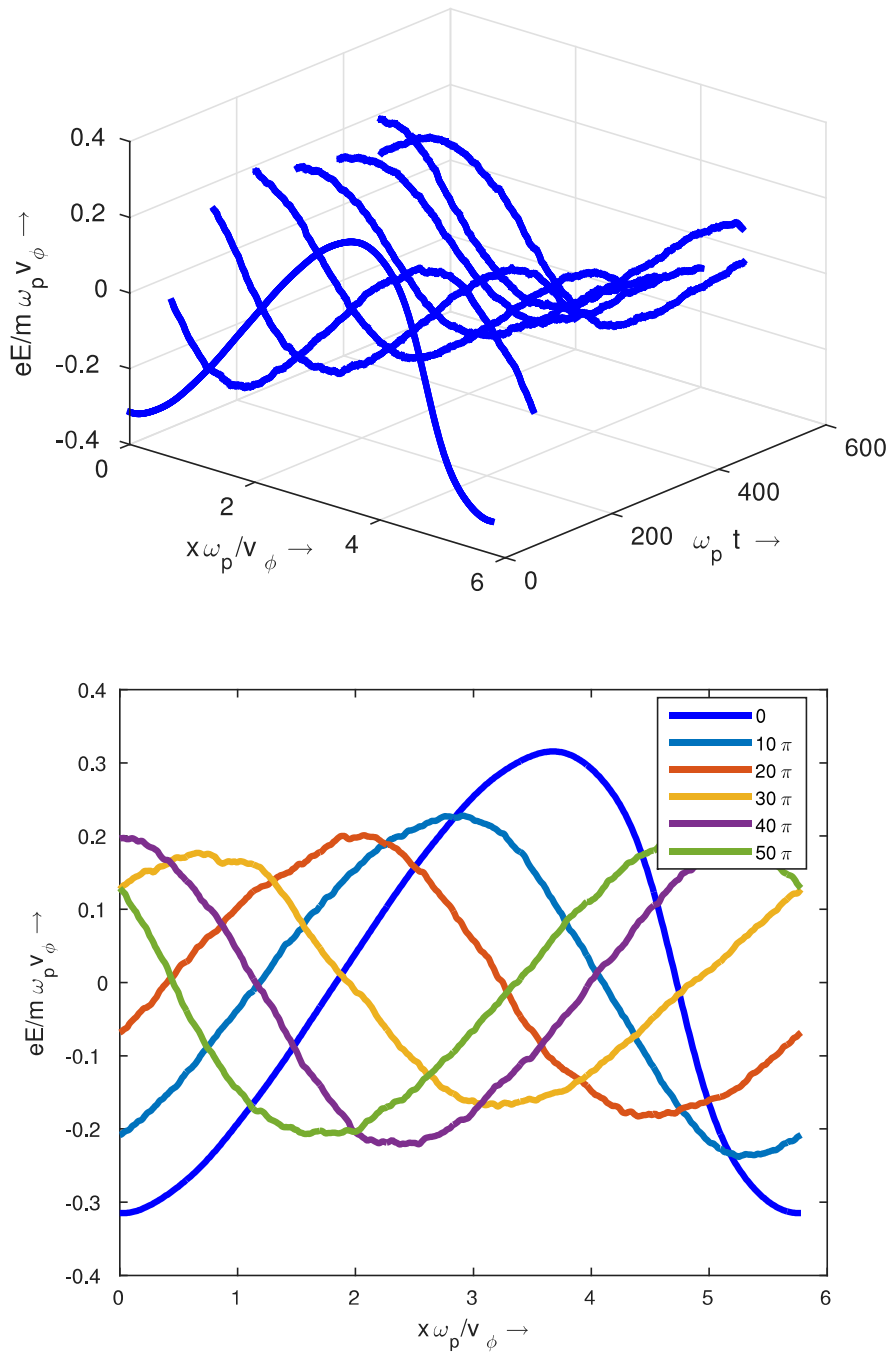


Figure 6.6: Space-time evolution of electric field (3D up, 2D down) for  $\beta = 0.1$  and  $\Delta = 0.98$  without any perturbation [ $eE_{max}/m\omega_p v_\phi$  at  $t = 0$  is below Coffey's limit (0.3155)].



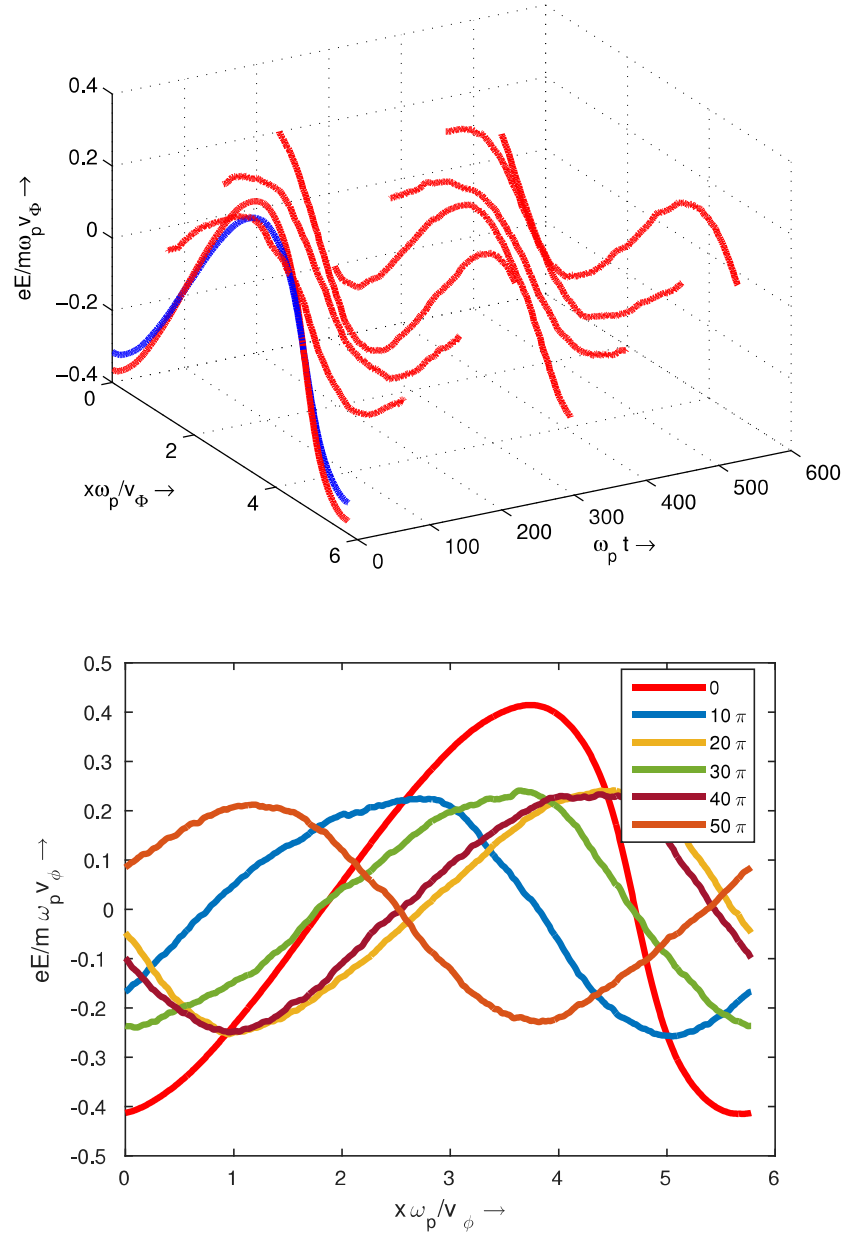


Figure 6.7: Space-time evolution of electric field (3D up, 2D down) for  $\beta = 0.1$  and  $\Delta = 0.98$  with a small amplitude perturbation ( $eE_{max}/m\omega_p v_\phi$  at  $t = 0$  is beyond Coffey's limit, 0.3155).

decided by the background electron's distribution which are making the wave and can be taken as the maximum electric field amplitude  $E_{max}$  that can be sustained by a freely running electron plasma wave in a Maxwellian plasma. We next

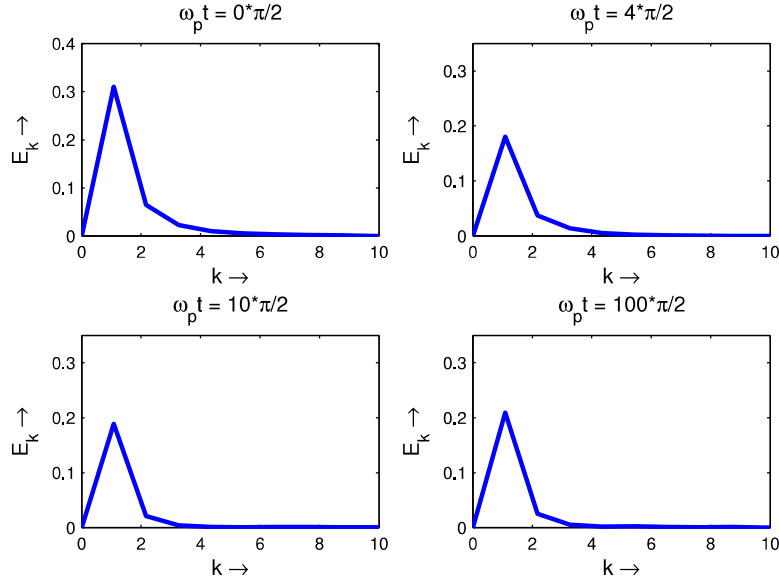


Figure 6.8: Snapshots of Fourier spectrum for  $\beta = 0.1$  and  $\Delta = 0.98$  without any perturbation [ $eE_{max}/m\omega_p v_\phi$  at  $t = 0$  is below Coffey's limit (0.3155)].

perform a thorough scan over  $v_{th}/v_\phi$  by varying the value of  $\beta (= 3v_{th}^2/v_\phi^2)$  from 0.1 to 0.25. The value of  $\Delta$  in each case is kept close to Coffey's wave breaking limit. As examples we present the wave profile (Figs. 6.10 - 6.13) for  $\beta = 0.15$  &  $\beta = 0.2$  without and with perturbation. For each value of  $\beta$  we have measured the maximum electric field amplitude  $E_{max}$  from our simulation results at a time when the wave self-consistently conforms itself with the background distribution. The magenta points in Fig. 6.14 show the values of  $E_{max}$  for different values of  $\beta$  measured from simulation. To compare our simulation results with Coffey's wave breaking limit (Eq. 6.11), the maximum electric field amplitudes (without applied perturbation) at  $t = 0$  are also plotted with red dots. These red dots are basically the numerical solution of Eq. 6.19. We observe that, the maximum electric field amplitude sustained by a electron plasma wave in a Maxwellian plasma is not as large as predicted by Coffey for a water-bag distribution. But it follows the same

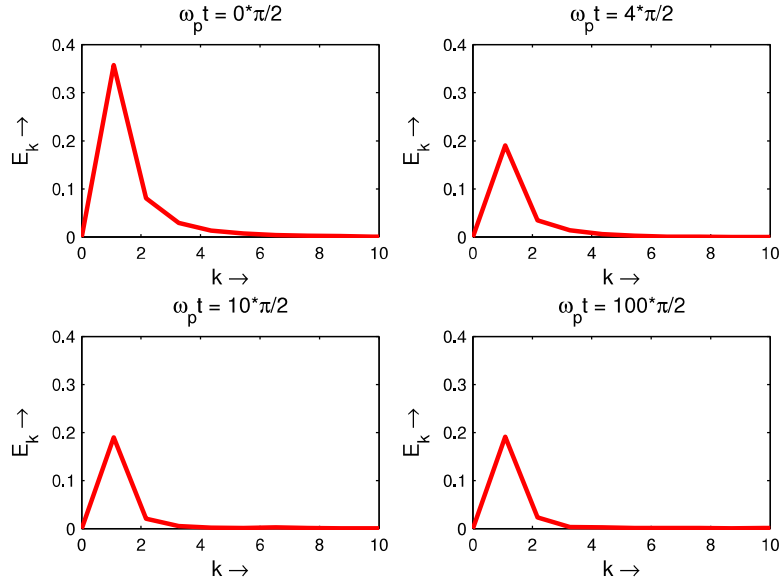


Figure 6.9: Snapshots of Fourier spectrum for  $\beta = 0.1$  and  $\Delta = 0.98$  with a small amplitude perturbation ( $eE_{max}/m\omega_p v_\phi$  at  $t = 0$  is beyond Coffey's limit, 0.3155).

scaling of  $\beta$  with different coefficients, which can be written as

$$E_{Maxwellian} = (1 - 2.84\beta^{1/4} + 2.06\beta^{1/2} - 0.07\beta)^{1/2} \quad (6.21)$$

These coefficients have been obtained by performing a least square fit of the simulation data.

Here, we would like to mention that, as  $\Delta$  and  $\beta$  change, frequency changes accordingly (as all velocities are normalized to  $v_\phi$ ), which results in different system length (plasma wavelength  $L_p$ ). Therefore Landau Damping rate of these waves also changes with  $\Delta$  and  $\beta$ . For a given  $\beta$  (say  $\beta = 0.1$ ), as  $\Delta$  varies from 0.2 to 0.98,  $k\lambda_D$  varies from 0.191 to 0.199. Therefore Landau damping rates ( $\gamma/\omega_p$ ) respectively range from  $6.24 \times 10^{-5}$  to  $1.62 \times 10^{-4}$ . For higher values of  $\beta$  (say  $\beta = 0.3$ ), as  $\Delta$  varies from 0.1 to 0.88,  $k\lambda_D$  varies from 0.3777 to 0.3932. Landau damping rates for these wave range from 0.2174 to 0.2536, resulting in decay of wave in  $\sim 5$ -6 plasma periods. Thus to verify Coffey's limit, we have limited our values of  $\beta$  to  $\beta < 0.3$ . For clarity in Fig.(6.15) we have shown the time evolution of electrostatic energy of an electron plasma wave for  $\beta = 0.35$  and  $\Delta = 0.1$ . From the figure we observe that, the energy decreases exponentially with time and

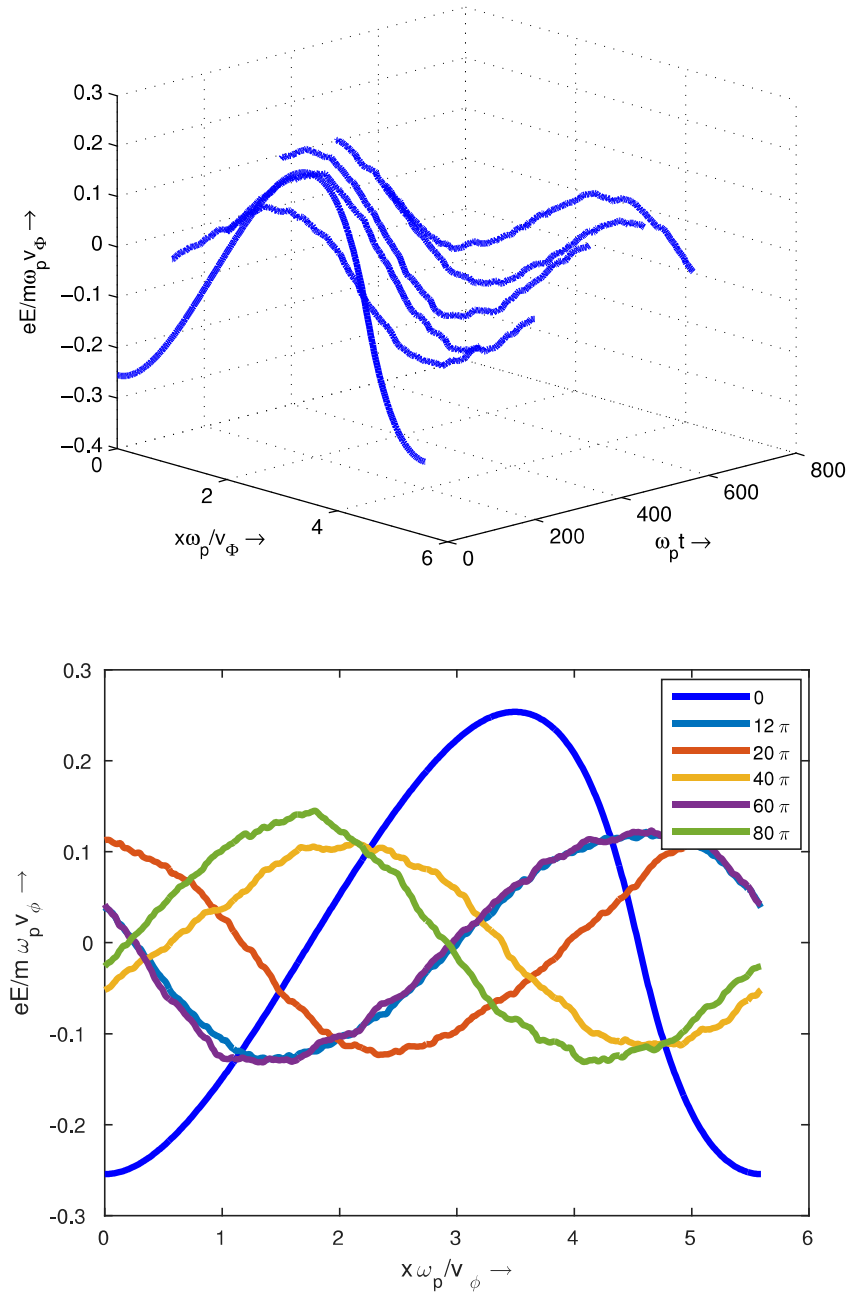


Figure 6.10: Space-time evolution of electric field (3D up, 2D down) for  $\beta = 0.15$  and  $\Delta = 0.965$  without any perturbation [ $eE_{max}/m\omega_p v_\phi$  at  $t = 0$  is below Coffey's limit (0.2510)].

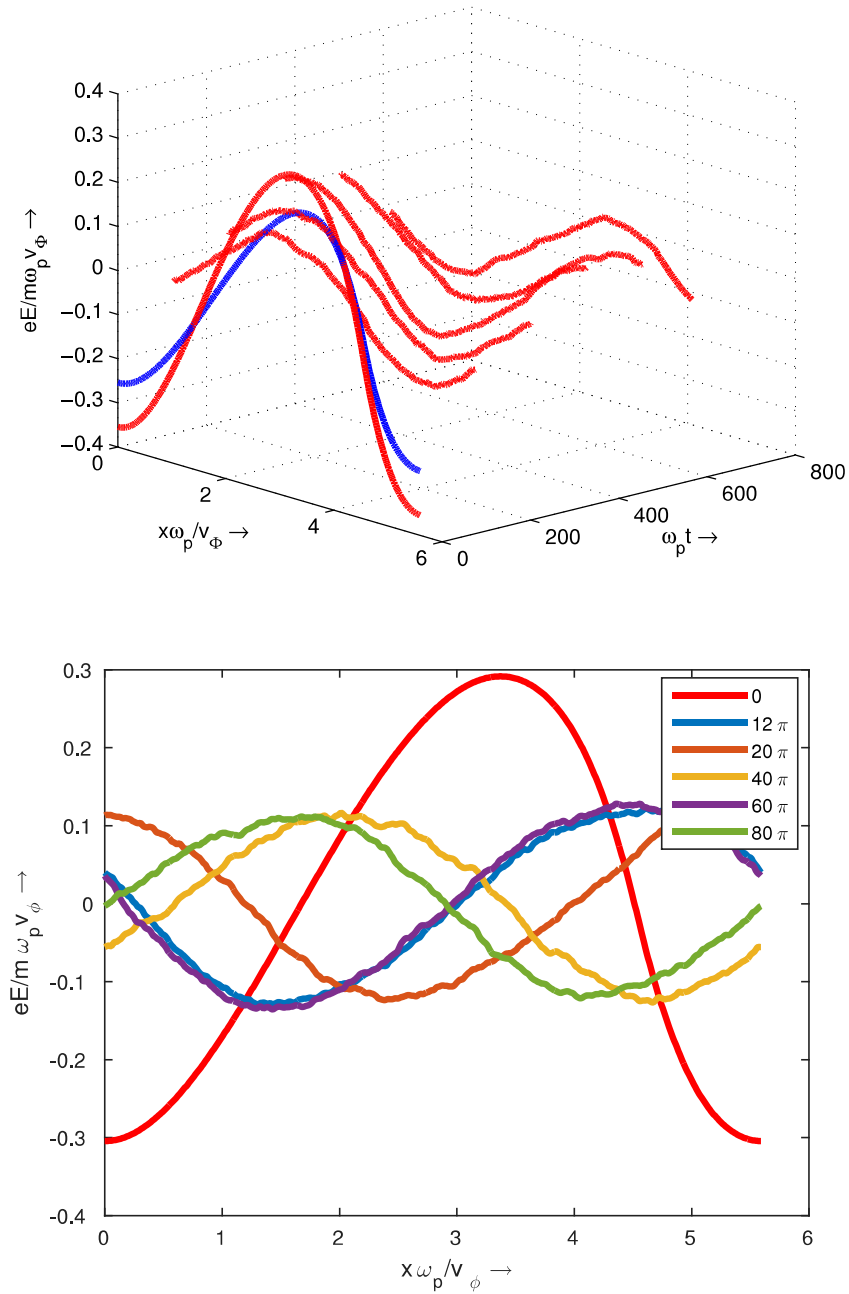


Figure 6.11: Space-time evolution of electric field (3D up, 2D down) for  $\beta = 0.15$  and  $\Delta = 0.965$  with a small amplitude perturbation [ $eE_{max}/m\omega_p v_\phi$  at  $t = 0$  is beyond Coffey's limit (0.2510)].

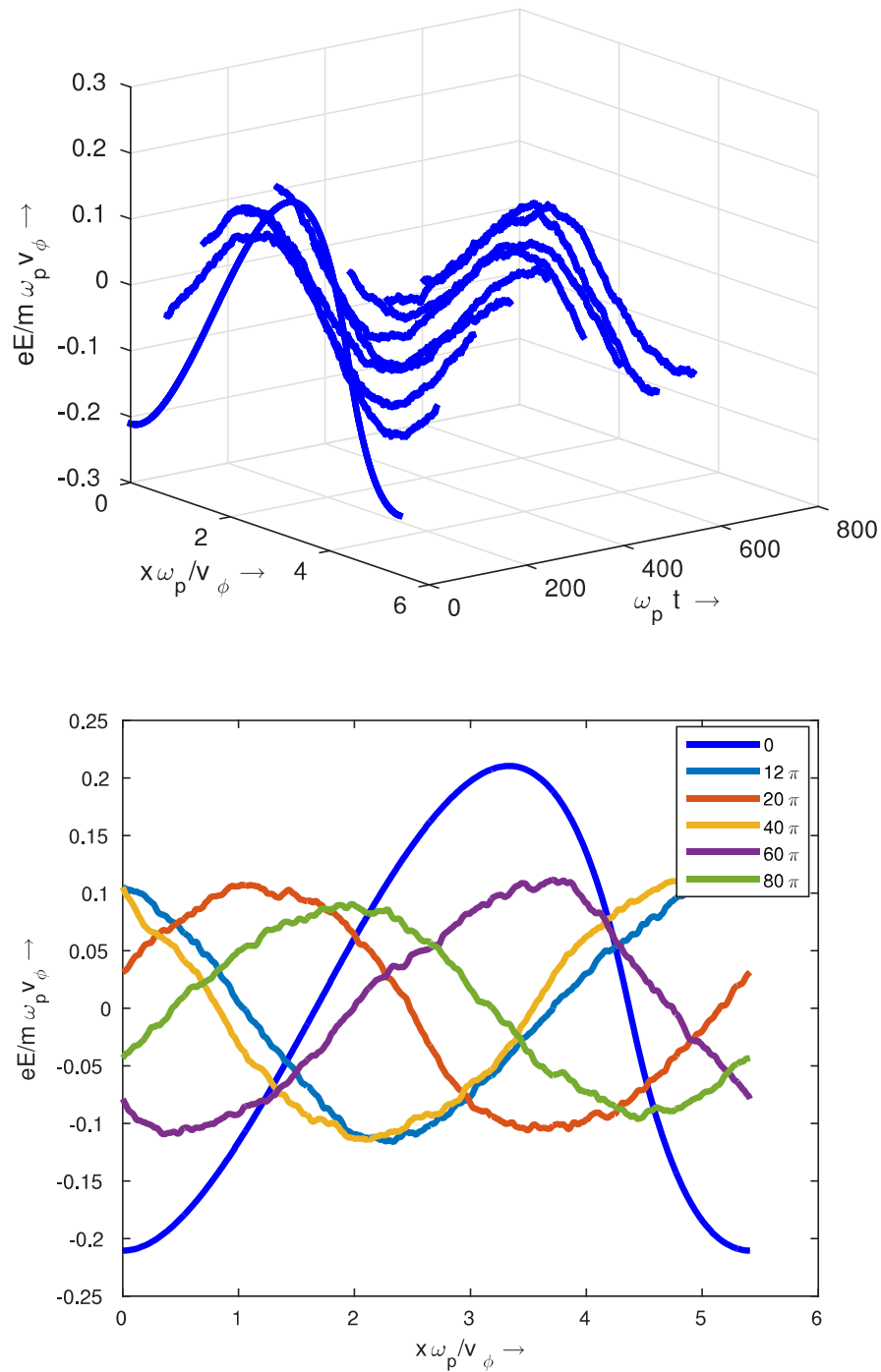


Figure 6.12: Space-time evolution of electric field (3D up, 2D down) for  $\beta = 0.2$  and  $\Delta = 0.9455$  without any perturbation [ $eE_{max}/m\omega_p v_\phi$  at  $t = 0$  is below Coffey's limit (0.2054)].

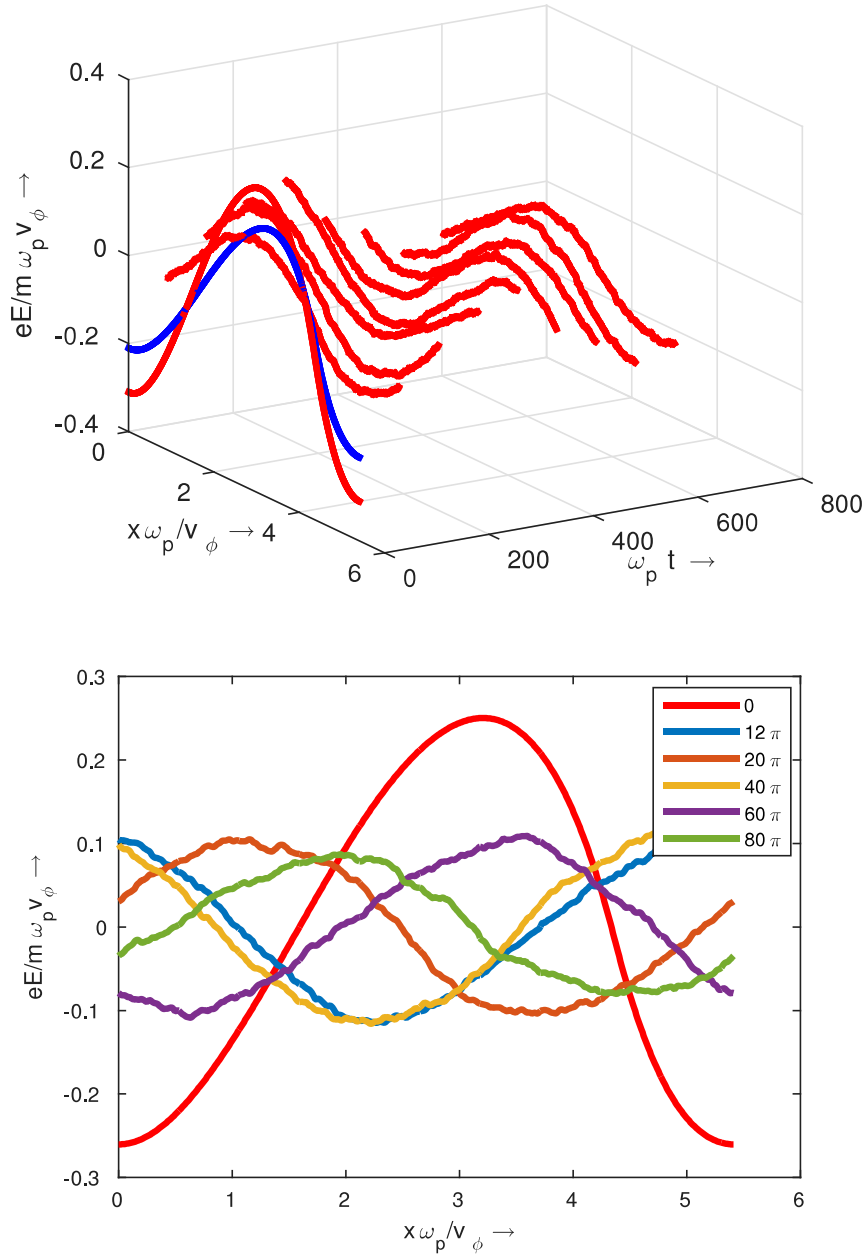


Figure 6.13: Space-time evolution of electric field (3D up, 2D down) for  $\beta = 0.2$  and  $\Delta = 0.9455$  with a small amplitude perturbation ( $eE_{max}/m\omega_p v_\phi$  at  $t = 0$  is beyond Coffey's limit, 0.2054).

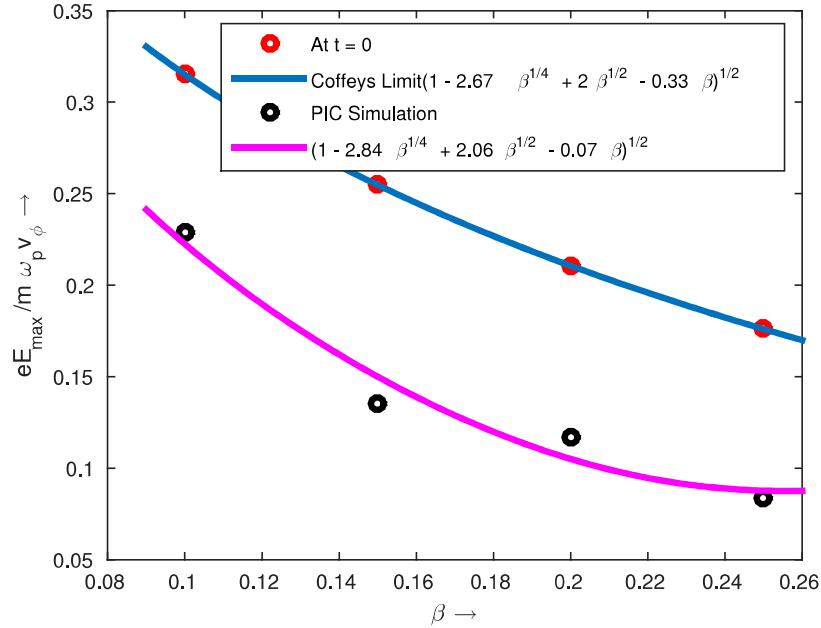


Figure 6.14:  $E_{max}$  as a function of  $\beta$

follows the theoretical Landau damping rate (shown by blue line) [1].

## 6.4 Summary

The maximum amplitude sustained by a large amplitude electron plasma wave in a Maxwellian has been studied using a Particle-in-Cell code. It is shown that Coffey's propagating wave solution which was derived by using a Water Bag distribution for electrons also represents a propagating wave albeit with a lower amplitude in a Maxwellian plasma. The stability of these waves towards a small amplitude longitudinal perturbation has been studied and it is observed that if the maximum amplitude of the initial perturbation exceeds  $[E_{Maxwellian}$  [given by Eq.(6.21)], within  $\sim$  few plasma period the initialized wave self-consistently conforms itself with the background distribution and propagates with an amplitude given by Eq.(6.21) for a large period of time ( $\sim 100$  plasma periods). This amplitude does not increase even after increasing the amplitude of the applied perturbation. By varying the initial electron temperature it has been found that the maximum electric field amplitude sustained by a self-consistent electron plasma wave in a Maxwellian plasma



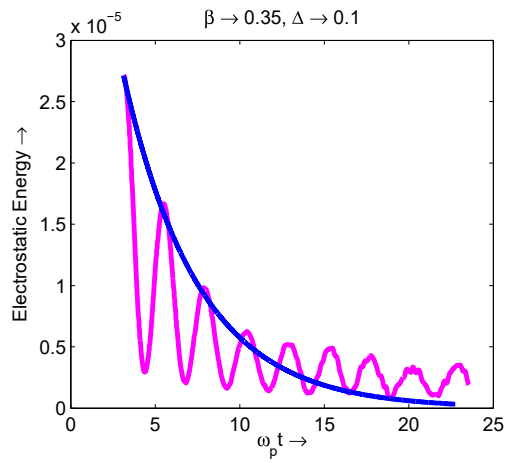


Figure 6.15: Time evolution of electrostatic energy for  $\beta = 0.35$  and  $\Delta = 0.1$

follows the similar scaling with electron temperature  $\beta$  given by Coffey but with different coefficients.

*Not only is the Universe  
stranger than we think, it is  
stranger than we can think.*

- Werner Heisenberg

# 7

## Breaking of Large Amplitude Relativistically Intense Electron Plasma Waves in a Warm Plasma

In this chapter, by performing Particle-in-Cell (PIC) simulations, we explicitly illustrate the effect of finite electron temperature on the space-time evolution and breaking of a large amplitude relativistically intense electron plasma wave. For this purpose we load a Jüttner-Synge [58] velocity distribution along with a Akhiezer - Polovin [27] type (travelling wave) initial condition in our code. We first show that for phase velocities for which  $\gamma_\phi \ll 1 + \frac{k_B T_e}{mc^2}$ , the wave damps within a few plasma period and essentially follows the relativistic Landau Damping rate predicted by Buti [59]. In the opposite regime (*i.e.* for  $\gamma_\phi \gg 1 + \frac{k_B T_e}{mc^2}$ ) we find that waves propagate through the system for a long period of time and in small amplitude limit follow the relativistic warm plasma dispersion relation [59–63]. Further we demonstrate that in the same regime (*i.e.* for  $\gamma_\phi \gg 1 + \frac{k_B T_e}{mc^2}$ ), for the phase velocities less than the velocity of light  $c$ , like the cold plasma Akhiezer - Polovin wave [33], in a warm plasma also, relativistically intense waves break via phase mixing when perturbed by an arbitrarily small amplitude longitudinal perturbation. Using our simulation results, we also show that the phase mixing time scale in a warm plasma can be interpreted using Dawson's formula [5] for phase mixing time for a non-relativistic cold inhomogeneous plasma, which is based on out of phase motion of neighbouring oscillators constituting the wave.

## 7.1 Introduction

This is the last topic that we explore in this thesis. In the previous chapter we have verified Coffey's [36] wave breaking limit for a Maxwellian plasma. Here we extend our previous study in the relativistic regime where the relativistic mass variation effects of the electrons are taken into account. Unlike the nonrelativistic warm plasma case, where Coffey's limit is the one and only existing theoretical wave breaking limit available in the literature (till date), the relativistic counterpart contains several theoretical results given by several group of authors in last three decades. These are as follows:

In 1988, Katsouleas and Mori [37,39], first extended the calculations carried out by Coffey [36] by including relativistic mass variation effects. By using a relativistic water bag model, an analytical expression for the maximum electric field amplitude ( $E_{KM}$ ) that can be sustained by a relativistically intense electron plasma wave in a warm plasma has been derived as a function of electron temperature and Lorentz factor ( $\gamma_\phi$ ), which can be written as

$$\frac{eE_{KM}}{m\omega_p c} = \lambda^{-1/4} \left[ \ln(2\gamma_\phi^{1/2} \beta^{1/4}) \right]^{1/2} \quad (7.1)$$

where  $\lambda = 3k_B T_e / mc^2$  is the normalised electron temperature. The authors [37, 39] strictly mentioned that the above expression [Eq.(7.1)] is valid only in the ultrarelativistic regime which is defined as  $\gamma_\phi^2 \lambda \gg 1$ . In the same year Rosenzweig [38] presented another expression of maximum electric field amplitude ( $E_{ROS}$ , in the limit  $v_\phi \rightarrow c$ ) as a function of electron temperature. The analytical expression for  $E_{ROS}$  is given by

$$\frac{eE_{ROS}}{m\omega_p c} = \left[ \frac{4}{9\lambda} \right]^{1/4} \quad (7.2)$$

Similar wave breaking limit [same as Eq.(7.2)] was obtained by Sheng and Meyerter-Vehn [40] in 1997, using a different set of equations [79–81]. Recently Schroeder *et. al.* [41, 42] proposed a new model of relativistic warm fluid theory and derived the following two expressions for wave breaking amplitude ( $E_{SES}$ ) in the limits  $\gamma_\phi^2 \lambda \gg 1$  and  $\gamma_\phi^2 \lambda \ll 1$  (laser wake field regime) respectively. These expressions

respectively can be written as

$$\left[ \frac{eE_{SES}}{m\omega_p c} \right]^2 = \left( \frac{2}{3} \right)^{3/2} \left( \frac{\lambda}{3} \right)^{-1/2} \left[ 1 - \left\{ \frac{\lambda}{2} \right\}^{1/2} \right]^3 \quad (7.3)$$

$$\left[ \frac{eE_{SES}}{m\omega_p c} \right]^2 = 2(\gamma_\phi - 1) - \gamma_\phi \left[ \frac{4}{3} (\gamma_\phi^2 \lambda)^{1/4} - (\gamma_\phi^2 \lambda)^{1/2} \right] \quad (7.4)$$

Later Trines *et. al.* [43] extended the calculations of Katsouleas & Mori [37,39] to the regime  $\gamma_\phi^2 \lambda \ll 1$  and derived the following expression of wave breaking limit

$$\left[ \frac{eE_{TN}}{m\omega_p c} \right]^2 = 2(\gamma_\phi - 1) - 2\gamma_\phi \left[ (\gamma_\phi^2 \lambda)^{1/4} - (\gamma_\phi^2 \lambda)^{1/2} \right] \quad (7.5)$$

All these theoretical results [37–43] clearly indicate that, thermal effects significantly reduces the wave breaking limit from the cold plasma Akhiezer - Polovin limit [27] ( $E_{AP}$ ). Physically it is expected, because the tendency of plasma density to increase to infinity at the breaking point is opposed by the thermal pressure term and the inclusion of thermal velocity of the particles in the direction of wave propagation enables them to get trapped at a lower amplitude of the wave.

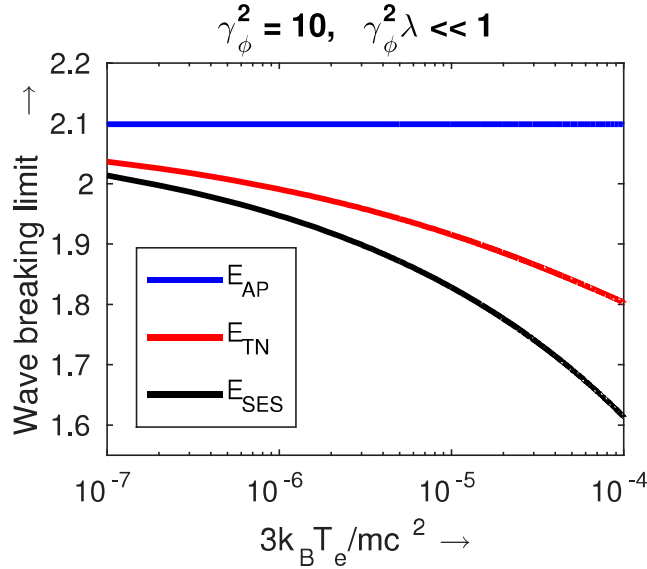


Figure 7.1: Wave breaking limit as a function of  $\lambda$  in laser wake field regime

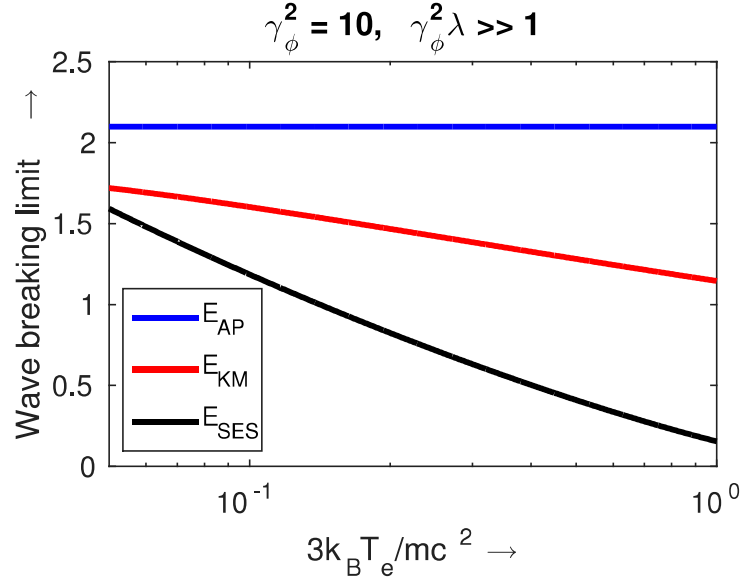


Figure 7.2: Wave breaking limit as a function of  $\lambda$  in ultrarelativistic regime

It should be noted here that, considerable amount of work has been contributed by several authors [37–43] to this subject over past three decades, mainly focusing on the theoretical analysis by assuming wave like solutions of relativistic Vlasov - Maxwell's equation and these results sometimes lead to different conclusions [43, 108, 109]. As for example, in Figs.(7.1) and (7.2) we have shown the variation of wave breaking limits derived by different authors (as discussed above) as a function of electron temperature  $\lambda (= 3k_B T_e / mc^2)$  for a fixed value of Lorentz factor ( $\gamma_\phi^2 = 10$ ). These figures clearly show differences in results obtained by different authors [37, 39, 41–43] even in the same parameter domain. The only similarity is that all the expressions in the regime  $\gamma_\phi^2 \lambda \ll 1$  approach the cold plasma Akhiezer - Polovin [11, 27] limit ( $E_{AP}$ ) in the limit  $\lambda \rightarrow 0$ . Here we would like to mention that although Trines *et. al.* [43, 108, 109] have made some attempt to resolve the above differences by giving mathematical arguments which are essentially based on Taub's inequality [110] and closure of the hierarchy of the relativistic fluid equations, but to the best of our knowledge, till date there is no consensus on a suitable theoretical model expression for studying the breaking of relativistically intense electron plasma waves in a thermal plasma. So at this present situation, it is imperative to conduct a numerical experiment on the space-time evolution and

breaking of a large amplitude relativistically intense plasma wave in a warm plasma with a relativistically correct velocity distribution. Thus, finally in this last chapter we carry out Particle-in-Cell (PIC) simulations in order to investigate the effect of electron temperature on the breaking of a relativistically intense electron plasma wave in a warm plasma where electron's velocity distribution is a Jüttner [58].

Our first aim would be to excite a travelling wave with relativistic speed in a Jüttner -Synge [58] plasma which propagates without damping for a large period of time and next to check its sensitivity towards a small amplitude longitudinal perturbation. Because it is also very crucial to check whether the above limits hold in the presence of a small amplitude perturbations or do they phase mix [29–33] like cold plasma Akhiezer - Polovin wave; as in a realistic experiment, there will always be some noises associated with the excited wave. From the present understanding it is expected that due to the applied perturbation, the characteristic frequency would acquire a spatial dependency which would lead to phase mixing [29–33]. Therefore, we measure the characteristics frequency of the wave at each position in space, for both the cases without and with the external perturbation.

Thus in order to reach our goal, in section 7.2, we first load Akhiezer - Polovin type initial conditions (parametrized by amplitude  $u_m$  and phase velocity  $\beta_\phi$ ) in our PIC code. Along with this, we also load a finite electron temperature (Jüttner - Synge distribution) to the background. Here we note that, the inclusion of non-zero electron temperature would try to damp the excited wave within a few plasma period by relativistic Landau damping effect - which would swamp out the wave breaking physics. This damping rate crucially depends on the phase velocity of the wave and the background electron temperature. It is expected that damping would be negligible for phase velocities near the velocity of light  $c$ . Therefore at the beginning we clearly delineate parameter regimes where either the phenomenon of Relativistic Landau Damping (regime 1) or the phenomenon of wave breaking (regime 2) would be dominant. In regime 1, we observe that the damping rate essentially follows the relativistic Landau damping rate derived first by Buti [59] in 1962. In the opposite regime (regime 2), we find that without any external perturbation the resultant wave propagates through the system for a long period of time and, in the low amplitude limit, it follows the relativistic warm plasma dispersion relation first given by Buti [59] and later derived by several other authors [60–63]. Further we find that, like a cold plasma Akhiezer - Polovin

wave, in a warm plasma also relativistically intense wave breaks when perturbed by an arbitrarily small amplitude longitudinal perturbation. Breaking occurs at an amplitude far below the existing theoretical limits [37–43] presented in the literature. We demonstrate that this breaking is a manifestation of the phase mixing phenomena [29–33], as mentioned above. We clearly show that after adding the external perturbation the characteristic frequency of the wave indeed becomes an explicit function of space which lead to wave breaking via phase mixing at an amplitude which is well below the existing theoretical limits. Further in section 7.3 we show that the results obtained from simulation indicate that the phase mixing time scale in a warm plasma can be interpreted using Dawson’s formula [5] for a non-relativistic cold inhomogeneous plasma, which is based on out of phase motion of neighbouring oscillators constituting the wave and separated by a distance equal to twice the amplitude of the oscillation/wave. Finally in section 7.4 we summarize this work and conclude.

## 7.2 Relativistic Particle-in-Cell Simulations Results

In this section we perform PIC simulations (method discussed in chapter-2) with periodic boundary conditions in order to study the effect of finite electron temperature on the maximum electric field amplitude that can be sustained by a relativistically intense electron plasma wave in a warm plasma. For this purpose we first load Akhiezer - Polovin [27] type initial conditions in our relativistic PIC code. Along with this a finite temperature is also added to the electrons by loading a Jüttner - Synge [58] velocity distribution which can be expressed as (loaded using inversion method [48], discussed in chapter -2):

$$f(p) = \frac{1}{2mcK_1(\frac{mc^2}{k_B T_e})} \exp \left[ -\frac{mc^2}{k_B T_e} \sqrt{1 + \frac{p^2}{m^2 c^2}} \right] \quad (7.6)$$

Here  $K_1$  is the modified Bessel function of second kind [97]. In terms of  $\lambda$ , Eq.(7.6) can be written as

$$f(p) = \frac{1}{2mcK_1(\frac{3}{\lambda})} \exp \left[ -\frac{3}{\lambda} \sqrt{1 + \frac{p^2}{m^2 c^2}} \right] \quad (7.7)$$

Ions are assumed to be infinitely massive providing a neutralizing positive background. Our simulation parameters are as follows: total number of particles  $N_p = 80,000$ , number of grid points  $N_G = 500$ , time step  $\Delta t = \pi/160$ . We use periodic boundary condition where the wavelength  $L$  depends on the amplitude of the Akhiezer - Polovin wave which in turn is decided by its input parameters  $u_m$  and  $\beta_\phi$ . Normalizations are as follows:  $x \rightarrow x\omega_p/c$ ,  $t \rightarrow \omega_p t$ ,  $n_e \rightarrow n_e/n_0$ ,  $v \rightarrow v/c$ ,  $p \rightarrow p/mc$ ,  $E \rightarrow eE/m\omega_p c$ . In the following two subsections, we present the results obtained from the relativistic PIC simulations carried out in the respective regimes where the relativistic Landau damping (regime 1) & wave breaking (regime 2) are dominant.

### 7.2.1 Regime 1 - Relativistic Landau Damping

We have already mentioned that our goal is to verify the existing theoretical results [37–43] on the maximum electric field amplitude that can be sustained by a relativistically intense wave in a warm plasma. For this purpose at the outset we should ensure ourself that the other effects would not interfere with the wave propagation. As the plasma under investigation contains a non-zero electron temperature, therefore it is possible that the temperature effect would try to damp the wave. As the waves are relativistically intense, here the reason for damping would be Relativistic Landau damping - first discovered by Buti [59] in 1962. By linearising relativistic Vlasov - Poisson's equations Buti [59] first wrote down the relativistic Landau damping rate ( $\epsilon$ ), which in the limit  $k_B T_e \gg mc^2$  can be expressed as [59]

$$\epsilon = -\frac{1}{4}\pi ck \left[ 1 - \frac{3\lambda}{4} \right] \quad (7.8)$$

The author [59] also mentioned that, “the damping is very strong in the case where phase velocity is small compared to  $c$ ”. In Fig.(7.3), we have shown the time evolution of electrostatic energy obtained from simulation for  $\beta_\phi = 0.5$ ,  $u_m = 0.1$ ,  $\lambda = 3$  in magenta colour. The blue line is the relativistic landau damping rate derived by Buti [59]. This figure shows that the damping rate follows the theoretical predictions made by Buti [59] which is given by Eq.(7.8). This damping rate decreases significantly as  $\beta_\phi$  increases. From the complete analysis of relativistic Landau damping rate it is shown that the damping rate is very small for wave



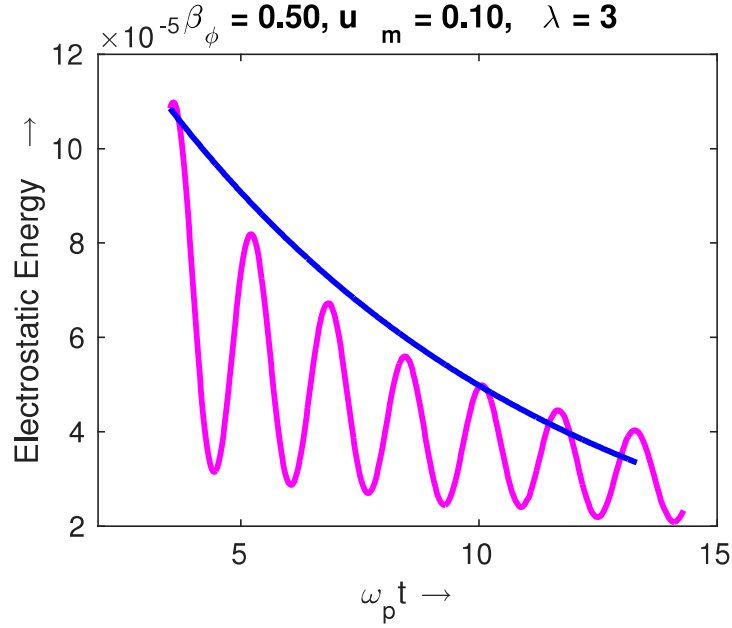


Figure 7.3: Time evolution of electrostatic energy at a fixed grid point for  $\beta_\phi = 0.5$ ,  $u_m = 0.1$ ,  $\lambda = 3$

Lorentz factor  $\gamma_\phi \gg 1 + \lambda/3$  [59,63]. When this inequality is reversed the damping becomes very strong and swamps out the wave propagation and hence the wave breaking physics.

For the sake of clarity, here we have shown a schematic diagram of relativistic velocity distribution function [Fig.(7.4)] where we have roughly depicted the parameter regimes (for  $\lambda = 1$ ) where either relativistic Landau damping or wave breaking would be dominant. From this figure we understand that to study wave breaking we need to work in the regime between the vertical black (corresponding to  $\beta_\phi = 0.68$ , for  $\gamma_\phi = 1 + \lambda/3$ ) and the red line (corresponding to  $\beta_\phi = 1$ ) where wave particle interaction is almost negligible. Therefore in the next subsection to explore the wave breaking physics, we keep the phase velocity of the Akhiezer - Polovin waves  $\beta_\phi = 0.95$  such that the relativistic Landau Damping rate remains small for the entire range of  $\lambda$  where we carry out the numerical experiment.

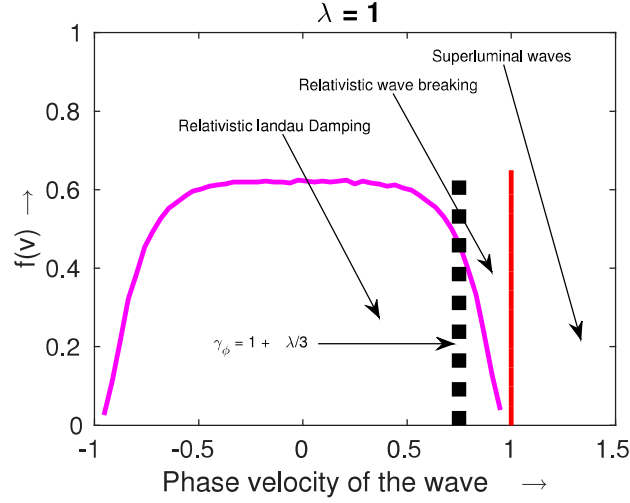


Figure 7.4: Parameter domains exhibiting relativistic Landau damping and wave breaking

### 7.2.2 Regime 2 - Wave breaking (via phase mixing)

Here, in all simulation runs we keep the phase velocity of the Akhiezer - Polovin wave at  $\beta_\phi = 0.95$ . Thus the relativistic Landau damping rate is negligible and the wave should propagate for a long period of time without damping or losing the periodicity. Figs.(7.5) and (7.6) respectively show the space time evolution of the electric field profile of a relativistically intense wave for  $\lambda = 5 \times 10^{-4}$  and  $\lambda = 10^{-2}$ . The value of  $u_m$  is taken as 0.30. From these figures we see that the wave propagates through the system without any damping and without losing periodicity for a large period of time. In Figs.(7.7) and (7.8), we have also plotted the time evolution of the electric field & density at a fixed grid point for two different initial temperature and observe that both are oscillating with a nearly constant amplitude. By measuring the time difference between two consecutive peaks from Figs.(7.7) and (7.8) we find that when a finite temperature is added with the pure Akhiezer - Polovin wave, the frequency does not remain  $\Omega_{ap}$  (frequency of the pure Akhiezer - Polovin wave propagating in a cold plasma, as studied in chapter - 4). In the small amplitude limit, we can estimate this characteristic frequency from the relativistic warm plasma dispersion relation [59, 61–63] which is followed by a relativistically intense electron plasma wave in a warm plasma. In

the limit  $k_B T_e / mc^2 \ll 1$  this dispersion relation can be written as

$$\Omega^2 = \omega_p^2 + k^2 c^2 \lambda - \frac{5}{6} \omega_p^2 \lambda \quad (7.9)$$

An elementary derivation of this dispersion relation is given in Appendix - C.

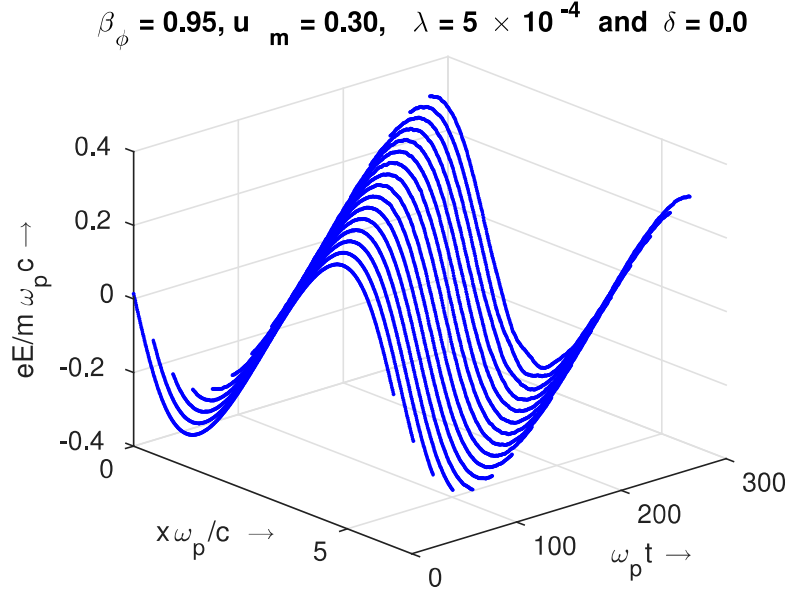


Figure 7.5: Space-time evolution of electric field for  $\beta_\phi = 0.95$ ,  $u_m = 0.3$ ,  $\lambda = 5 \times 10^{-4}$  and  $\delta = 0.0$

Here, we verify this dispersion relation for two different amplitudes  $u_m = 0.1$  &  $0.3$  by changing the values of  $\lambda$  and  $k$ . In Figs.(7.9) and (7.10), we respectively show the variation of frequency  $\Omega$  as a function of  $\lambda$  and  $k$  for fixed value of other parameters. In these figures the points are obtained from PIC simulations and the continuous lines are the theoretical relativistic dispersion relation given by Eq.(7.9). Note that, for amplitude  $u_m = 0.1$  we see a better matching as compared to  $u_m = 0.3$ . This is expected, as this dispersion relation is obtained by linearising the Vlasov - Poisson's equations, the excited wave is supposed to follow it only in the low amplitude limit.

Now we add a very small amplitude sinusoidal velocity perturbation with a maximum amplitude  $\delta$  to this large amplitude Akhiezer - Polovin wave with same mode number as the large amplitude Akhiezer - Polovin wave ( $k_{ap}$ ). In Figs.(7.11)

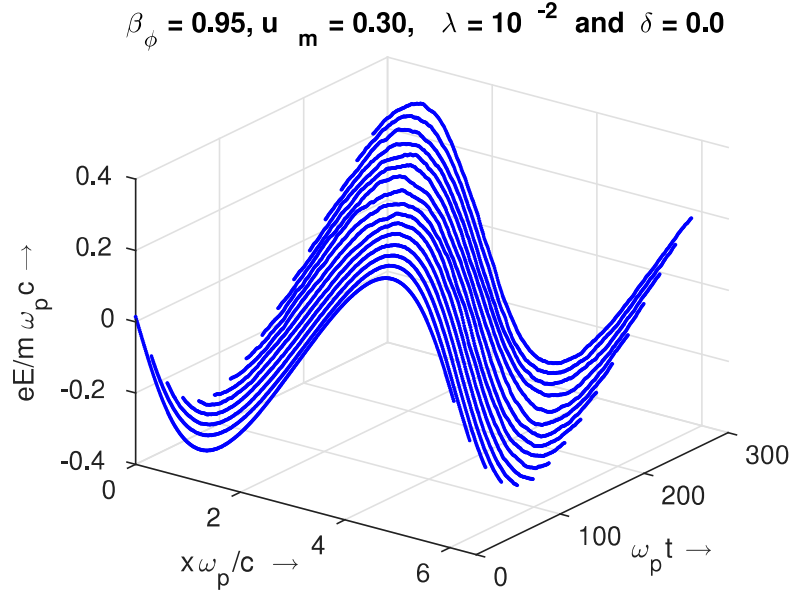


Figure 7.6: Space-time evolution of electric field for  $\beta_\phi = 0.95$ ,  $u_m = 0.3$ ,  $\lambda = 10^{-2}$  and  $\delta = 0.0$

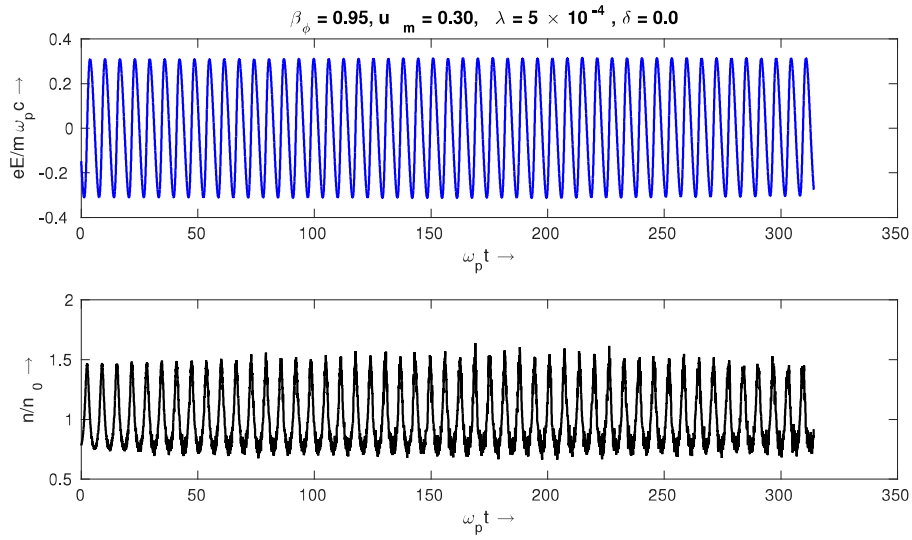


Figure 7.7: Time evolution of electric field & density at a fixed grid point for  $\beta_\phi = 0.95$ ,  $u_m = 0.3$ ,  $\lambda = 5 \times 10^{-4}$  and  $\delta = 0.0$

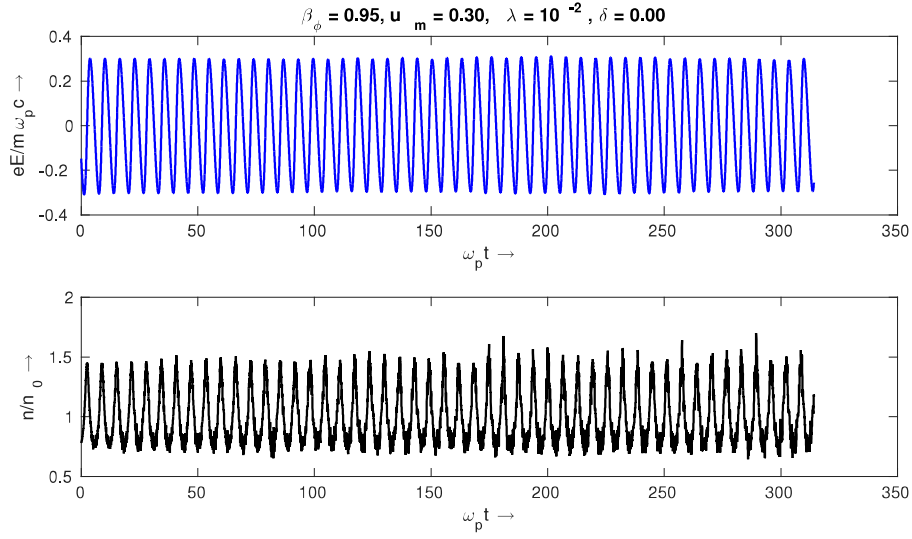


Figure 7.8: Time evolution of electric field & density at a fixed grid point for  $\beta_\phi = 0.95$ ,  $u_m = 0.3$ ,  $\lambda = 0.01$  and  $\delta = 0.0$

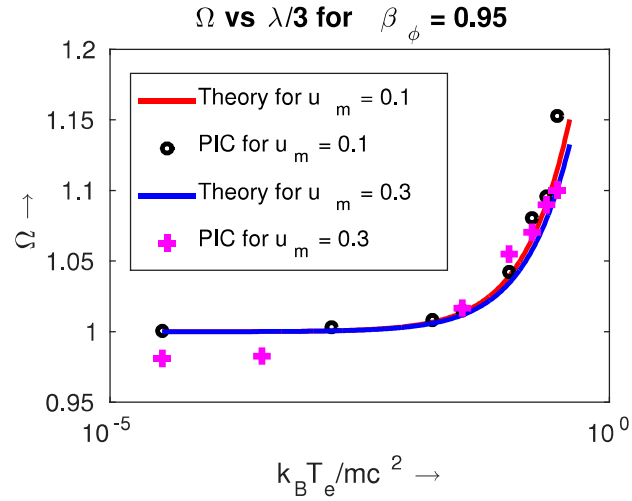


Figure 7.9:  $\Omega$  as a function of  $\lambda$ , for  $\beta_\phi = 0.95$ ,  $u_m = 0.10, 0.30$ ,  $\delta = 0.0$

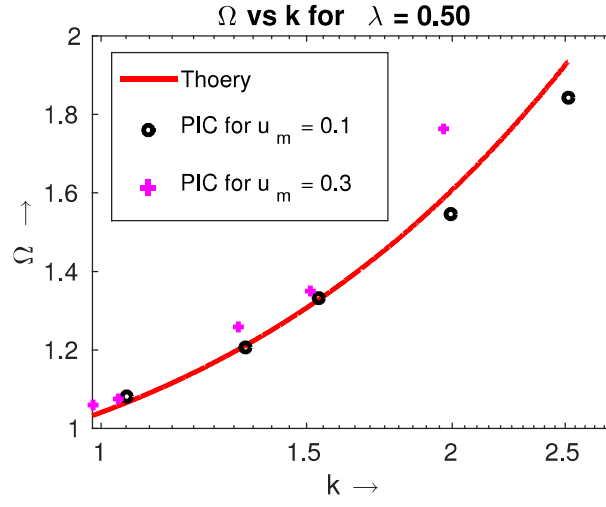


Figure 7.10:  $\Omega$  as a function of  $k$ , for  $u_m = 0.10, 0.30$ ,  $\delta = 0.0$  ( $\lambda$  is taken as 0.5)

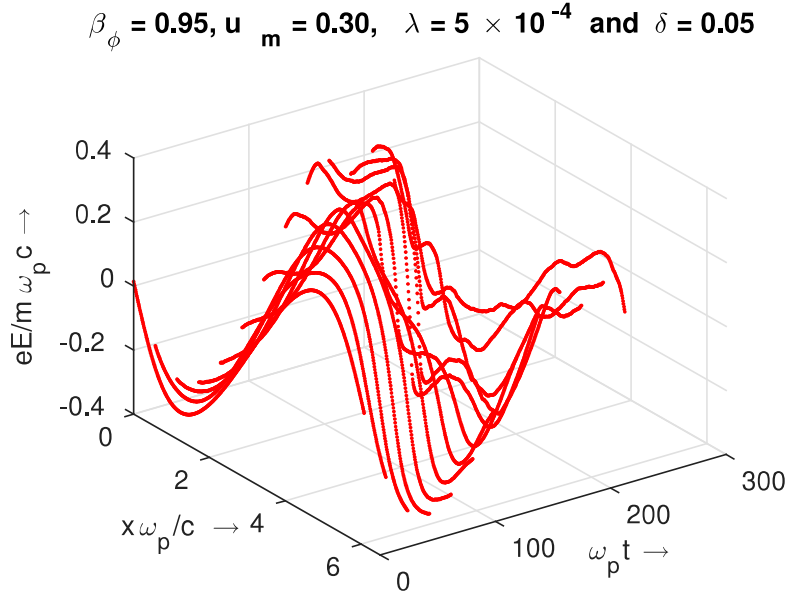


Figure 7.11: Space-time evolution of electric field for  $\beta_\phi = 0.95$ ,  $u_m = 0.3$ ,  $\lambda = 5 \times 10^{-4}$  and  $\delta = 0.05$

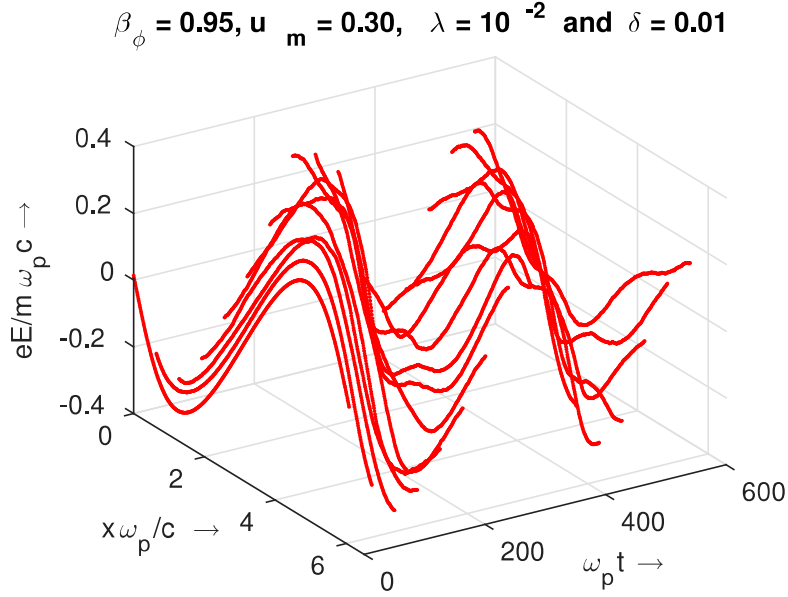


Figure 7.12: Space-time evolution of electric field for  $\beta_\phi = 0.95, u_m = 0.3, \lambda = 10^{-2}$  and  $\delta = 0.01$

and (7.12) we show that the space -time evolution of the resultant electric field of the perturbed wave for two different values of  $\lambda$  and  $\delta$ . Similarly, in Figs.(7.13) and (7.14), we have plotted the time evolution of the perturbed electric field and density at a fixed grid point for the same parameters. Both the figures are exhibiting gradual deformation of the wave electric field and density profile which show that as time progresses the wave profile deforms and after a certain time (decided by  $u_m, \beta_\phi, \lambda$  and  $\delta$ ) the wave amplitude becomes modulated. We define wave breaking time (phase mixing time) as the time when the “first dip” appears in the time evolution plot [Figs.(7.13) and 7.14]. We expect that this breaking is manifested via the process of phase mixing, as after adding the perturbation the characteristic frequency could become a function of space. To confirm our prediction we have measured the initial total energy (“ $a$ ”) of each particle (electron sheet) for both the cases without and with perturbation. Then the characteristic frequencies of the motion of the particles have been evaluated by using the general expression of frequency for a relativistic harmonic oscillator, which is given by (derived in

## Chapter 7. Breaking of Large Amplitude Relativistically Intense Electron Plasma Waves in a Warm Plasma

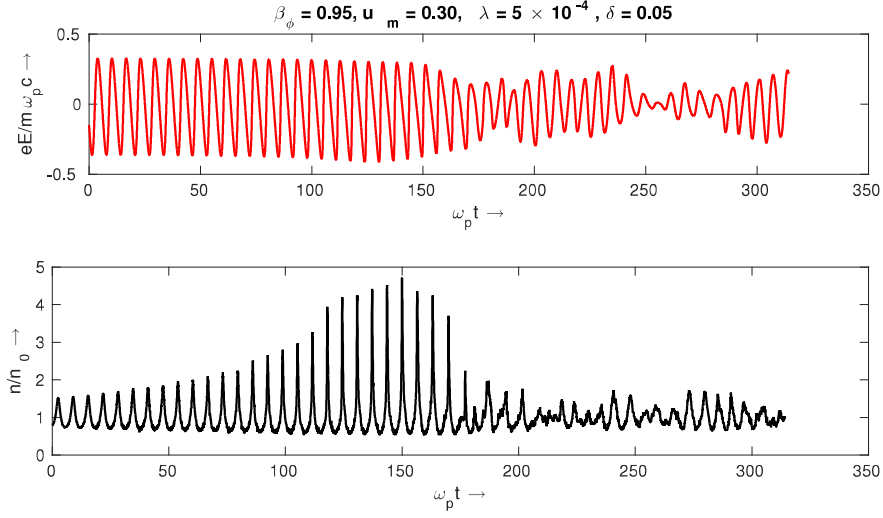


Figure 7.13: Time evolution of electric field & density at a fixed grid point for  $\beta_\phi = 0.95$ ,  $u_m = 0.3$ ,  $\lambda = 5 \times 10^{-4}$  and  $\delta = 0.05$

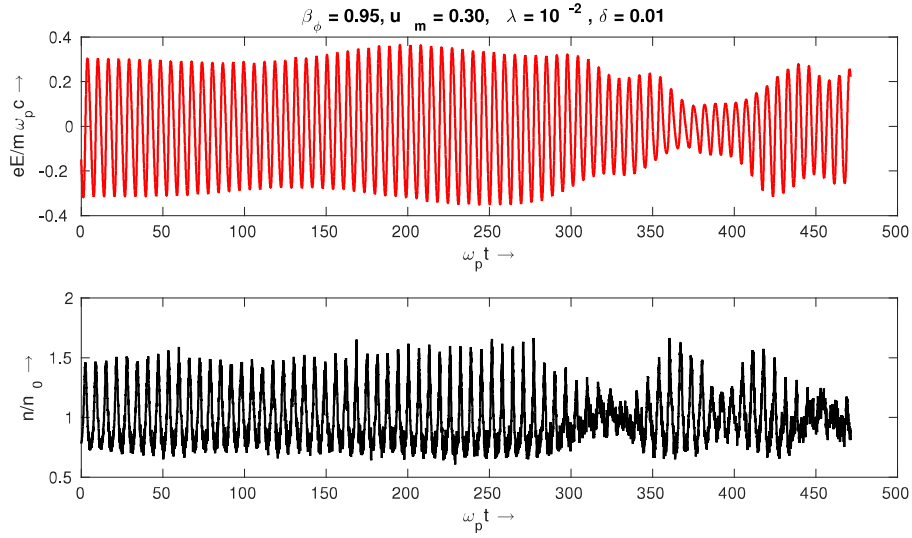


Figure 7.14: Time evolution of electric field & density at a fixed grid point for  $\beta_\phi = 0.95$ ,  $u_m = 0.3$ ,  $\lambda = 10^{-2}$  and  $\delta = 0.01$



Chapter-4)

$$\Omega = \omega_p \frac{\pi}{2} \frac{r'}{[2E(r) - r'K(r)]} \quad (7.10)$$

where  $E(r)$  and  $K(r)$  are complete elliptic integrals of second and first kind [97] respectively,  $r^2 = (a - 1)/(a + 1)$  and  $r' = (1 - r^2)^{1/2}$ . In Figs.(7.15) and (7.16) we have respectively plotted the frequency (averaged over a cell) as a function of space for the cases without and with perturbation for a fixed electron temperature ( $\lambda = 0.01$ ). We observe that in Fig.(7.16), after adding the perturbation, the frequency indeed becomes a function of position as the total energy “ $a$ ” becomes an explicit function of the space; this is absent in Fig.(7.15) as for  $\delta = 0$  the energy of each particle remains independent of their respective equilibrium position.

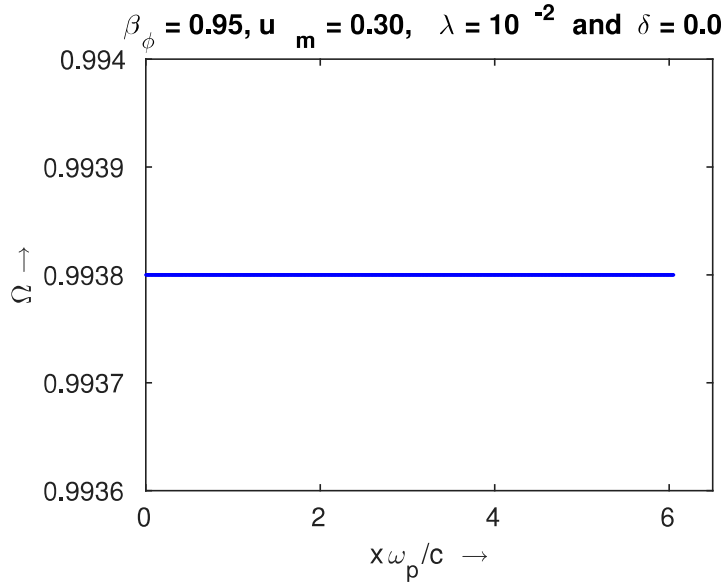


Figure 7.15: Frequency of the wave as a function of the position for  $\beta_\phi = 0.95$ ,  $u_m = 0.3$ ,  $\lambda = 0.01$  and  $\delta = 0.0$

The occurrence of phase mixing has been again confirmed by plotting the Fourier spectrum of electric field amplitude ( $E_k$ ) at different instants of time for both the cases without (left) and with perturbation (right). Compare these two figures (blue and red) in Fig.(7.17). It shows that, after adding the perturbation, as the time progresses the amplitude of the primary mode ( $k_{ap}$ ) reduces significantly (red curves) with the simultaneous growth in higher order modes. It is clear from the Fig.(7.17) that a significant amount of energy has been transferred to the

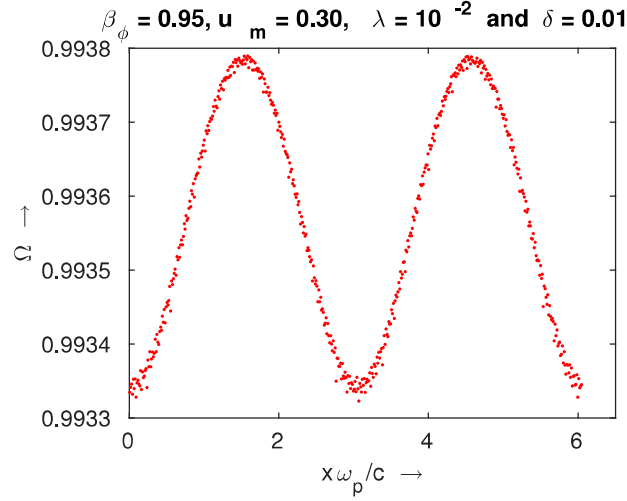


Figure 7.16: Frequency of the wave as a function of the position for  $\beta_\phi = 0.95$ ,  $u_m = 0.3$ ,  $\lambda = 0.01$  and  $\delta = 0.01$

higher harmonics which is another signature of wave breaking via phase mixing process reported by other authors [29–31]. As a consequence some of the electrons will acquire energy from the wave and accelerate to much higher energies.

A clear manifestation of the phase mixing process *i.e* generation of energetic electrons can be seen by plotting the evolution of electron phase - space. In Figs.(7.18) and (7.19) we have respectively plotted the evolution of electron phase space for the cases without and with perturbation. From these figures we observe that in the presence of a small amplitude perturbation, the number of energetic particles increases significantly after wave breaking and thus confirms wave breaking via the gradual process of phase mixing which had been reported earlier by several authors in different contexts [14,16,20,22,111]. We also note that the phase space plots for the unperturbed case remain unchanged from the initial stage of excitation.

### 7.3 Estimation of Phase Mixing Time

As we have found that after adding a small amplitude sinusoidal velocity perturbation the characteristic frequency acquires a spatial dependency, therefore we also expect that in a warm plasma the wave breaking time (phase mixing time) can also be estimated from Dawson’s formula [5] for phase mixing time given for a non-

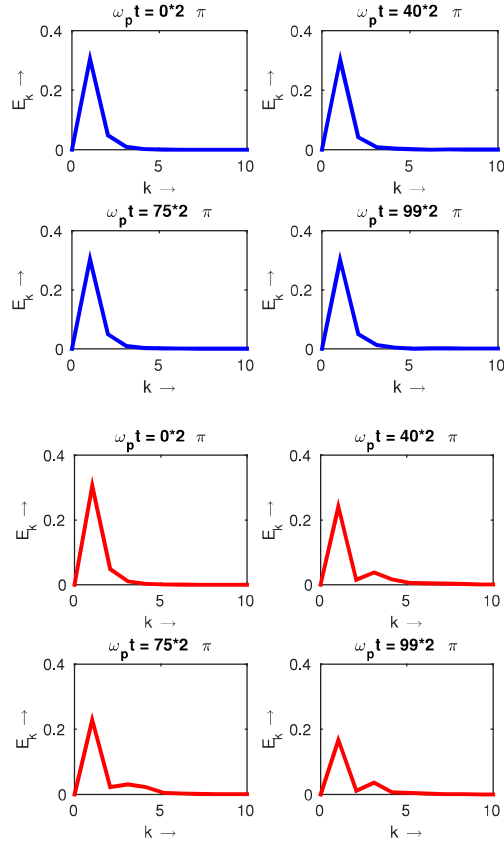


Figure 7.17: Fourier spectrum of electric field for  $\beta_\phi = 0.95$ ,  $u_m = 0.3$ ,  $\lambda = 0.01$  and  $\delta = 0.0$  (blue),  $0.01$ (red) at different time steps

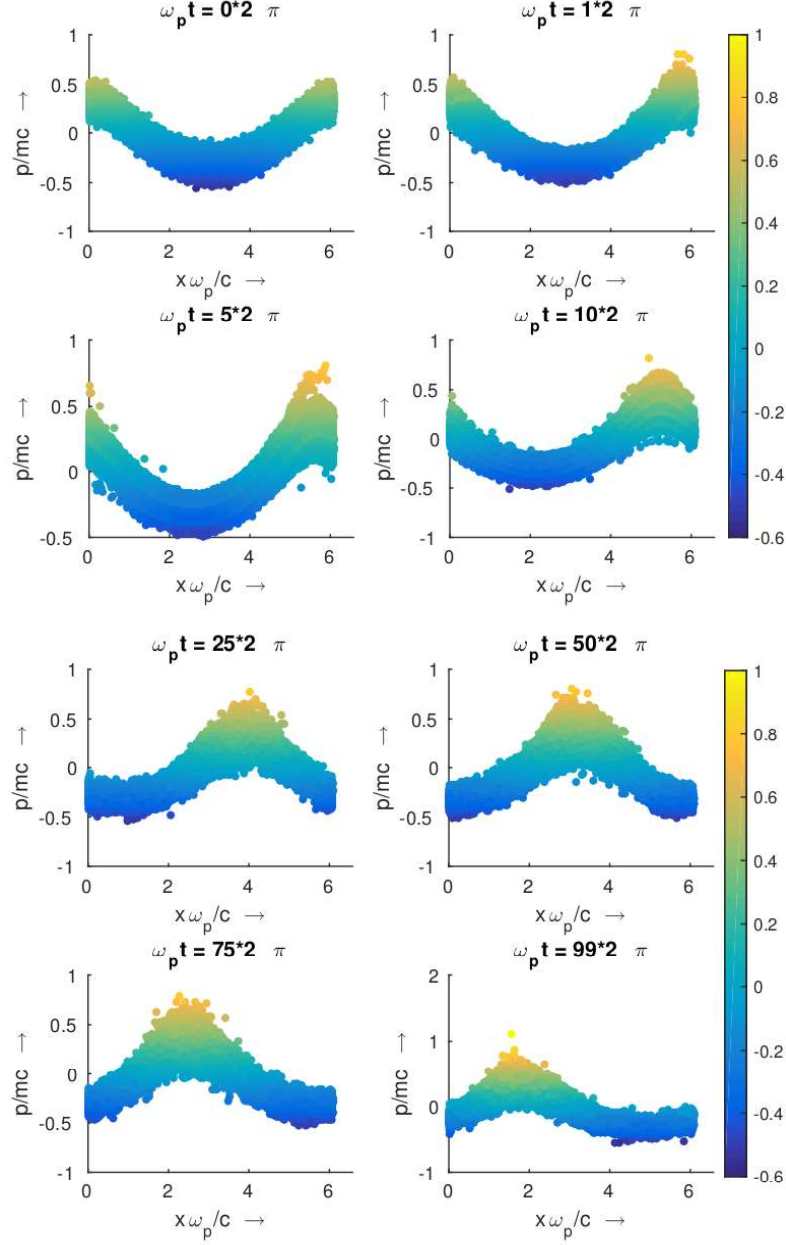


Figure 7.18: Snapshots of phase space for  $\beta_\phi = 0.95$ ,  $u_m = 0.3$ ,  $\lambda = 0.01$  and  $\delta = 0.0$  at different time steps

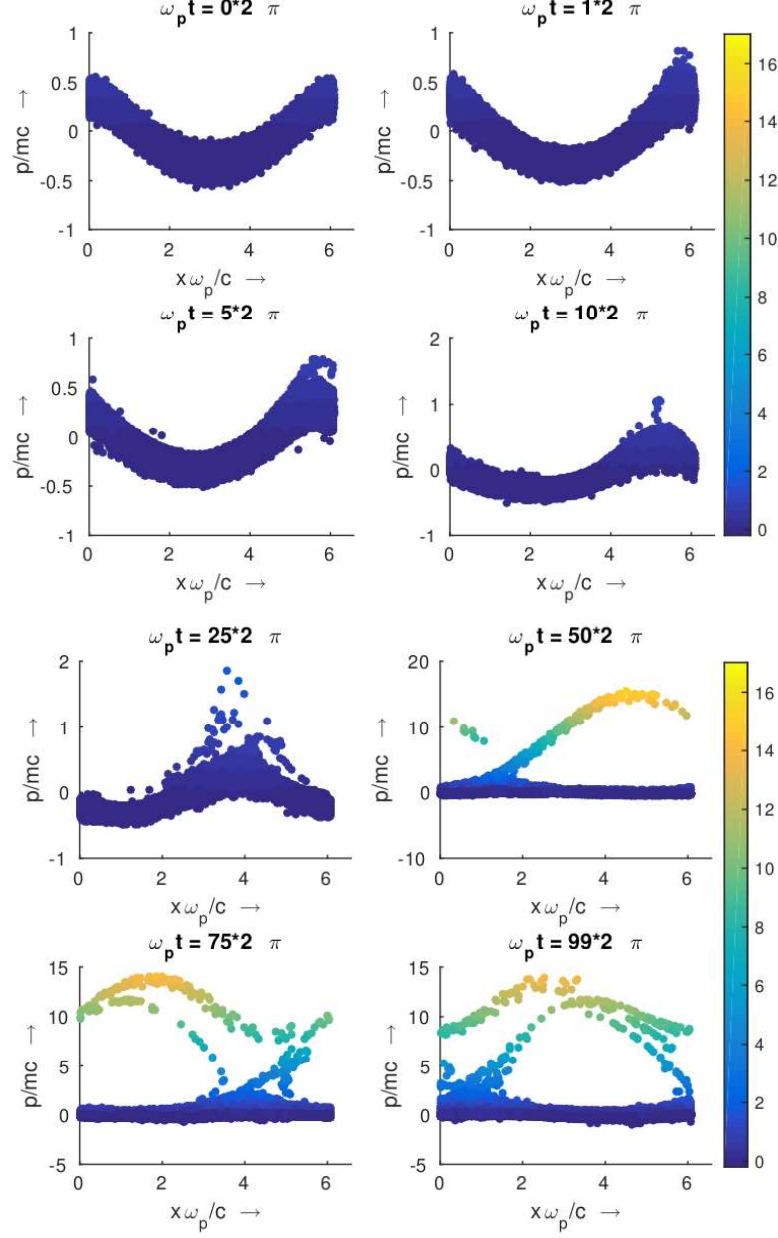


Figure 7.19: Snapshots of phase space for  $\beta_\phi = 0.95$ ,  $u_m = 0.3$ ,  $\lambda = 0.01$  and  $\delta = 0.01$  at different time steps

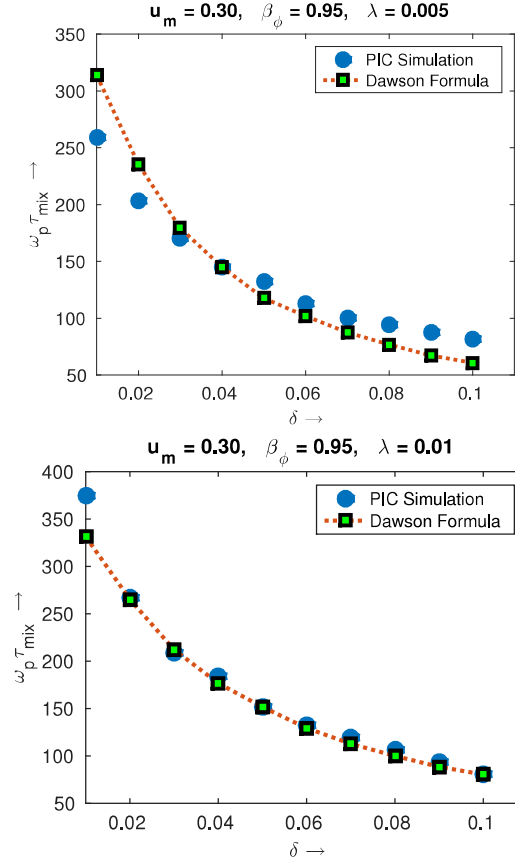


Figure 7.20: Phase mixing time as a function of  $\delta$  for  $\lambda = 5 \times 10^{-3}$  and  $10^{-2}$

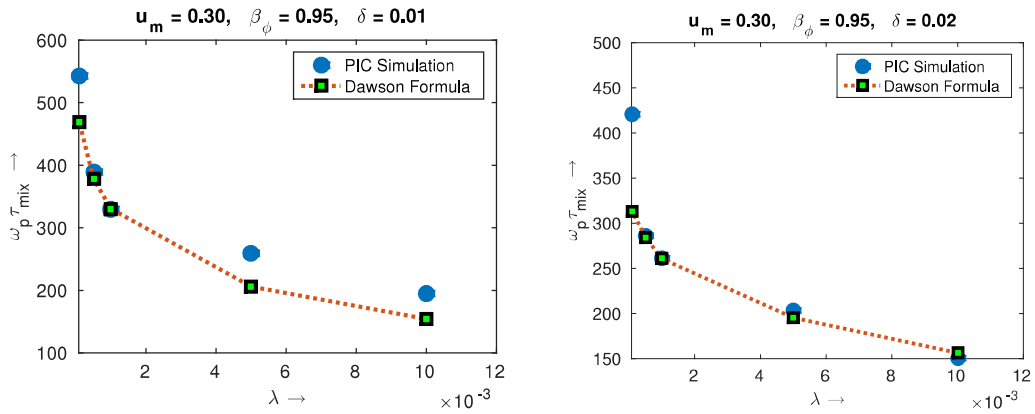


Figure 7.21: Phase mixing time as a function of  $\lambda$  for  $\delta = 0.01$  and  $0.02$

relativistic cold inhomogeneous plasma. This formula was based on out of phase motion of neighbouring sheets constituting the wave and separated by a distance equal to twice the amplitude of the oscillation/wave. Now in order to calculate the phase mixing time scale using Dawson's formula we first measure the derivative  $d\Omega/dx$  from Fig.(7.16) and note its maximum value.  $\xi_{max}$  is calculated by measuring the initial displacement of all the particles from their respective equilibrium positions at  $t = 0$ . Thus by measuring the values of  $d\Omega/dx$  and  $\xi_{max}$  from simulation data, we calculate the phase mixing time scale by using Dawson's formula which is  $\omega_p t_{mix} \sim \frac{\pi}{2\xi_{max} d\Omega/dx}$ . Now in order to verify this scaling on the amplitude of the perturbation ( $d\Omega/dx$  depend on the amplitude of the perturbation  $\delta$ ) we repeat the above numerical experiment such that the maximum velocity amplitude of Akhiezer - Polovin wave is kept fixed at  $u_m = 0.30$  and amplitude of the perturbation  $\delta$  is varied from 0.01 to 0.1. Fig.(7.20) shows the variation of phase mixing time as a function of the amplitude of the applied velocity perturbation  $\delta$  for two different values of  $\lambda = 5 \times 10^{-3}$  and  $10^{-2}$ . The simulation results clearly indicate that as the amplitude of the perturbation is increased, phase mixing time decreases. Next we vary the electron temperature keeping the values of  $u_m$  and  $\delta$  fixed. Fig.(7.21) shows the variation of phase mixing time as a function of electron temperature for two different values of fixed  $\delta = 0.01$  and  $0.02$ . This figure indicates that the phase mixing time decreases with increasing the electron temperature  $\lambda$ . In both two figures blue points are the phase mixing time measured by observing the appearance of first dip of the wave electric field, while the green squares are the phase mixing time scale estimated by using Dawson's formula. These figures show that Dawson's phase mixing time formula clearly captures the underlying physics. The close match between simulation and analytical results (Dawson's phase mixing time formula) supports the role played by phase mixing process in the breaking of relativistically intense electron plasma waves in a warm plasma.

## 7.4 Summary and Discussions

In summary, the breaking of a large amplitude relativistically intense electron plasma wave in a warm plasma has been studied by loading a Jüttner - Synge

distribution along with a Akhiezer - Polovin type initial conditions in a relativistic Particle-in-Cell code. It has been observed that in the regime where wave Lorentz factor  $\gamma_\phi \ll 1 + \lambda/3$ , the wave damps in a few plasma period and swamps out the wave breaking physics. The results obtained from simulations indicate that the damping rate essentially follows the relativistic Landau damping rate predicted by Buti [59]. In the opposite regime we have found that the wave propagates through the system for a long period of time and in the small amplitude limit, the frequency of the resultant mode follows the relativistic warm plasma dispersion relation  $\Omega^2 = \omega_p^2 + k^2 c^2 \lambda - 5\omega_p^2 \lambda/6$ . Next we have shown that when a small amplitude longitudinal sinusoidal velocity perturbation is added to this Akhiezer - Polovin wave, the wave breaks via the process of phase mixing at an amplitude far below its conventional theoretical breaking limits that exist in the literature [37–43]. As for example, in Figs.(7.11) and (7.12), the wave breaks at an amplitude  $eE/m\omega_p c \sim 0.3$ , which is far below the wave breaking limits obtained from the models given by Katsouleas-Mori [37] & Trines *et. al.* [43] ( $eE/m\omega_p c \sim 1.8033$ ), Rosenzweig [38] and Sheng *et. al.* [40] ( $eE/m\omega_p c \sim 8.1648$ ) and Schroeder *et. al.* [41,42] ( $eE/m\omega_p c \sim 1.6137$ ). Here we have explicitly shown by carrying out a PIC simulation that, relativistically intense plasma waves in a warm plasma breaks via the process of phase mixing even at  $eE/m\omega_p c \sim 0.3$  when perturbed longitudinally by a small amplitude perturbation. Therefore in experiments it is impossible to reach  $eE/m\omega_p c \sim 1$ , as in a realistic experiment, it is natural to expect some noise which would break the wave via phase mixing. We have also illustrated that this phase mixing time can be predicted from the Dawson's formula [5] for phase mixing time scale for a non-relativistic cold inhomogeneous plasma, which is based on out of phase motion of neighbouring oscillators constituting the wave and separated by a distance equal to twice the amplitude of the oscillation/wave.





*There is no real ending. It's  
just the place where you stop  
the story.*

- Frank Herbert

# 8

## Conclusion and Future Scope

This chapter contains conclusions and summary of our work studied in this thesis. Directions for further research are also enumerated.

### 8.1 Conclusions and Summary

In this thesis, by performing analytical calculations and computer experiments, we present a thorough investigation and understanding on the formation, evolution and breaking of variety of relativistically intense longitudinal electron plasma oscillations/waves that a homogeneous unmagnetized plasma (cold and warm) can support. We have started our research from the cold plasma wave breaking (via phase mixing) physics, both analytically and numerically, by using Dawson sheet model. Then we have gradually extended our focus of attention to the wave breaking physics in a warm plasma by using Particle-in-Cell (PIC) simulation method because sheet simulation method has some limitations here. A detailed description of Sheet simulation method and a brief overview of PIC simulation method have been given in Chapter -2.

Then in chapter -3, we have studied the space-time evolution and breaking (via phase mixing) of a large amplitude relativistically intense wave packet (specified by its amplitude  $\delta$  and spectral width  $\Delta k$ ) in a cold plasma by using Dawson sheet model. The equation of motion of a sheet has been solved and an expression for frequency correct upto fourth order of the oscillation amplitude has been derived by using Lindstedt - Poincaré perturbation method (for complete derivation see Appendix -A). Then an analytical expression for phase mixing time scale has been

obtained by using Dawson's reasoning [5] and it has been found that the phase mixing time ( $\tau_{mix}$ ) of this wave packet crucially depends on the relative magnitude of the amplitude  $\delta$  and dimensionless spectral width  $\Delta k/k$  of the wave packet; for  $\Delta k/k \leq 2\omega_p^2\delta^2/c^2k^2$ ,  $\tau_{mix}$  scales with  $\delta$  as  $1/\delta^5$  and for  $\Delta k/k > 2\omega_p^2\delta^2/c^2k^2$ ,  $\tau_{mix}$  scales with  $\delta$  as  $1/\delta^3$ . We have also verified our theoretical results by a simulation code which is based on Dawson Sheet Model for three different values of  $\Delta k$ . In this code, at each time step we have carefully checked the particle crossing condition and the phase mixing time has been measured as the time taken by any two adjacent sheets to cross over. In every case we have found a reasonably good fit between the theoretical and simulation results.

Next, in chapter -4, we have studied the space-time evolution and breaking of a very special kind of wave - longitudinal Akhiezer - Polovin mode in a cold plasma. A longitudinal Akhiezer - Polovin mode actually represents a travelling wave in a cold plasma parametrized by its maximum fluid velocity ( $u_m$ ) and phase velocity ( $\beta_\phi$ ), studied first by Akhiezer and Polovin in 1956 by including the relativistic mass variation effect of the electrons. The authors found that, the maximum electric field amplitude that can be sustained by this wave is given by  $E_{AP} = \sqrt{2(\gamma_\phi - 1)}$ . However, in 2012 Verma *et. al.* by performing extensive numerical simulation, showed that even a longitudinal Akhiezer - Polovin wave breaks through the gradual process of phase mixing at an amplitude well below its wave breaking limit, when it is subjected to an arbitrarily small amplitude longitudinal perturbation. Here we have presented an analytical expression for the phase mixing time scale for this longitudinal Akhiezer - Polovin mode by using Dawson sheet model. At first, we have given an exact analytical solution of equation of motion of a sheet and found the initial conditions needed to excite Akhiezer - Polovin mode having a characteristic frequency  $\omega_{ap}$  independent of space. Then we have perturbed these initial conditions with a small amplitude external perturbation with a velocity amplitude  $\delta$  & wavelength  $k_{ap}$  (same as the longitudinal Akhiezer - Polovin wave) and derived an expression for frequency  $\Omega_{per}$  in weakly relativistic limit. We have observed that, in this situation, the characteristic frequency of the wave explicitly contains a space dependent term due to which neighbouring electrons (which govern the wave motion) gradually go out of phase and eventually cross causing the wave to break via phase mixing at arbitrarily small initial perturbation. By using Dawson's argument, we also

obtained an analytical expression for this phase mixing time scale which shows that the longitudinal Akhiezer - Polovin wave breaks in a time scale given by  $\sim \frac{2\pi\beta_\phi}{3\delta} \left[ \frac{1}{u_m^2} - \frac{1}{4} \right]$ . Next, in order to verify our theoretical results, we have numerically followed the space-time evolution of longitudinal Akhiezer - Polovin wave, by using a code based on Dawson sheet model. We have observed that, without any external perturbation ( $\delta = 0$ ), the wave propagates through the system without any change in its amplitude. But, when it is perturbed by a small amplitude perturbation, we have found that as time progresses, the density profile becomes more and more spiky as energy is irreversibly transferred to higher and higher harmonics. Due to longitudinal perturbation, the energy which was initially loaded on the Akhiezer - Polovin mode goes to higher harmonics, then partially returns to the original mode, again goes to higher harmonics and so on. We have explicitly shown that this partial back-and-forth sloshing of energy between different harmonics eventually results in accumulation of energy at higher harmonics and interaction of these high harmonics with the particles (sheets) accelerates the particles, causing the initial delta-function momentum distribution to spread. We have also found that the analytical expression derived by us shows a reasonably good fit to the observed numerical results, thus vindicating our weakly relativistic calculation.

Another manifestation of breaking of nonlinear electron plasma oscillations via phase mixing have been observed by changing the geometry or pattern of the oscillation (from planar to cylindrical and spherical) and explicitly illustrated in Chapter -5. In this chapter we have extended Dawson's earlier work [5] by including relativistic mass variation effects. First, we have extended the Dawson sheet model from planar to cylindrical and spherical geometry and derived the fluid variables by using the conservation of number of particles and Gauss's Law. The equation of motion of a sheet has also been derived and has been solved in weakly relativistic limit using a perturbative method *viz.* Lindstedt - Poincaré perturbation method upto fourth order in oscillation amplitude (for complete derivation see Appendix -B). We have observed that in general the expressions for frequencies acquire spatial dependency which ultimately lead to breaking via phase mixing [5, 28-33, 68]. Analytical expressions for phase mixing time scales as a function of the amplitude of the applied perturbation ( $\Delta$ ) have been derived which indicate that for both relativistic cylindrical and spherical oscillations, phase mixing time scales inversely with the cube of the amplitude of the applied perturbation. We observe that, for

nonrelativistic case also the variation of phase mixing time with the amplitude of the applied perturbation follows the same scaling law. Inclusion of relativistic effects [55, 56] only hastens the phase mixing time but the scaling law remains unchanged. We also verify our analytically obtained scaling law by Sheet Simulation code. For cylindrical and spherical oscillations, fluid variables depend only on the radial coordinate of the oscillating species (here the electron sheets) *i.e.* they are radially symmetric in nature. As Bessel functions and Spherical Bessel functions [97] form a complete orthogonal set (basis functions) in cylindrical and spherical coordinate systems respectively, then any arbitrary perturbation imposed in these systems can be written as a superposition of these basis functions (Fourier Bessel Series) in their respective coordinate system [101, 102]. Therefore to excite an oscillation in cylindrically and spherically symmetric system we use Bessel functions and Spherical Bessel functions respectively as an initial perturbation. Here also we have found that, as the time progresses, the density becomes more and more spiky and at the time of breaking the density becomes singular.

Here we would like to note that the density singularity is an artefact of cold fluid plasma model. In fact, when non-linear density perturbations are excited in a large amplitude plasma wave, electron pressure and hence thermal effects may become important as the electron thermal pressure may not allow the density compression to build upto such high values as predicted by the simple cold plasma fluid model. Therefore, under this condition a warm plasma theory is required. In 1971, Coffey [36] investigated the phenomenon of wave breaking for an electron plasma wave (nonrelativistic) in a warm plasma by using the simplest distribution *i.e.* “water-bag” distribution [39, 57] for electrons and showed that maximum electric field amplitude explicitly depends on the electron temperature and decreases monotonically with increasing electron temperature which is typically known as Coffey’s limit.

In Chapter - 6, by using a 1D Particle-in-Cell (PIC) simulation code, we have numerically investigated the maximum electric field amplitude that can be sustained by a “self-consistent” freely running electron plasma wave (Langmuir wave) in a warm plasma where electron’s velocity distribution is a Maxwellian. We have also studied the stability of this wave towards a small amplitude longitudinal perturbation. From simulation we have observed that Coffey’s propagating wave solution [36], which was derived using a “water-bag” distribution for electrons, also

represents a self-consistent propagating wave in a Maxwellian plasma albeit with a lower amplitude. In addition to this we have shown that if the amplitude of the initial perturbation exceeds Coffey's wave breaking limit, within a few plasma periods the initialized wave self-consistently conforms itself with the background distribution and settled at an amplitude below Coffey's limit for a large period of time ( $\sim 100$  plasma periods) provided the Landau damping rate is very weak. We have found that this final self-consistent wave amplitude does not increase even after increasing the perturbation amplitude and thus can be taken as maximum sustainable electric field amplitude. By changing the electron temperature, we have repeated our experiment and found that maximum electric field amplitude that can be sustained by a self-consistent electron plasma wave in a Maxwellian plasma follows a similar scaling given by Coffey [36] but with slightly different coefficients.

Finally in Chapter -7, we have explored the effect of electron temperature on the space-time evolution of a relativistically intense electron plasma wave in a warm plasma by conducting numerical experiment using 1D PIC code. In order to study the space time evolution and stability of these waves towards a small amplitude longitudinal perturbation in a warm plasma, we have loaded Akhiezer - Polovin [27] type initial conditions in our PIC code. Along with this, a finite electron temperature (Jüttner-Synge distribution [58]) has been added. At first, we have observed that for phase velocities for which  $\gamma_\Phi \ll 1 + k_B T_e / mc^2$ , the wave damps within a few plasma period and essentially follows the relativistic Landau Damping rate given by Buti [59]. In the opposite regime ( $\gamma_\Phi \gg 1 + k_B T_e / mc^2$ ) we have found that the wave propagates through the system for a long period of time and in small amplitude limit essentially follows the relativistic warm plasma dispersion relation [59–63] (an elementary derivation is given in Appendix-C). Further we demonstrate that in the same regime (*i.e.* for  $\gamma_\Phi \gg 1 + \frac{k_B T_e}{mc^2}$ ), for the phase velocities less than the velocity of light  $c$ , like the cold plasma Akhiezer - Polovin wave [33], in a warm plasma also, relativistically intense waves break via phase mixing when perturbed by an arbitrarily small amplitude longitudinal perturbation. This is far below the existing theoretical results on warm plasma wave breaking available in the literature [37–44]. By measuring the characteristic frequency of the wave (by measuring the initial energy of the particles constituting the wave) at each position, we have found that after adding the external perturbation the

characteristic frequency of the wave becomes a function of space which ultimately breaks the wave via phase mixing. Here the phase mixing time (wave breaking time) has been defined when the “first dip” appears in the time evolution plot of the perturbed electric field. Like the cold plasma case, here we have also seen the generation of higher and higher harmonics and as a consequence the generation of energetic particles with the progress of time. Variations of phase mixing time for a wide range of input parameters have been studied. Using our simulation results, we also show that the phase mixing time scale in a warm plasma can be interpreted using Dawson’s formula [5] for phase mixing time for a non-relativistic cold inhomogeneous plasma, which is based on out of phase motion of neighbouring oscillators constituting the wave.

## 8.2 Future Scope

As the present thesis focuses on the formation, evolution and breaking of variety of relativistically intense longitudinal electron modes that a homogeneous unmagnetized plasma (cold and warm) can support, one can think of several possible improvements in the present study. In the following we enumerate some of the possible future directions leading from the present study.

1. First of all, here it should be noted that, the present study explores the physics of the breaking of longitudinal waves in a cold & warm plasma and the study has been carried out in one - dimension (1-D) where the variables are allowed to vary only along one direction (the direction of propagation). In 2D, relativistically intense plasma waves excited by a finite width, short laser pulse or by a pulse with a sharp leading edge in an underdense plasma has a specific horseshoe (or “D shape”) structure where the curvature of the constant phase surfaces increases with the distance from the pulse. The curvature radius decreases until it is comparable to the electron displacement in the nonlinear plasma wave leading to a new type of self-intersection of the electron trajectories. This is called transverse wave breaking which occurs at much lower wave amplitudes than the conventional 1-D wave break, studied first by Bulanov *et. al.* [112]. The inclusion of transverse direction yields interesting consequences on the space - time evolution of the oscillation/wave

and thus will be interesting to explore in future.

2. We understand that phase mixing leading to wave breaking occurs at arbitrarily small amplitude in a homogeneous plasma, provided (i) the background ions have a finite mass and/or (ii) the excited plasma wave is relativistically intense because in these cases the characteristic frequency acquires a spatial dependency. In this thesis, we have focused our attention only on the relativistically intense oscillations/waves in a homogeneous plasma where ions are at rest. In the very ultrarelativistic regime ( $\gamma_\phi$  very high), when the mass of the electron becomes extremely high, the effect of ion motion can be important. Therefore it will be interesting to explore the effect of self-consistent ion motion (which arise because of low frequency ponderomotive forces) on the space-time evolution of relativistic intense waves in a cold and warm plasma. Moreover, an analytical expression for the phase mixing time scale for relativistically intense oscillations/ waves as a function of the mass ratio and amplitude of the applied perturbation is yet to be discovered. To derive an analytical formula for this phase mixing time scale (as a function of the mass ratio and amplitude of the applied perturbation) and its verification by Particle-in-Cell method will be an interesting future work.
3. In chapters -3, 4 and 5 we have explored the wave breaking physics in a cold plasma by using the sheet simulation method [96]. All the modes have been studied up to the phase mixing time. Physics of these modes beyond wave breaking (phase mixing) needs to be explored as it may have direct relevance in particle acceleration experiments. It is also interesting to know the type of distributions that will be formed after the breaking of these waves. In Ref. [74] it has been demonstrated that for nonrelativistic cold plasma oscillations, after wave breaking all the initialized energy does not end up as the random kinetic energy of the particles, but some fraction always remains with two oppositely propagating coherent BGK [75] like modes with supporting trapped particle distributions and further demonstrated that the amplitude of this mode follows Coffey's limit [36]. Therefore one question naturally comes. Do the relativistically intense oscillations/waves lead to coherent structures after long time evolution (breaking) ? If they do, then what is the maximum electric field amplitude of these modes ? These questions



are unanswered yet and will be exciting to explore in future.

4. In chapter - 5, we have mentioned about “turn around time” [56] for spherical wave - the time at which the wave changes its direction of propagation. It has been strictly mentioned that the turn around occurs when the frequency of the wave acquires a spatial dependency [56] and an analytical expression for this turn around time has also been derived by the authors of Ref. [56]. But, the verification for this time scale by changing the amplitude of the perturbation has never been attempted. In this thesis, we have shown that, for oscillations in cylindrical geometry the characteristic frequency acquires a spatial dependency. Therefore it is expected that, cylindrical waves will also turn around after a certain time scale. In future, we wish to estimate the turn around time theoretically and by using the sheet simulation code we wish to verify them.

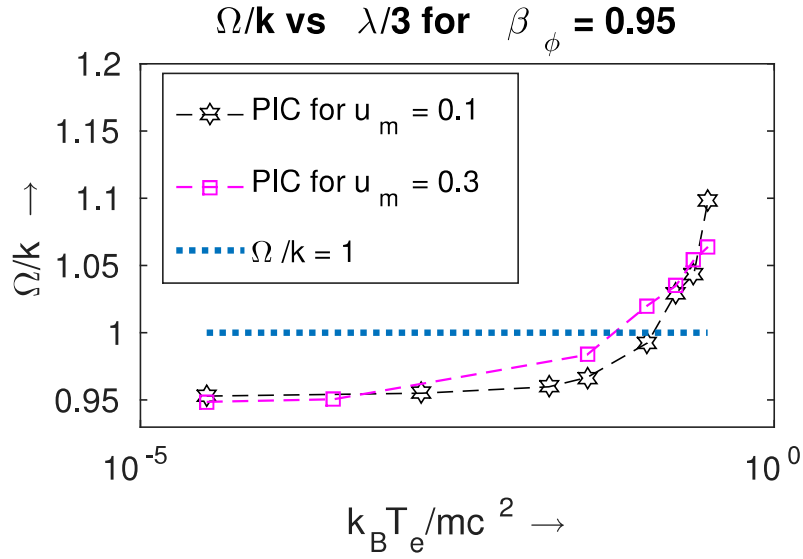


Figure 8.1:  $\Omega/k$  as a function of  $\lambda$ , for  $\beta_\phi = 0.95$ ,  $u_m = 0.10, 0.30$ ,  $\delta = 0.0$

5. In chapter - 7, simulations have been performed for a relatively small range of  $\lambda = 10^{-4} - 10^{-2}$ . In fact, we have found that, in higher temperature limit, the phase velocity of the wave exceeds the velocity of light  $c$  and thus becomes superluminal. In Fig.(8.1), we have shown the variation of

the phase velocity of the resultant wave (Akhiezer - Polovin [27] with a Juttner-Synge distribution [58]) as a function of electron temperature  $\lambda$ . This figure indicates that in higher temperature limit, the phase velocity exceeds the velocity of light  $c$ . Moreover we have found that, these superluminal waves do not exhibit phase mixing even under the application of the external perturbation. As for example, here we have shown the space-time evolution of the electric field profile & snapshots of electron phase space without [Fig.8.2 and Fig.8.3] and with perturbation [Fig.8.4 and Fig.8.5] respectively.

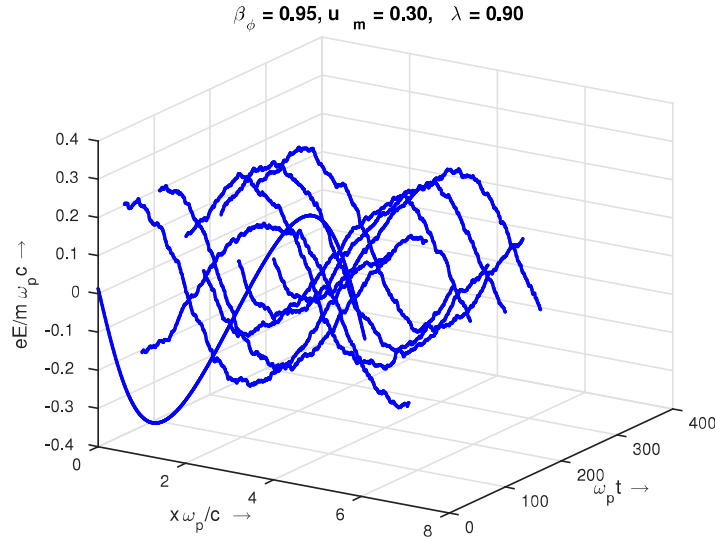


Figure 8.2: Space-time evolution of electric field for  $\beta_\phi = 0.95$ ,  $u_m = 0.3$ ,  $\lambda = 0.90$  and  $\delta = 0.0$

From Fig.(8.2), we observe that, the wave propagates even under the external perturbation without any breaking. Moreover, from Fig.(8.4) and Fig.(8.5), we find that there is no symptom of wave breaking via phase mixing. Our study indicates that, for superluminal waves, the characteristic frequency does not acquire any spatial dependency when it is subjected by an external perturbation and thus does not exhibit phase mixing. We wish to analyse the reason behind this further in the future.

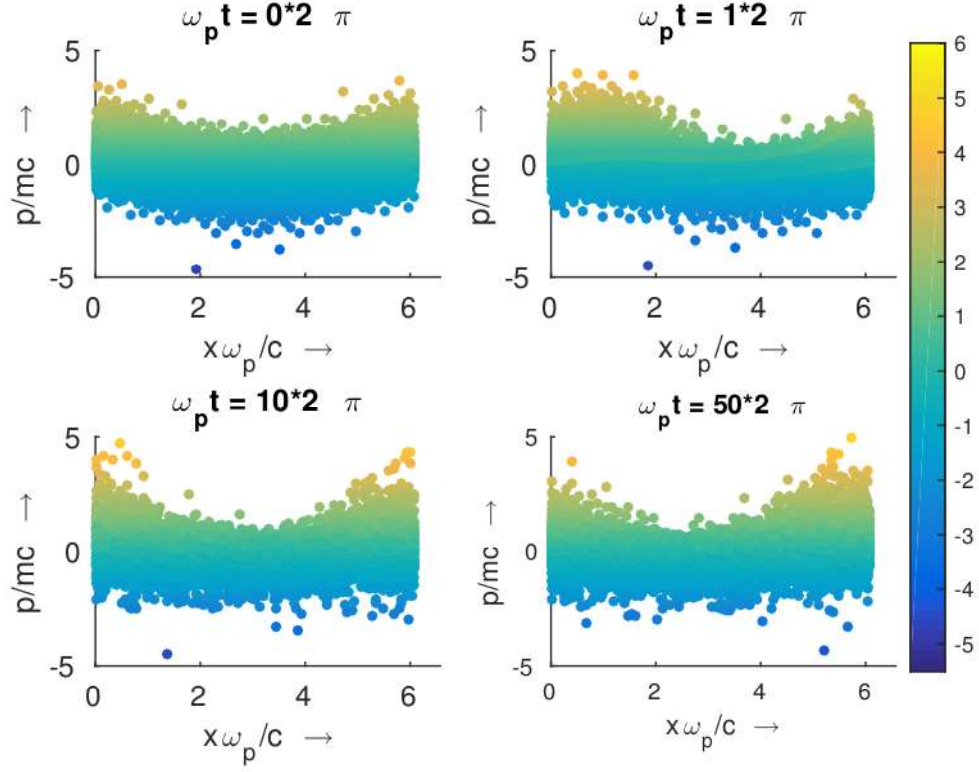


Figure 8.3: Snapshots of electron phase space for  $\beta_\phi = 0.95$ ,  $u_m = 0.3$ ,  $\lambda = 0.90$  and  $\delta = 0.0$  at different time steps

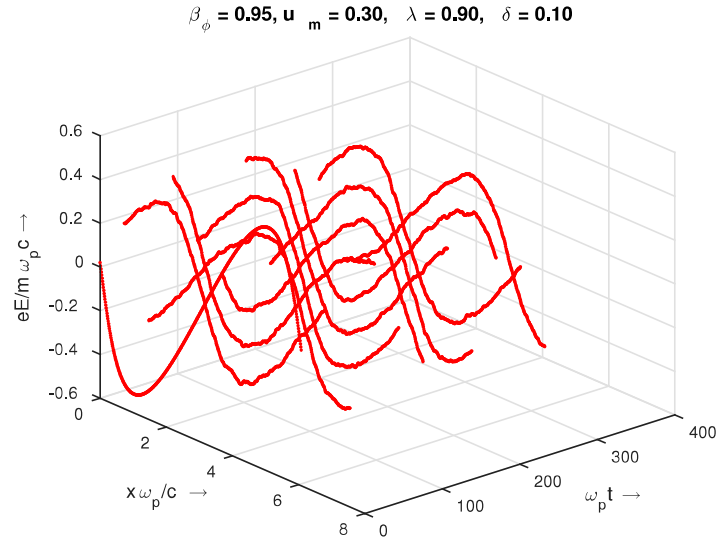


Figure 8.4: Space-time evolution of electric field for  $\beta_\phi = 0.95$ ,  $u_m = 0.3$ ,  $\lambda = 0.90$  and  $\delta = 0.1$

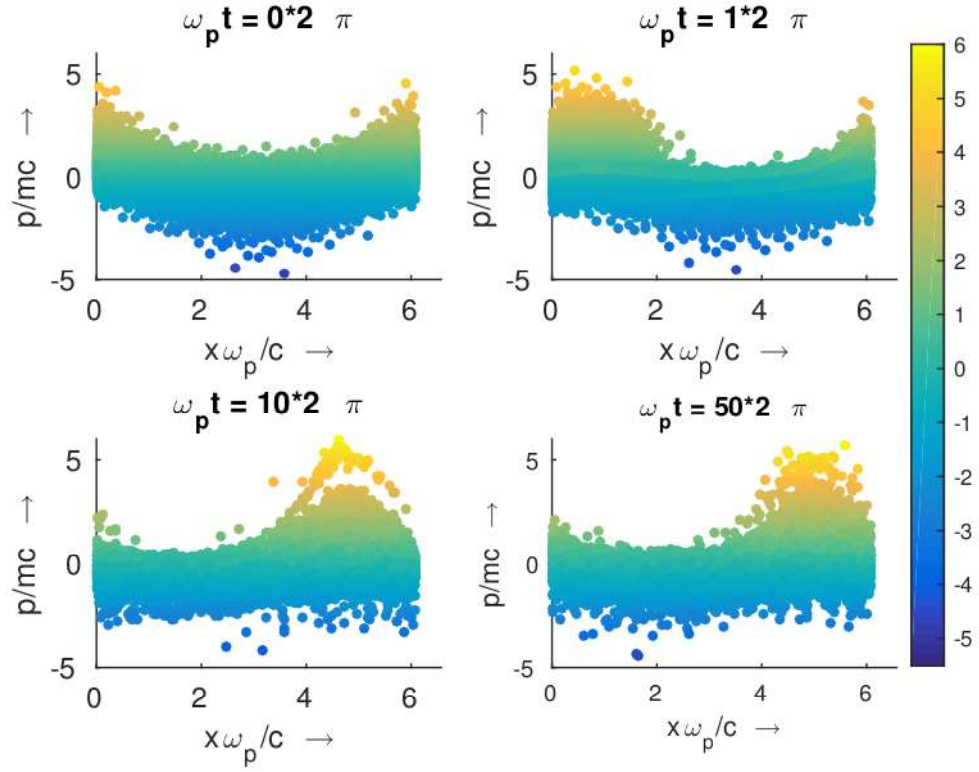
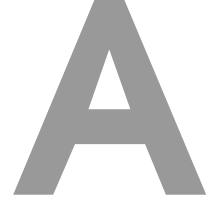


Figure 8.5: Snapshots of electron phase space for  $\beta_\phi = 0.95$ ,  $u_m = 0.3$ ,  $\lambda = 0.90$  and  $\delta = 0.1$  at different time steps

# Appendices





## Lindstedt - Poincaré Perturbation Technique (In Planar Geometry)

Here we give a solution of the equation of motion of a sheet (derived in chapter -3) and derive the expression for frequency  $\Omega$  in the weakly relativistic limit. We essentially follow the Lindstedt - Poincaré perturbation technique [54] and take a general wave packet like initial condition specified by its amplitude  $\delta$  and spectral width  $\Delta k$  (same as in chapter -3). The equation of motion of a sheet including the relativistic mass variation effect can be written as

$$\frac{\ddot{\xi}}{\left(1 - \frac{\dot{\xi}^2}{c^2}\right)^{3/2}} + \omega_p^2 \xi = 0 \quad (\text{A.1})$$

In weakly relativistic limit ( $\xi, \dot{\xi} \ll 1$ ), the above equation can be approximated as

$$\ddot{\xi} + \omega_p^2 \xi - \frac{3}{2} \omega_p^2 \xi \frac{\dot{\xi}^2}{c^2} + \frac{3}{8} \omega_p^2 \xi \frac{\dot{\xi}^4}{c^4} \approx 0 \quad (\text{A.2})$$

The above equation can be separated into following two equations:

$$\ddot{\xi} + \omega_p^2 \xi + \epsilon_1 \xi \dot{\xi}^2 \approx 0 \quad (\text{A.3})$$

$$\ddot{\xi} + \omega_p^2 \xi + \epsilon_2 \xi \dot{\xi}^4 \approx 0 \quad (\text{A.4})$$

where,  $\epsilon_1 = -\frac{3}{2} \frac{\omega_p^2}{c^2}$  and  $\epsilon_2 = \frac{3}{8} \frac{\omega_p^2}{c^4}$ . In the following two sections, we respectively solve Eqs.(A.3) and (A.4) by Lindstedt - Poincaré perturbation technique [54].

## Appendix A. Lindstedt - Poincaré Perturbation Technique (In Planar Geometry)

The initial conditions are as follows:

$$\xi(x, 0) = -\frac{\omega_p \delta}{2c} \left[ \frac{1}{k} \cos(kx) + \frac{1}{k + \Delta k} \cos(k + \Delta k)x \right] \quad (\text{A.5})$$

and

$$v(x, 0) = \frac{\omega_p \delta}{2} \left[ \frac{1}{k} \sin(kx) + \frac{1}{k + \Delta k} \sin(k + \Delta k)x \right] \quad (\text{A.6})$$

Eq.(A.5) represents the position perturbation of the sheets due the density perturbation of the form  $n(x, 0) = n_0 \left[ 1 + \delta \cos \left( \frac{\Delta k}{2} x \right) \cos \left( k + \frac{\Delta k}{2} x \right) \right]$ .

### A.1 Perturbative Solution of $\ddot{\xi} + \omega_p^2 \xi + \epsilon_1 \xi \dot{\xi}^2 \approx 0$ :

The equation is

$$\ddot{\xi} + \omega_p^2 \xi + \epsilon_1 \xi \dot{\xi}^2 \approx 0$$

Now we expand the displacement  $\xi$  and the oscillation frequency  $\Omega(x_{eq})$  in series as:  $\xi = \xi_0 + \epsilon_1 \xi_1 + \epsilon_1^2 \xi_2 + \dots$  and  $\Omega^2 = \omega_p^2 + \epsilon_1 \omega_1^2 + \epsilon_1^2 \omega_2^2 + \dots$  [54]. Therefore

$$\dot{\xi} = \dot{\xi}_0 + \epsilon_1 \dot{\xi}_1 + \epsilon_1^2 \dot{\xi}_2 + \dots \quad (\text{A.7})$$

and

$$\ddot{\xi} = \ddot{\xi}_0 + \epsilon_1 \ddot{\xi}_1 + \epsilon_1^2 \ddot{\xi}_2 + \dots \quad (\text{A.8})$$

Using the series expansions of  $\xi$ ,  $\dot{\xi}$ ,  $\ddot{\xi}$  and  $\Omega^2$ , Eq.(A.3) can be re-framed as

$$(\ddot{\xi}_0 + \epsilon_1 \ddot{\xi}_1 + \epsilon_1^2 \ddot{\xi}_2 + \dots) + (\Omega^2 - \epsilon_1 \omega_1^2 - \epsilon_1^2 \omega_2^2 - \dots)(\xi_0 + \epsilon_1 \xi_1 + \epsilon_1^2 \xi_2 + \dots) = -\epsilon_1 (\xi_0 + \epsilon_1 \xi_1 + \epsilon_1^2 \xi_2 + \dots)(\dot{\xi}_0 + \epsilon_1 \dot{\xi}_1 + \epsilon_1^2 \dot{\xi}_2 + \dots)^2 \quad (\text{A.9})$$

Equating the coefficients of  $\epsilon_1^0$  from the both side of Eq.(A.9), we get

$$\ddot{\xi}_0 + \Omega^2 \xi_0 = 0 \quad (\text{A.10})$$

The solution of the above equation is

$$\xi_0 = A \cos(\Omega t + \phi_0) \quad (\text{A.11})$$



## Appendix A. Lindstedt - Poincaré Perturbation Technique (In Planar Geometry)

Using the initial conditions given by Eqs.(A.5) and (A.6), the value of  $A$  and  $\phi_0$  come out respectively as

$$A(x) = \frac{\delta}{2k} \left[ 1 + \frac{k^2}{(k + \Delta k)^2} + \frac{2k}{(k + \Delta k)} \cos(\Delta k x) \right]^{1/2} \quad (\text{A.12})$$

and

$$\phi_0(x) = \tan^{-1} \left\{ \frac{\left[ \frac{\cos(kx)}{k} + \frac{\cos(k+\Delta k)x}{(k+\Delta k)} \right]}{\left[ \frac{\sin(kx)}{k} + \frac{\sin(k+\Delta k)x}{(k+\Delta k)} \right]} \right\} \quad (\text{A.13})$$

Now equating the coefficients of  $\epsilon_1^1$  from the both side of Eq.(A.9), we get

$$\ddot{\xi}_1 + \Omega^2 \xi_1 = \omega_1^2 \xi_0 - \xi_0 \dot{\xi}^2 \quad (\text{A.14})$$

Using the expression for  $\xi_0$  from Eq.(A.11), Eq.(A.14) becomes

$$\ddot{\xi}_1 + \Omega^2 \xi_1 = \omega_1^2 A \cos(\Omega t + \phi_0) - A^3 \Omega^2 \cos(\Omega t + \phi_0) \sin^2(\Omega t + \phi_0) \quad (\text{A.15})$$

$$\ddot{\xi}_1 + \Omega^2 \xi_1 = \left( \omega_1^2 A - \frac{A^3 \Omega^2}{4} \right) \cos(\Omega t + \phi_0) - \frac{A^3 \Omega^2}{4} \cos 2(\Omega t + \phi_0) \quad (\text{A.16})$$

The equations for  $\xi_1$  and  $\xi_2$  should not contain any secular terms. Therefore

$$\omega_1^2 = \frac{A^2 \Omega^2}{4} \quad (\text{A.17})$$

Now, we have

$$\Omega^2 \approx \omega_p^2 + \epsilon_1 \omega_1^2$$

Putting the values of  $\epsilon_1$  and  $\omega_1^2$ , we get

$$\Omega^2 \approx \omega_p^2 - \frac{3 \omega_p^2}{2} \frac{A^2 \Omega^2}{c^2} \quad (\text{A.18})$$

$$\Omega \approx \omega_p \left[ 1 - \frac{3}{16} \frac{\omega_p^2 A^2}{c^2} \right] \quad (\text{A.19})$$

Putting the value of  $A$  from Eq.(A.12), the expression for frequency finally becomes

$$\Omega \approx \omega_p \left[ 1 - \frac{3 \omega_p^2 \delta^2}{64 c^2} \left\{ \frac{1}{k^2} + \frac{1}{(k + \Delta k)^2} + \frac{2 \cos(\Delta k x_l)}{k(k + \Delta k)} \right\} \right] \quad (\text{A.20})$$

## Appendix A. Lindstedt - Poincaré Perturbation Technique (In Planar Geometry)

Now from Eq.(A.16), we can write

$$\ddot{\xi}_1 + \Omega^2 \xi_1 = \frac{A^3 \Omega^2}{4} \cos 2(\Omega t + \phi_0) \quad (\text{A.21})$$

The solution of Eq.(A.21) can be written as

$$\begin{aligned} \xi_1(x_{eq}, \tau) = & \frac{3\xi(x_{eq})^3}{16} \cos(\Omega\tau + 2\phi_0) \\ & - \frac{\xi(x_{eq})^3}{16} \cos(\Omega\tau - 2\phi_0) - \frac{\xi(x_{eq})^3}{8} \cos 2(\Omega\tau + \phi_0) \end{aligned} \quad (\text{A.22})$$

Now equating the coefficients of  $\epsilon_1^2$  from the both side of Eq.(A.9), we get

$$\ddot{\xi}_2 + \Omega^2 \xi_2 = \omega_2^2 \xi_0 + \omega_1^2 \xi_1 - \xi_1 \dot{\xi}_0^2 - 2\xi_0 \xi_1 \dot{\xi}_1 \quad (\text{A.23})$$

Substituting the values of  $\xi_0$  &  $\xi_1$  from Eqs.(A.11) & (A.23) respectively and following the similar way as above (vanishing the resonant term), the expression for  $\Omega$  becomes,

$$\omega \approx \omega_p \left[ 1 - \frac{9\omega_p^4 \delta^4}{1024c^4} \left\{ \frac{\cos(kx_l)}{k} + \frac{\cos(k + \Delta k)x_l}{(k + \Delta k)} \right\}^4 \right] \quad (\text{A.24})$$

Thus, using Eqs.(x20) and (x22b), the expression for frequency  $\Omega$  can be written as

$$\begin{aligned} \Omega \approx 1 - \frac{3\omega_p^2 \delta^2}{64c^2} \left[ \frac{1}{k^2} + \frac{1}{(k + \Delta k)^2} + \frac{2\cos(\Delta k x_l)}{k(k + \Delta k)} \right] \\ - \frac{9\omega_p^4 \delta^4}{1024c^4} \left\{ \frac{\cos(kx_l)}{k} + \frac{\cos(k + \Delta k)x_l}{(k + \Delta k)} \right\}^4 \end{aligned} \quad (\text{A.25})$$

## A.2 Perturbative Solution of $\ddot{\xi} + \omega_p^2 \xi + \epsilon_2 \xi \dot{\xi}^4 \approx 0$ :

Now the second equation is

$$\ddot{\xi} + \omega_p^2 \xi + \epsilon_2 \xi \dot{\xi}^4 \approx 0$$

## Appendix A. Lindstedt - Poincaré Perturbation Technique (In Planar Geometry)

Like the previous subsection, here also we expand the displacement  $\xi$  and the oscillation frequency  $\Omega(x_{eq})$  in series as:  $\xi = \xi_0 + \epsilon_2 \xi_1 + \epsilon_2^2 \xi_2 + \dots$  and  $\Omega^2 = \omega_p^2 + \epsilon_2 \omega_1^2 + \epsilon_2^2 \omega_2^2 + \dots$  [54]. Therefore

$$\dot{\xi} = \dot{\xi}_0 + \epsilon_2 \dot{\xi}_1 + \epsilon_2^2 \dot{\xi}_2 + \dots \quad (\text{A.26})$$

and

$$\ddot{\xi} = \ddot{\xi}_0 + \epsilon_2 \ddot{\xi}_1 + \epsilon_2^2 \ddot{\xi}_2 + \dots \quad (\text{A.27})$$

Using the series expansions of  $\xi$ ,  $\dot{\xi}$ ,  $\ddot{\xi}$  and  $\Omega^2$ , Eq.(A.4) can be written as

$$(\ddot{\xi}_0 + \epsilon_2 \ddot{\xi}_1 + \epsilon_2^2 \ddot{\xi}_2 + \dots) + (\Omega^2 - \epsilon_2 \omega_1^2 - \epsilon_2^2 \omega_2^2 - \dots)(\xi_0 + \epsilon_2 \xi_1 + \epsilon_2^2 \xi_2 + \dots) = -\epsilon_2 (\xi_0 + \epsilon_2 \xi_1 + \epsilon_2^2 \xi_2 + \dots)(\dot{\xi}_0 + \epsilon_2 \dot{\xi}_1 + \epsilon_2^2 \dot{\xi}_2 + \dots)^4 \quad (\text{A.28})$$

Equating the coefficients of  $\epsilon_2^0$  from the both side of Eq.(A.28), we get

$$\ddot{\xi}_0 + \Omega^2 \xi_0 = 0 \quad (\text{A.29})$$

The solution of the above equation is same as Eq.(A.11), where  $A$  and  $\phi_0$  are respectively given by Eq.(A.12) and Eq.(A.13) Now equating the coefficients of  $\epsilon_2^1$  from the both side of Eq.(A.28), we get

$$\ddot{\xi}_1 + \Omega^2 \xi_1 = \omega_1^2 \xi_0 - \xi_0 \dot{\xi}^4 \quad (\text{A.30})$$

Using the expression for  $\xi_0$ , Eq.(A.30) becomes

$$\ddot{\xi}_1 + \Omega^2 \xi_1 = \omega_1^2 A \cos(\Omega t + \phi_0) - A^5 \Omega^4 \cos(\Omega t + \phi_0) \sin^4(\Omega t + \phi_0) \quad (\text{A.31})$$

$$\ddot{\xi}_1 + \Omega^2 \xi_1 = \left( \omega_1^2 A - \frac{A^5 \Omega^4}{8} \right) \cos(\Omega t + \phi_0) - \frac{A^5 \Omega^4}{16} \{ 3 \cos 3(\Omega t + \phi_0) - \cos 5(\Omega t + \phi_0) \} \quad (\text{A.32})$$

The equations for  $\xi_1$  and  $\xi_2$  should not contain any secular terms. Therefore

$$\omega_1^2 = \frac{A^4 \Omega^4}{8} \quad (\text{A.33})$$

## Appendix A. Lindstedt - Poincaré Perturbation Technique (In Planar Geometry)

Now, we have

$$\Omega^2 \approx \omega_p^2 + \epsilon_2 \omega_1^2$$

Putting the values of  $\epsilon_2$ ,  $\omega_1^2$  &  $A$  and solving for  $\Omega$ , we get

$$\Omega \approx \omega_p \left[ 1 + \frac{3\omega_p^4 \delta^4}{1024c^4} \left\{ \frac{1}{k^2} + \frac{1}{(k + \Delta k)^2} + \frac{2\cos(\Delta k x_l)}{k(k + \Delta k)} \right\}^2 \right] \quad (\text{A.34})$$

Now, taking all the terms [from Eqs.(A.25) and (A.34)], the final expression for the frequency stands as (this is because at each step of the perturbation technique one is solving a linear equation driven by solution obtained from the previous step)

$$\begin{aligned} \frac{\Omega}{\omega_p} \approx 1 - \frac{3\omega_p^2 \delta^2}{64c^2} \left[ \frac{1}{k^2} + \frac{1}{(k + \Delta k)^2} + \frac{2\cos(\Delta k x_l)}{k(k + \Delta k)} \right] - \frac{3\omega_p^4 \delta^4}{1024c^4} \times \\ \left[ 3 \left\{ \frac{\cos(k x_l)}{k} + \frac{\cos(k + \Delta k) x_l}{(k + \Delta k)} \right\}^4 - \left\{ \frac{1}{k^2} + \frac{1}{(k + \Delta k)^2} + \frac{2\cos(\Delta k x_l)}{k(k + \Delta k)} \right\}^2 \right] \quad (\text{A.35}) \end{aligned}$$

As mentioned in chapter-3, now it is clear that the term  $3 \left\{ \frac{\cos(k x_l)}{k} + \frac{\cos(\Delta k + \Delta k) x_l}{(k + \Delta k)} \right\}^4$  comes from the second order correction in the Lindstedt- Poincaré series due to the term  $-(3/2)\xi\dot{\xi}^2$  in equation  $\ddot{\xi} + \xi - \frac{3}{2}\xi\dot{\xi}^2 + \frac{3}{8}\xi\dot{\xi}^4 \approx 0$  and the other term  $\left\{ \frac{1}{k^2} + \frac{1}{(k + \Delta k)^2} + \frac{2\cos(\Delta k x_l)}{k(k + \Delta k)} \right\}^2$  comes from to the first order correction in the Lindstedt-Poincaré series due to the next higher order term in the series expansion of  $\xi(1 - \dot{\xi}^2)^{3/2}$ , which is  $(3/8)\xi\dot{\xi}^4$  in the above equation.

# B

## Lindstedt - Poincaré Perturbation Technique (In Cylindrical and Spherical Geometry)

Here we respectively derive an expression for cylindrical and spherical oscillations from the equation of motion of a sheet in their respective coordinate system. We essentially follow the Lindstedt - Poincaré perturbation technique [54] and solve the equations in weakly relativistic limit.

For cylindrical and spherical oscillations, the equation of motion of an oscillating sheet in weakly relativistic limit can be written in the following generalized form

$$\ddot{\rho} + \omega_p^2 \rho + \epsilon_1 \rho \dot{\rho}^2 + \epsilon_2 \rho^2 + \epsilon_3 \rho^3 = 0 \quad (\text{B.1})$$

This equation can be separated in to the following two equations :

$$\ddot{\rho} + \omega_p^2 \rho + \epsilon_1 \rho \dot{\rho}^2 = 0 \quad (\text{B.2})$$

and

$$\ddot{\rho} + \omega_p^2 \rho + \epsilon_2 \rho^2 + \epsilon_3 \rho^3 = 0 \quad (\text{B.3})$$

Here Eqs.(B.2) and (B.3) are respectively indicate the correction for relativistic effects and geometrical effects. Eq.(B.3) can again be separated in to following two equations

$$\ddot{\rho} + \omega_p^2 \rho + \epsilon_2 \rho^2 = 0 \quad (\text{B.4})$$

and

$$\ddot{\rho} + \omega_p^2 \rho + \epsilon_3 \rho^3 = 0 \quad (\text{B.5})$$

We take the following initial conditions : at  $t = 0$ ,  $\rho = A_0$  and  $\dot{\rho} = 0$ . The solution of Eq.(B.4) and an expression for frequency have been given in Appendix- A. This frequency of oscillation ( $\Omega$ ) correct upto the second order of oscillation amplitude can be written as

$$\Omega = \omega_p \left[ 1 + \epsilon_1 \frac{A_0^2}{8} \right] \quad (\text{B.6})$$

Here the term  $\epsilon_1 \frac{A_0^2}{8}$ , arises due to the relativistic correction. In the following two subsections we respectively solve Eqs.(B.4) and (B.5) and derive an expression for frequency.

## B.1 Perturbative solution of $\ddot{\rho} + \omega_p^2 \rho + \epsilon_2 \rho^2 = 0$

Like previous case, here also we proceed in the same manner. First we expand  $\rho$  and  $\Omega$  in the following way :

$$\rho = \rho_0 + \epsilon_2 \rho_1 + \epsilon_2^2 \rho_2 + \dots$$

$$\Omega^2 = \omega_p^2 + \epsilon_2 \omega_1^2 + \epsilon_2^2 \omega_2^2 + \dots$$

$$\dot{\rho} = \dot{\rho}_0 + \epsilon_2 \dot{\rho}_1 + \epsilon_2^2 \dot{\rho}_2 + \dots$$

and

$$\ddot{\rho} = \ddot{\rho}_0 + \epsilon_2 \ddot{\rho}_1 + \epsilon_2^2 \ddot{\rho}_2 + \dots$$

Using the series expansions of  $\rho$ ,  $\dot{\rho}$ ,  $\ddot{\rho}$  and  $\Omega^2$ , Eq.(B.4) can be written as

$$(\ddot{\rho}_0 + \epsilon_2 \ddot{\rho}_1 + \epsilon_2^2 \ddot{\rho}_2 + \dots) + (\Omega^2 - \epsilon_2 \omega_1^2 - \epsilon_2^2 \omega_2^2 - \dots)(\rho_0 + \epsilon_2 \rho_1 + \epsilon_2^2 \rho_2 + \dots) = -\epsilon_2 (\xi_0 + \epsilon_2 \xi_1 + \epsilon_2^2 \xi_2 + \dots)^2 \quad (\text{B.7})$$

Equating the coefficients of  $\epsilon_2^0$  from the both side of Eq.(B.7), we get

$$\ddot{\rho}_0 + \Omega^2 \rho_0 = 0 \quad (\text{B.8})$$

## Appendix B. Lindstedt - Poincaré Perturbation Technique (In Cylindrical and Spherical Geometry)

Using the initial conditions, the solution can be written as

$$\rho_0 = A_0 \cos(\Omega t) \quad (\text{B.9})$$

Now, equating the coefficients of  $\epsilon_2^1$  from the both side of Eq.(B.7), we can write

$$\ddot{\rho}_1 + \Omega^2 \rho_1 = -\rho_0^2 + \omega_1^2 \rho_0 \quad (\text{B.10})$$

Putting the value of  $\rho_0$ , the above equation transforms to

$$\ddot{\rho}_1 + \Omega^2 \rho_1 = -\frac{A_0^2}{2}(1 + \cos 2\Omega t) + \omega_1^2 A_0 \cos \Omega t \quad (\text{B.11})$$

The term with frequency  $\Omega$  on the R.H.S of Eq.(B.11) causes a spurious resonance in the system. This would cause  $\rho_1$  to diverge. In order to have a finite  $\rho_1$ , we need to remove the resonance causing term from the R.H.S of Eq.(B.11), removal of this requires  $\omega_1 = 0$ . Thus

$$\ddot{\rho}_1 + \Omega^2 \rho_1 = -\frac{A_0^2}{2}(1 + \cos 2\Omega t) \quad (\text{B.12})$$

The solution can be written as

$$\rho_1 = -\frac{A_0^2}{2\Omega^2} + \frac{A_0^2}{3\Omega^2} \cos \Omega t + \frac{A_0^2}{6\Omega^2} \cos 2\Omega t \quad (\text{B.13})$$

Now, equating the coefficients of  $\epsilon_2^2$  from the both side of Eq.(B.7), we can write

$$\ddot{\rho}_2 + \Omega^2 \rho_2 = -2\rho_0 \rho_1 + \omega_2^2 \rho_0 \quad (\text{B.14})$$

Putting the values of  $\rho_0$  and  $\rho_1$  respectively from Eqs.(B.9) and (B.13), we get

$$\ddot{\rho}_2 + \Omega^2 \rho_2 = -\frac{A_0^3}{6\Omega^2} \cos 3\Omega t - \frac{A_0^3}{3\Omega^2} (1 + \cos 2\Omega t) + \left( \omega_2^2 A_0 + \frac{5A_0^3}{6\Omega^2} \right) \cos \Omega t \quad (\text{B.15})$$

Removing the resonant term, we get

$$\omega_2^2 A_0 = -\frac{5A_0^3}{6\Omega^2} \quad (\text{B.16})$$

Now using the series expansion of  $\Omega^2$ , we can write

$$\Omega^2 = \omega_p^2 + \epsilon_2 \omega_1^2 + \epsilon_2^2 \omega_2^2$$

The above equation can be simplified to

$$\Omega = \omega_p \left[ 1 - \frac{5}{12} \frac{\epsilon_2^2 A_0^2}{\omega_p^4} \right] \quad (\text{B.17})$$

## B.2 Perturbative solution of $\ddot{\rho} + \omega_p^2 \rho + \epsilon_3 \rho^3 = 0$

Using the series expansions of  $\rho$ ,  $\dot{\rho}$ ,  $\ddot{\rho}$  and  $\Omega^2$ , Eq.(B.5) can be written as

$$\begin{aligned} &(\ddot{\rho}_0 + \epsilon_3 \ddot{\rho}_1 + \epsilon_3^2 \ddot{\rho}_2 + \dots) + (\Omega^2 - \epsilon_3 \omega_1^2 - \epsilon_3^2 \omega_2^2 - \dots) \times \\ &(\rho_0 + \epsilon_3 \rho_1 + \epsilon_3^2 \rho_2 + \dots) = -\epsilon_3 (\xi_0 + \epsilon_3 \xi_1 + \epsilon_3^2 \xi_2 + \dots)^3 \end{aligned} \quad (\text{B.18})$$

The zeroth order solution is as same as Eq.(B.9). Equating the coefficients of  $\epsilon_3^1$  from the both side of Eq.(B.18), we can write

$$\ddot{\rho}_1 + \Omega^2 \rho_1 = -\rho_0^3 + \omega_1^2 \rho_0 \quad (\text{B.19})$$

Putting the value of  $\rho_0$ , the above equation transforms to

$$\ddot{\rho}_1 + \Omega^2 \rho_1 = -\frac{A_0^3}{4} \cos 3\Omega t + (\omega_1^2 A_0 - \frac{3A_0^3}{4}) \cos \Omega t \quad (\text{B.20})$$

As before, there is a resonating term on the R.H.S and

$$\omega_1^2 A_0 - \frac{3A_0^3}{4} = 0$$

Now using the series expansion of  $\Omega^2$ , we can write

$$\Omega^2 = \omega_p^2 + \epsilon_3 \omega_1^2$$



The above equation can be simplified to

$$\Omega = \omega_p \left[ 1 + \frac{3}{8} \frac{\epsilon_3 A_0^2}{\omega_p^2} \right] \quad (\text{B.21})$$

Now, Eq.(B.20) becomes

$$\ddot{\rho}_1 + \Omega^2 \rho_1 = -\frac{A_0^3}{4} \cos 3\Omega t \quad (\text{B.22})$$

The solution of  $\rho_1$  is given by

$$\rho_1 = \frac{A_0^3}{32\Omega^2} (\cos 3\Omega t - \cos \Omega t) \quad (\text{B.23})$$

Now, equating the coefficients of  $\epsilon_3^2$  from the both side of Eq.(B.7), we can write

$$\ddot{\rho}_2 + \Omega^2 \rho_2 = -3\rho_0^2 \rho_1 + \omega_1^2 \rho_1 + \omega_2^2 \rho_0 \quad (\text{B.24})$$

Now putting the expression of  $\rho_1$  in the above equation and following the same procedure, we get

$$\Omega = \omega_p \left[ 1 + \epsilon_3^2 \frac{A_0^4}{128\omega_p^4} \right] \quad (\text{B.25})$$

Combining Eqs.(B.21) and (B.25), the expression for frequency can be penned as

$$\Omega = \omega_p \left[ 1 + \frac{3}{8} \frac{\epsilon_3 A_0^2}{\omega_p^2} + \epsilon_3^2 \frac{A_0^4}{128\omega_p^4} \right] \quad (\text{B.26})$$

Finally combining Eqs.(B.26) and (B.17), the final expression for frequency stands as

$$\Omega = \omega_p \left[ 1 + \epsilon_1 \frac{A_0^2}{8} - \frac{5}{12} \frac{\epsilon_2^2 A_0^2}{\omega_p^4} + \frac{3}{8} \frac{\epsilon_3 A_0^2}{\omega_p^2} + \epsilon_3^2 \frac{A_0^4}{128\omega_p^4} \right] \quad (\text{B.27})$$

### B.3 Frequency of Oscillation in Cylindrical Geometry:

In cylindrical geometry, the equation of motion of an oscillating sheet (in weakly relativistic limit) is given by

$$\ddot{\rho} - \frac{3}{2} \frac{r_0^2 \omega_p^2}{c^2} \rho \dot{\rho}^2 + \omega_p^2 \rho - \frac{\omega_p^2}{2} \rho^2 + \frac{\omega_p^2}{2} \rho^3 = 0 \quad (\text{B.28})$$

Comparing Eq.(B.28) with Eq.(B.1), we get  $\epsilon_1 = -\frac{3}{2} \frac{r_0^2 \omega_p^2}{c^2}$ ,  $\epsilon_2 = -\frac{\omega_p^2}{2}$  and  $\epsilon_3 = \frac{\omega_p^2}{2}$ . Putting these values in Eq.(B.27), the expression for frequency of an oscillating sheet in a cylindrical geometry can be written as (this is because at each step of the perturbation technique one is solving a linear equation driven by solution obtained from the previous step)

$$\Omega_{cy}(rel) = \omega_p \left[ 1 - \frac{3\omega_p^2}{16} \frac{r_0^2 \rho_0(r_0)^2}{c^2} + \frac{\rho_0(r_0)^2}{12} + \frac{\rho_0(r_0)^4}{512} \right] \quad (\text{B.29})$$

In nonrelativistic limit  $\epsilon_1 \rightarrow 0$  and the above expression stands as

$$\Omega_{cy}(nonrel) = \omega_p \left[ 1 + \frac{\rho_0(r_0)^2}{12} + \frac{\rho_0(r_0)^4}{512} \right] \quad (\text{B.30})$$

### B.4 Frequency of Oscillation in Spherical Geometry:

In cylindrical geometry, the equation of motion of an oscillating sheet (in weakly relativistic limit) is given by

$$\ddot{\rho} - \frac{3}{2} \frac{r_0^2 \omega_p^2}{c^2} \rho \dot{\rho}^2 + \omega_p^2 \rho - \omega_p^2 \rho^2 + \frac{4\omega_p^2}{3} \rho^3 = 0 \quad (\text{B.31})$$

Similarly, comparing Eq.(B.31) with Eq.(B.1), we get  $\epsilon_1 = -\frac{3}{2} \frac{r_0^2 \omega_p^2}{c^2}$ ,  $\epsilon_2 = -\omega_p^2$  and  $\epsilon_3 = \frac{4\omega_p^2}{3}$ . Putting these values in Eq.(B.27), the expression for frequency of an oscillating sheet in a spherical geometry can be written as (this is because at each step of the perturbation technique one is solving a linear equation driven by

## Appendix B. Lindstedt - Poincaré Perturbation Technique (In Cylindrical and Spherical Geometry)

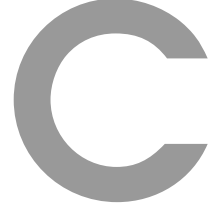
solution obtained from the previous step)

$$\Omega_{cy}(rel) = \omega_p \left[ 1 - \frac{3\omega_p^2}{16} \frac{r_0^2 \rho_0(r_0)^2}{c^2} + \frac{\rho_0(r_0)^2}{12} + \frac{\rho_0(r_0)^4}{72} \right] \quad (\text{B.32})$$

In nonrelativistic limit  $\epsilon_1 \rightarrow 0$  and the above expression becomes

$$\Omega_{cy}(nonrel) = \omega_p \left[ 1 + \frac{\rho_0(r_0)^2}{12} + \frac{\rho_0(r_0)^4}{72} \right] \quad (\text{B.33})$$





# Derivation of Relativistic Warm Plasma Dispersion Relation

Here we give an elementary derivation of the dispersion relation followed by a relativistically intense wave in a warm plasma. We follow the steps used by Pegoraro and Porcelli [60].

## C.1 Derivation of Linear Dispersion Relation

We start from the 1-D relativistic Vlasov equation which can be written as

$$\frac{\partial f_R}{\partial t} + v \frac{\partial f_R}{\partial z} - eE \frac{\partial f_R}{\partial p_z} = 0 \quad (\text{C.1})$$

$f_R$  is the relativistic distribution function. We separate the distribution function  $f_R$  into an equilibrium part  $f_{R0}$  which is in the equilibrium rest frame and a perturbed part  $f_{R1}$ , where we assume that  $|f_{R1}| \ll |f_{R0}|$ . We also take  $f_{R0}$  to be given by the Jüttner-Synge distribution

$$f_{R0}(p) = n_0 \frac{\alpha}{4m^3 K_2(\alpha)} \exp \left[ -\alpha(1 + p^2/m^2)^{1/2} \right] \quad (\text{C.2})$$

where,  $\alpha = \frac{m}{k_B T_e}$  is the inverse of the relevant temperature ( $c = 1$ ),  $n_0$  is the equilibrium density in the proper frame. As we are looking for the wave like solution of the form  $\exp \iota(kz - \omega t)$  (propagating wave along the  $z$ -direction), therefore we

## Appendix C. Derivation of Relativistic Warm Plasma Dispersion Relation

can put  $\frac{\partial}{\partial t} = -\iota\omega$  and  $\frac{\partial}{\partial z} = -\iota k$ . Therefore linearising Eq.(C.1), we get

$$-\iota\omega f_{R1} + \iota k f_{R1} = eE_1 \left( \frac{\partial f_{R0}}{\partial p_z} \right) \quad (\text{C.3})$$

$E_1$  is the perturbed electric field.

$$f_{R1} = \iota \left( \frac{eE}{w} \right) \left( \frac{\partial f_{R0}}{\partial p} \right) \left[ 1 - \frac{kv}{\omega} \right]^{-1} \quad (\text{C.4})$$

Now, from Poisson's equation

$$\frac{\partial E}{\partial z} = -4\pi en_1 \quad (\text{C.5})$$

$n_1$  is the perturbed electron density.

$$\iota k E_1 = -4\pi \int f_{R1} d^3p \quad (\text{C.6})$$

From Eq.(C.2), we can write

$$\frac{\partial f_{R0}}{\partial p_z} = -\frac{\alpha^2 n_0}{4\pi m^4 K_2(\alpha)} \exp \left[ -\alpha(1 + p^2/m^2 c^2)^{1/2} \right] \frac{p_z/m}{(1 + p^2/m^2)^{1/2}} \quad (\text{C.7})$$

Now, putting the value of  $f_{R1}$  from Eq.(C.4) in Eq.(C.6), we get

$$k = -\frac{4\pi e^2}{\omega} \int \left( \frac{\partial f_{R0}}{\partial p_z} \right) \left[ 1 - \frac{kp_z}{m\omega(1 + p^2/m^2 c^2)^{1/2}} \right]^{-1} d^3p \quad (\text{C.8})$$

$$k = -\frac{4\pi e^2}{\omega} \int \left( \frac{\partial f_{R0}}{\partial p_z} \right) \sum_{j=0}^{\infty} \left( \frac{k}{\omega} \right)^j \left[ \frac{p_z/m}{(1 + p^2/m^2 c^2)^{1/2}} \right]^j d^3p$$

$$\omega^2 = -4\pi e^2 \int \left( \frac{\partial f_{R0}}{\partial p_z} \right) \sum_{j=0}^{\infty} \left( \frac{k}{\omega} \right)^{j-1} \left[ \frac{p_z/m}{(1 + p^2/m^2 c^2)^{1/2}} \right]^j d^3p \quad (\text{C.9})$$

## Appendix C. Derivation of Relativistic Warm Plasma Dispersion Relation

Taking  $p_z = p \cos \theta$ ,  $d^3p = 4\pi p^2 \sin \theta d\theta d\phi$  and using Eq.(C.7), the above equation modifies to

$$\omega^2 = \frac{\omega_p^2 \alpha^2}{2K_2(\alpha)} \sum_{j=0}^{\infty} \left(\frac{k}{\omega}\right)^{j-1} \int_{\theta=0}^{\pi} \cos \theta^{(j+1)} \sin \theta d\theta \times \int_{x=0}^{\infty} \exp[-\alpha(1+x^2)^{1/2}] \frac{x^{j+3}}{(1+x^2)^{\frac{(j+1)}{2}}} dx \quad (\text{C.10})$$

where  $x = p/m$ . The above equation can again be simplified as

$$\omega^2 = \frac{\omega_p^2 \alpha^2}{2K_2(\alpha)} \sum_{j=0}^{\infty} \left(\frac{k}{\omega}\right)^{j-1} \left[ \int_{y=-1}^{+1} y^{(j+1)} dy \right] I_{j+3,j+1}(\alpha) \quad (\text{C.11})$$

where,

$$I_{m,n}(\alpha) = \int_{x=0}^{\infty} \exp[-\alpha(1+x^2)^{1/2}] \frac{x^m}{(1+x^2)^{\frac{n}{2}}} dx$$

and by putting  $y = \cos \theta$

$$\int_{\theta=0}^{\pi} \cos \theta^{(j+1)} \sin \theta d\theta = \int_{y=-1}^{+1} y^{(j+1)} dy$$

Now for

$$j = 0, \int_{y=-1}^{+1} y^{(j+1)} dy = 0$$

$$j = 1, \int_{y=-1}^{+1} y^{(j+1)} dy = 2/3$$

$$j = 2, \int_{y=-1}^{+1} y^{(j+1)} dy = 2/3$$

$$j = 3, \int_{y=-1}^{+1} y^{(j+1)} dy = 2/5$$

To first order in  $(k/\omega)^2$ , Eq.(C.11) can be expanded as

$$\begin{aligned} \omega^2 &= \frac{\omega_p^2 \alpha^2}{2K_2(\alpha)} \left[ \frac{2}{3} I_{4,2}(\alpha) + \frac{2}{5} \left(\frac{k}{\omega}\right)^2 I_{6,4}(\alpha) \right] \\ \omega^2 &= \frac{\omega_p^2 \alpha^2}{K_2(\alpha)} \left[ \frac{1}{3} I_{4,2}(\alpha) + \frac{1}{5} \left(\frac{k}{\omega}\right)^2 I_{6,4}(\alpha) \right] \end{aligned} \quad (\text{C.12})$$

## C.2 Case 1: $\alpha \gg 1$ , Weakly Relativistic limit

For  $n \geq 2$ , the integrals  $I_{m,n}(\alpha)$  can be evaluated for large values of  $\alpha$  using the saddle point method, which is given by [60]

$$I_{m,n}(\alpha) = \left[ \frac{\pi}{2\alpha^{m+1}} \right]^{1/2} \frac{(m+1)!!}{(m+1)} \exp(-\alpha) \times \left[ 1 + \frac{(m+1)}{8\alpha} (m-1) - 4(n-1) \right] \quad (\text{C.13})$$

Using the above expression, we get

$$I_{4,2}(\alpha) = 3 \left[ \frac{\pi}{2\alpha^5} \right]^{1/2} \exp(-\alpha) \left[ 1 - \frac{5}{8\alpha} \right] \quad (\text{C.14})$$

and

$$I_{6,4}(\alpha) = 15 \left[ \frac{\pi}{2\alpha^7} \right]^{1/2} \exp(-\alpha) \left[ 1 - \frac{49}{8\alpha} \right] \quad (\text{C.15})$$

For large  $\alpha$ , the modified Bessel function can be written as

$$K_\nu(\alpha) = \sqrt{\frac{\pi}{2\alpha}} \exp(-\alpha) \left[ 1 + \frac{4\nu^2 - 1}{8\alpha} + \frac{(4\nu^2 - 1)(4\nu^2 - 9)}{2!(8\alpha)^2} \right] \quad (\text{C.16})$$

Now substituting the values of  $I_{4,2}(\alpha)$ ,  $I_{6,4}(\alpha)$  and  $K_2(\alpha)$  respectively using Eqns.(C.14), (C.15) and (C.16) in Eq.(C.12), the dispersion relation becomes

$$\omega^2 = \omega_p^2 \left( 1 - \frac{5}{2\alpha} \right) + 3 \frac{k^2}{\alpha} \quad (\text{C.17})$$

This is the dispersion relation followed by a relativistically intense electron plasma wave in a warm plasma having nonrelativistic initial temperature. The similar dispersion relation has also been derived rigorously by several authors [59, 61–63].

## C.3 Case 2: $\alpha \ll 1$ , Strongly Relativistic limit

We know that [60]

$$I_{m,n}(\alpha) = I_{m-2,n-2}(\alpha) - I_{m-2,n}(\alpha) \quad (\text{C.18})$$



## Appendix C. Derivation of Relativistic Warm Plasma Dispersion Relation

Therefore, the integral  $I_{4,2}$  can be simplified as

$$I_{4,2}(\alpha) = I_{0,-2}(\alpha) - 2I_{0,0}(\alpha) + I_{0,2}(\alpha) \quad (\text{C.19})$$

Now we note that  $I_{0,n+1}(\alpha) = Ki_n(\alpha)$ , where  $Ki_n(\alpha)$  is the repeated integral of Modified Bessel function defined as

$$Ki_n(\alpha) = \int_{\alpha}^{\infty} Ki_{n-1}(\alpha) dx$$

with  $Ki_0(\alpha) = K_0(\alpha)$ . Therefore, Eqn.(C.19) becomes

$$I_{4,2}(\alpha) = Ki_{-3}(\alpha) - 2I_{0,0}(\alpha) + Ki_1(\alpha) \quad (\text{C.20})$$

Now,  $Ki_{-r}(\alpha) = (-1)^r \frac{d^r}{d\alpha^r} K_0(\alpha)$  and in the limit  $\alpha \ll 1$ ,  $K_0(\alpha) = -\ln(\alpha)$ . Thus,

$$Ki_{-3}(\alpha) = (-1)^3 \frac{d^3}{d\alpha^3} [-\ln(\alpha)] = \frac{2}{\alpha^3} \quad (\text{C.21})$$

Next, for  $\alpha \ll 1$ ,

$$Ki_1(\alpha) = \int_{\alpha}^{\infty} K_0(t) dt \sim \frac{\pi}{2} \quad (\text{C.22})$$

and

$$I_{0,0}(\alpha) = \int_0^{\infty} \exp[-\alpha(1+t^2)] dt = K_1(\alpha) \sim \frac{1}{\alpha} \quad (\text{C.23})$$

where we have used  $K_{\nu}(\alpha) \sim \frac{1}{2} \Gamma(\nu) \frac{\alpha^{-\nu}}{2}$  for  $\alpha \ll 1$ . Thus the final form of the integral can be written as

$$I_{4,2}(\alpha) = \frac{2}{\alpha^3} - \frac{2}{\alpha} + \frac{\pi}{2} \quad (\text{C.24})$$

since  $\alpha \ll 1$ , only the first term will contribute and the above Eqn. becomes

$$I_{4,2}(\alpha) \sim \frac{2}{\alpha^3} \quad (\text{C.25})$$

Similarly using Eqn.(C.18), the integral  $I_{6,4}(\alpha)$  can be modified as

$$I_{6,4}(\alpha) = I_{0,-2}(\alpha) - 3I_{0,0}(\alpha) + 3I_{0,0}(\alpha) - I_{0,4}(\alpha) \quad (\text{C.26})$$

## Appendix C. Derivation of Relativistic Warm Plasma Dispersion Relation

$$I_{6,4}(\alpha) = \frac{2}{\alpha^3} - \frac{3}{\alpha} + 3\frac{\pi}{2}(\alpha) - Ki_3(\alpha) \quad (\text{C.27})$$

Now,

$$Ki_3(\alpha) = \int_0^\infty \frac{e^{-\alpha \cosh t}}{\cosh^3 t} dt \quad (\text{C.28})$$

In the limit  $\alpha \ll 1$ , the value of above integral is given by  $\sim \frac{\pi}{4}$ . Thus, from Eqn.(C.27), the final form of the integral  $I_{6,4}(\alpha)$  becomes

$$I_{6,4}(\alpha) = \frac{2}{\alpha^3} - \frac{3}{\alpha} + 3\frac{\pi}{2}(\alpha) - \frac{\pi}{4} \quad (\text{C.29})$$

We see that, here also the first term on the R. H. S of the above Eqn. will contribute in the limit  $\alpha \ll 1$ . Thus using Eqns.(C.25) and (C.29), Eqn.(C.12) can be simplified as

$$\omega^2 \approx \omega_p^2 \frac{\alpha}{3} + \frac{\omega_p^2 k^2 \alpha}{5 \omega^2} \quad (\text{C.30})$$

which finally gives

$$\omega^2 = \omega_p^2 \frac{\alpha}{3} + \frac{3}{5} k^2 \quad (\text{C.31})$$

This is the dispersion relation followed by a relativistically intense electron plasma wave in a warm plasma having relativistic initial temperature.

# Bibliography

- [1] Francis F. Chen. Introduction to plasma physics and controlled fusion. *Plenum Press*, 1983.
- [2] Nicholas A. Krall and Alvin. W Trivelpiece. Principles of plasma physics. *McGraw-Hill*, 1973.
- [3] Ronald C Davidson. Methods in nonlinear plasma theory. *Academic Press*, 1972.
- [4] R. O. Dendy. Plasma dynamics. *Clarendon Press, Oxford*, 1990.
- [5] J. M. Dawson. Nonlinear electron oscillations in a cold plasma. *Physical Review*, 113(2):383, 1959.
- [6] R. C. Davidson and P. P. J. M. Schram. Nonlinear oscillations in a cold plasma. *Nuclear Fusion*, 8(3):168, 1968.
- [7] D. Bohm and E. P. Gross. Theory of plasma oscillations. a. origin of medium-like behaviour. *Physical Review*, 75(12):1851, 1949.
- [8] T. Tajima and J.M. Dawson. Laser electron accelerator. *Phys. Rev. Lett.*, 43, 1979.
- [9] J. B. Rosenzweig. Nonlinear plasma dynamics in the plasma wake field accelerator. *Phys. Rev. Lett.*, 58:555, 1987.
- [10] William L Kruer. The physics of laser plasma interactions. *Avalon Publishing*, 2003.
- [11] Paul Gibbon. Short pulse laser interactions with matter: An introduction. *Dover Publications, INC, New York*.
- [12] Peter Mulser and Dieter Bauer. High power laser-matter interaction. *Springer*, 2010.
- [13] A. V. Borovsky, A. L. Galkin, O. B. SHiryaev, and T. Auguste. Laser physics at relativistic intensities. *Springer*, 2003.

- [14] Eric Esarey, Phillip Sprangle, Jonathan Krall, and Antonio Ting. Overview of plasma-based accelerator concepts. *IEEE Transactions on Plasma Science*, 24(2):252, 1996.
- [15] Donald Umstadter. Review of physics and applications of relativistic plasmas driven by ultra-intense lasers. *Physics of Plasmas*, 8(5):1774–1785, 2001.
- [16] E. Esarey, C. B. Schroder, and W. P. Leemans. Physics of laser-driven plasma-based electron accelerators. *Rev. Mod. Phys.*, 81:1229, 2009.
- [17] Max Tabak, James Hammer, Michael E. Glinsky, William L. Kruer, Scott C. Wilks, John Woodworth, E. Michael Campbell, Michael D. Perry, and Rodney J. Mason. Ignition and high gain with ultrapowerful lasers\*. *Physics of Plasmas*, 1(5):1626–1634, 1994.
- [18] M. Honda, A. Nishiguchi, H. Takabe, H. Azechi, and K. Mima. Kinetic effects on the electron thermal transport in ignition target design. *Physics of Plasmas*, 3(9):3420–3424, 1996.
- [19] S. Sengupta, A. S. Sandhu, G. K. Kumar, A. Das, and P. K. Kaw. Short laser pulse induced generation of hot electrons and their anomalous stopping in overdense plasmas. *Nuclear Fusion*, 45(11):1377–1385, 2005.
- [20] A. Modena, Z. Nazmudin, A. E. Dangor, C. E. Clayton, K. A. Marsh, C. Joshi, V. Malka, C. B. Darrow, C. Danson, D. Neely, and F. N. Walsh. Electron acceleration from the breaking of relativistic plasma waves. *Nature*, 377:606, 1995.
- [21] A. Modena, Z. Nazmudin, A. E. Dangor, C. E. Clayton, K. A. Marsh, C. Joshi, V. Malka, C. B. Darrow, and C. Danson. Observation of raman forward scattering and electron acceleration in the relativistic regime. *IEEE Transactions on Plasma Science*, 24:289–295, 1996.
- [22] J. Faure, Y. Glinec, A. Pukhov, S. Kiselev, S. Gordienko, E. Lefebvre, J. P. Rousseau, F. Burgy, and V. Malka. A laser-plasma accelerator producing monoenergetic electron beams. *Nature*, 431:541–544, Sep2004.

- [23] S. P. D. Mangles, C. D. Murphy, Z. Najmudin, A. G. R. Thomas, J. L. Collier, A. E. Dangor, E. J. Divall, P. S. Foster, J. G. Gallacher, C. J. Hooker, D. A. Jaroszynski, A. J. Langley, W. B. Mori, P. A. Norreys, F. S. Tsung, R. Viskup, B. R. Walton, and K. Krushelnick. Monoenergetic beams of relativistic electrons from intense laser-plasma interactions. *Nature*, 431:535–538, Sep2004.
- [24] C. G. R. Geddes, Cs. Toth, J. van Tilborg, E. Esarey, C. B. Schroeder, D. Bruhwiler, C. Nieter, J. Cary, and W. P. Leemans. High-quality electron beams from a laser wakefield accelerator using plasma-channel guiding. *Nature*, 431:538–541, Sep2004.
- [25] Thomas Katsouleas. Accelerator physics: Electrons hang ten on laser wake. *Nature*, 431:515–516, Sep2004.
- [26] V. Malka, J. faure, Y. A. gauduel, E. Lefebvre, A. Rousse, and K. T. Phuoc. Principles and applications of compact laserâ€šplasma accelerators. *Nature Phys.*, 4:447, 2008.
- [27] A. I. Akhiezer and R. V Polovin. Theory of wave motion of a electron plasma. *JETP*, 3(5):696–705, 1956.
- [28] E Infeld and G. Rowlands. Relativistic bursts. *Phys. Rev. Lett.*, 62(10):1122, 1989.
- [29] Sudip Sengupta and Predhiman K. Kaw. Phase mixing of nonlinear plasma oscillations in an arbitrary mass ratio cold plasma. *Phys. Rev. Lett.*, 82(9):1867, 1999.
- [30] Sudip Sengupta, Vikrant Saxena, Predhiman K. Kaw, Abhijit Sen, and Amita Das. Phase mixing of relativistically intense waves in a cold homogeneous plasma. *Phys. Rev. E*, 79:026404, Feb 2009.
- [31] Sudip Sengupta, Predhiman Kaw, Vikrant Saxena, Abhijit Sen, and Amita Das. Phase mixing/wave breaking studies of large amplitude oscillations in a cold homogeneous unmagnetized plasma. *Plasma Physics and Controlled Fusion*, 53(7):074014, 2011.

- [32] Sudip Sengupta. Breaking of relativistically intense longitudinal space charge waves: A description using dawson sheet model. *AIP Conf. Proc.*, 1582:191, 2014.
- [33] Prabal Singh Verma, Sudip Sengupta, and Predhiman Kaw. Breaking of longitudinal akhiezer-polovin waves. *Phys. Rev. Lett.*, 108:125005, 2012.
- [34] E. Infeld, G. Rowlands, and S. Torvén. Ion density cavities can cause non-linear plasma oscillations to peak. *Phys. Rev. Lett.*, 62(19):2269, 1989.
- [35] G. Botha, T. Arber, V. M. Nakariakov, and F. P Keenan. A developed stage of alfvén wave phase mixing. *Astronomy and Astrophysics*, 363:1186, 2000.
- [36] T. P. Coffey. Breaking of large amplitude plasma oscillations. *Phys. Fluids*, 14:1402, 1971.
- [37] T. Katsouleas and W. B. Mori. Wave-breaking amplitude of relativistic oscillations in a thermal plasma. *Phys. Rev. Lett.*, 61:90–93, Jul 1988.
- [38] J. B. Rosenzweig. Trapping, thermal effects and wave breaking in the non-linear plasma wake-field accelerator. *Phys. Rev. A*, 38:3634, 1988.
- [39] W. B. Mori and T. Katsouleas. Wavebreaking of longitudinal plasma oscillations. *Physica Scripta*, T30:127, 1990.
- [40] Z. M. Sheng and J. Meyer-ter Vehn. Relativistic wave breaking in warm plasmas. *Phys. Plasmas*, 4:493, 1997.
- [41] C. B. Schroeder, E. Esarey, and B. A. Shadwick. Warm wave breaking of nonlinear plasma waves with arbitrary phase velocities. *Phys. Rev. E*, 72:055401, 2005.
- [42] C. B. Schroeder, E. Esarey, B. A. Shadwick, and W. P. Leemans. Trapping, dark current, and wave breaking in nonlinear plasma waves. *Phys. Plasmas*, 13:033103, 2006.
- [43] R. M. G. M. Trines and P. A. Norreys. Wave-breaking limits for relativistic electrostatic waves in a one-dimensional warm plasma. *Phys. Plasmas*, 13:123102, 2006.

- [44] C. B. Schroeder and E. Esarey. Relativistic warm plasma theory of nonlinear laser-driven electron plasma waves. *Phys. Rev. E*, 81:056403, 2010.
- [45] John M. Dawson. Particle simulation of plasmas. *Rev. Mod. Phys.*, 55:403, 1983.
- [46] W. Press et al. Numerical recipes: The art of scientific computing. *Cambridge University Press*, 1992.
- [47] Birdsall C. K. Particle-in-cell charged-particle simulations, plus monte carlo collisions with neutral atoms, pic-mcc. *IEEE Trans. on Plasma Science*, 19(2):65, 1991.
- [48] C. K. Birdsall and A. B. Langdon. Plasma physics via computer simulation. *Adam Hilger*.
- [49] Sudip Sengupta. Particle simulation of quark-antiquark plasma. *PhD Thesis*, 2002.
- [50] L. M. Gorbunov and V. I. Kirsanov. Excitation of plasma waves by an electromagnetic wave packet. *Sov Phys. JETP*, 66(2):290, 1987.
- [51] J. B. Rosenzweig, P. Schoessow, B. Cole, W. Gai, R. Konecny, J. Norem, and J. Simpson. Experimental measurement of nonlinear plasma wake fields. *Phys. Rev. A*, 39(3):1586(R), 1989.
- [52] C. D. Decker, W. B. Mori, and T. Katsouleas. Particle-in-cell simulations of raman forward scattering from short-pulse high-intensity lasers. *Phys. Rev. E*, 50(5):3338(R), 1994.
- [53] Vikrant Saxena, Amita Das, Sudip Sengupta, Predhiman Kaw, and Abhijit Sen. Stability of nonlinear one-dimensional laser pulse solitons in a plasma. *Phys. Plasmas*, 14(7):072307, 2007.
- [54] Ali Hasan Nayfeh. Perturbation methods. *John Wiley and sons*, 1973.
- [55] L. M. Gorbunov, A. A. Frolov, E. V. Chizhonkov, and N. E. Andreev. Breaking of nonlinear cylindrical plasma oscillations. *Plasma Phys. Rep.*, 36(4):345, 2010.

- [56] S. S. Bulanov, A. Maksimchuk, C. B. Schoreder, A. G. Zhidkov, E. Esarey, and W. P. Leemans. Relativistic spherical plasma waves. *Phys. Plasmas*, 19:020702, 2012.
- [57] P. Bertrand and M. R. Fiex. Nonlinear electron plasma oscillation: The water bag model. *Phys. Lett.*, 28A(1):68, 1968.
- [58] J. L. Synge. The relativistic gas. *North- Holland Publishing Company*, 1957.
- [59] B. Buti. Plasma oscillations and Landau damping in a relativistic gas. *Phys. Fluids.*, 5:1, 1962.
- [60] F. Pegoraro and F. Porcelli. Equation of state for relativistic plasma waves. *Physics of Plasmas*, 27:1665, 1984.
- [61] P. Misra. The study of electromagnetic cusp solitons. *Jour. Plasma. Phys.*, 14(3):529, 1975.
- [62] Rémi Hakim. Introduction to relativistic statistical mechanics: Classical and quantum. *World Scientific*, 2011.
- [63] Donald Melrose. Quantum plasmadynamics. *Springer*, 2006.
- [64] Prabal Singh Verma, Sudip Sengupta, and Predhiman Kaw. Nonlinear evolution of an arbitrary density perturbation in a cold homogeneous unmagnetized plasma. *Phys. Plasmas*, 18:012301, 2011.
- [65] D. A. Diver and E. W. Liang. Modelling nonlinear electrostatic oscillations in plasmas. *Phys. Plasmas*, 23:122103, 2016.
- [66] P. K. Kaw, A. T. Lin, and J. M. Dawson. Quasiresonant mode coupling of electron plasma waves. *Phys. Fluids.*, 16:1967, 1973.
- [67] E. Infeld and G. Rowlands. Langmuir oscillations against a single-ion pulse or cavity background. *Phys. Rev. A*, 42:838, 1990.
- [68] J. F. Drake, Y. C. Lee, K. Nishikawa, and N. L. Tsintsadze. Breaking of large-amplitude waves as a result of relativistic electron-mass variation. *Phys. Rev. Lett.*, 36(4):196, 1976.



- [69] Prabal Singh Verma, Sudip Sengupta, and Predhiman Kaw. Bernstein-green-kruskal waves in relativistic cold plasma. *Phys. Plasmas.*, 19:032110, 2012.
- [70] Ratan Kumar Bera, Sudip Sengupta, and Amita Das. Fluid simulation of relativistic electron beam driven wakefield in a cold plasma. *Phys. Plasmas.*, 22:073109, 2015.
- [71] R. K. Bera, Arghya Mukherjee, Sudip Sengupta, and Amita Das. Relativistic electron beam driven longitudinal wake-wave breaking in a cold plasma. *Phys. Plasmas.*, 23:083113, 2016.
- [72] E Infeld and G. Rowlands. Nonlinear oscillations in a warm plasma. *Phys. Rev. Lett.*, 58:2063.
- [73] B. S. Bauer, A. Y. Wong, V. K. Decyk, and G. Resenthal. Experimental observation of superstrong electron plasma waves and wave breaking. *Phys. Rev. Lett.*, 68(25), 1992.
- [74] Prabal Singh Verma, Sudip Sengupta, and Predhiman Kaw. Residual bernstein-green-kruskal-like waves after one-dimensional electron wave breaking in a cold plasma.
- [75] Ira B Bernstein, John M. Greene, and Martin D. Kruskal. Exact nonlinear plasma oscillations. *Phys. Rev.*, 108:546, 1957.
- [76] R. M. G. M. Trines. Wave-breaking limits for nonquasistatic oscillations in a warm one-dimensional electron plasma. *Phys. Rev. E*, 79:056406, 2009.
- [77] William L. Kruer. Wavebreaking amplitudes in warm, inhomogeneous plasmas. *Phys. Fluids.*, 22:1111, 1979.
- [78] A Bergmann and P. Mulser. Breaking of resonantly excited electron plasma waves. *Phys. Rev. E*, 47(5):3585, 1993.
- [79] William A Newcomb. Warm relativistic electron fluid. *Phys. Fluids*", 25, 1982.

- [80] William A. Newcomb. Warm relativistic electron fluid. ii. small  $m/e$  limit. *Phys. Fluids.*, 29.
- [81] John G. Siambis. Relativistic fluid equations for intense electron beams. *Phys. Fluids*, 30:896, 1987.
- [82] Sergei V. Bulanov, Timur Zh. Esirkepov, Masaki Kando, James K. Koga, Alexander S. Pirozhkov, Tatsufumi Nakamura, Stepan S. Bulanov, Carl B. Schroeder, Eric Esarey, Francesco Califano, and Francesco Pegoraro. On the breaking of a plasma wave in a thermal plasma. i. the structure of the density singularity. *Phys. Plasmas.*, 19:113102, 2012.
- [83] Anna Grassi, Fedeli, Andrea Macchi, Sergei Bulanov, and Francesco Pegoraro. Phase space dynamics after the breaking of a relativistic langmuir wave in a thermal plasma. *Euro Phys. J. D.*, 68, 2014.
- [84] G. G. Stokes. On the theory of oscillatory waves. *Phys. Rev. Lett.*, 8:441, 1847.
- [85] G. B. Whitham. Linear and nonlinear waves. *Wiley-Interscience*, New York, 1974.
- [86] D. D. Camassa, Rand Holm. An integrable shallow water equation with peaked solitons. *Phys. Rev. Lett.*, 1661:71, 1993.
- [87] Arsen G. Khachatryan. Ion motion and finite temperature effect on relativistic strong plasma waves. *Phys. Rev. E*, 58:7799.
- [88] R. W. Hockney and J. W. Eastwood. Computer simulation using particles. *Adam Hilger*, 1988.
- [89] D. C. Rapaport. The art of molecular dynamics simulation - numerics, algorithms, parallelization, applications. *Cambridge University Press*, 1995.
- [90] Michael Griebel, Stephan Knapek, and Gerhard Zumbusch. Numerical simulation in molecular dynamics. *Springer*.
- [91] Elaine S. Oran and Jay P. Boris. Numerical simulation of reactive flow. *Cambridge University Press*, 1987.

- [92] H. Matsumoto and Y. Omura. Computer space plasma physics: Simulation techniques and software. *Terra Scientific Publishing Company*, 1993.
- [93] J. Búchner, C. T. Dum, and M. Scholer. Space plasma simulation. *Springer*, 2003.
- [94] G. Lehmann, E. W. Laedke, and K. H. Spatschek. Localized wake-field excitation and relativistic wave-breaking. *Phys. Plasmas*, 14(10):103109, 2007.
- [95] N. N. Bogoliubov and Y. A. Mitropolsky. Asymptotic methods in the theory of non-linear oscillations. *Hindustan Publishing Corporation*, 1961.
- [96] Berni Alder, Sidney Fernbach, and Manuel Rotenberg. Methods in computational physics - volume 9 - plasma physics. *Academic Press*, 1970.
- [97] M. Abramowitz and I. A. Stegun. Handbook of mathematical functions. *Imperial College Press, London*, 2005.
- [98] Vladimir Osherovich and J. Fainberg. Dependence of frequency of nonlinear cold plasma cylindrical oscillations on electron density. *Phys. Plasmas*, 11, 2004.
- [99] J. R. Marquès, J. P. Geindre, F. Amiranoff, P. Audebert, J. C. Gauthier, A. Antonetti, and G. Grillon. Temporal and spatial measurements of the electron density perturbation produced in the wake of an ultrashort laser pulse. *Phys. Rev. Lett.*, 76(19):3566, 1996.
- [100] J. R. Marquès, F. Dorchies, P. Audebert, J. P. Geindre, F. Amiranoff, J. C. Gauthier, G. Hammoniaux, A. Antonetti, P. Chessa, P. Mora, and T. M. Antonsen Jr. Frequency increase and damping of nonlinear electron plasma oscillations in cylindrical symmetry. *Phys. Rev. Lett.*, 78:3463, 1997.
- [101] J. D. Jackson. Classical electrodynamics. *Wiley and Sons, New York*, 1998.
- [102] Goerge. B. Arfken, Hans J. Weber, and Frank E. Harris. Mathematical methods for physicists. *Academic, San Diego*, 1995.
- [103] A. W. Trappiece and R. W. Gould. Space charge waves in cylindrical plasma columns. *Journal of Appl. Phys.*, 30:1764, 1959.

- [104] Wallace M. Manheimer. Nonlinear development of an electron plasma wave in a cylindrical waveguide. *Phys. Fluids.*, 12:2426, 1969.
- [105] J. Juul Rasmussen. Finite amplitude electron plasma waves in a cylindrical waveguide. *Plasma. Phys.*, 20:997, 1978.
- [106] Thomas P. Hughes and Edward Ott. Nonlinear space charge waves on cylindrical electron beams and plasmas. *Phys. Fluids.*, 23:2265, 1980.
- [107] A. Bergmann and H. Schnabl. The influence of electron trapping on stationary langmuir waves. *Phys. Fluids*, 31.
- [108] C. B. Schroeder, E Esarey, and Shadwick B. A. Comment on wave-breaking limits for relativistic electrostatic waves in a one- dimensional warm plasma [phys. plasmas13, 123102 (2006)]. *Phys. Plasmas*, 14:084701, 2007.
- [109] R. M. G. M. Trines and P. A. Norreys. Response to “comment on ‘wave-breaking limits for relativistic electrostatic waves in a one-dimensional warm plasma’ ” [phys. plasmas14, 084701 (2007)]. *Phys. Plasmas*, 14:084702, 2007.
- [110] A. H. Taub. Relativistic rankine-hugoniot equations. *Phys. Rev.*, 74(3):328.
- [111] G. Malka and J. L. Miquel. Experimental confirmation of ponderomotive-force electrons produced by an ultrarelativistic laser pulse on a solid target. *Phys. Rev. Lett.*, 77:75–78, Jul 1996.
- [112] S. V. Bulanov, F. Pegoraro, A. M. Pukhov, and A. S. Sakharov. Transverse wake-wave breaking. *Phys. Rev. Lett.*, 78:4205, 1997.